2016

Minimizing Decoherence in Optical Fiber for Long Distance Quantum Communication

Manish Kumar Gupta
Louisiana State University and Agricultural and Mechanical College, manishh.gupta@gmail.com

MINIMIZING DECOHERENCE IN OPTICAL FIBER FOR LONG DISTANCE QUANTUM COMMUNICATION

A Dissertation

Submitted to the Graduate Faculty of the
Louisiana State University and
Agricultural and Mechanical College
in partial fulfillment of the
requirements for the degree of
Doctor of Philosophy

in

The Department of Physics and Astronomy

by
Manish Kumar Gupta
B.E., Visvesvaraya Technological University, 2003
M.S., Louisiana State University, 2014
August 2016

Dedicated to my beloved grandparents.

Acknowledgments

I sincerely want to thank my Ph.D. advisor Dr. Jonathan P. Dowling for giving me an opportunity to study physics and allowing me to work in the quantum science and technology group. Without his support and constant guidance, it would be impossible to reach this point in my life. He understood my abilities and weaknesses and provided me a ground to reform myself into a physicist from a computer engineer. He never demotivated me when my calculations were wrong or when I did not know something fundamental. I remember once I told him that I am not happy with my published papers because they are based on very small ideas and his response was ".. I did a very small calculation, where I showed a new method for calculating a density matrix...it has a lot of citations..". His terrific personality had a huge impact on my outlook towards research and other non-academic things in my life.

I also thank my co-advisor Dr. Hwang Lee, who constantly corrected my calculation errors, provided suggestion and gave me ample amount of time for discussion without appointments. He motivated and guided me in every respect from figuring out the solutions to the various research problem, to applying for jobs.

I also thank Dr. Mark M. Wilde for personally teaching me quantum information along with technique to develop LaTex notes into a final paper. I finally thank Dr. Georgios Veronis, Dr. Warren W. Johnson and Dr. Mark Davidson for accepting to be on my committee.

I also acknowledge travel support from the Coates Foundation, LSU and Graduate Research Assistantship from Dr. Jonathan P. Dowling and Dr. Mark M. Wilde. I also thank all the staff members of the Department of Physics and Astronomy, specially Arnell Jackson for helping me file all the official documents and Ophelia Dudley and Carol Duran for helping me with travel arrangements.

This period of time at LSU was demanding for me but with the support of my family and friends I was able to reach this point in my career. I would like to thank all my friends

and family: Brajesh Gupt, Kaushik P. Seshadreesan, Ashkan Baluchi, Kebie Jiang, Zhihao Xiao, Haoyu Qi, Sidharth Das, Chenglong You, Robert Lanning, Geeta Verma, Nilesh Singh, Kathiresan Selvam, Smitha Sivapragasam and other QST members. I finally thank my father Mr. Rampujan Prasad Gupta and my mother Mrs. Sudha Gupta and my sisters Pushpanjali and Geetanjali for constant support. If I forget to thank my brothers-in-law Mr. Sushant Prasd and Mr. Akshay Pratap Singh then it would be unfair because they motivated me to join LSU and I thank them for providing me with support and motivation.

Table of Contents

List of Tables

List of Figures

Abstract

In this research work, I have derived analytical models for decoherence of quantum states of light and developed techniques based on Dynamical Decoupling (DD) to preserve the quantum state of polarization qubit and Orbital Angular Momentum (OAM) qudit in single-mode, multi-mode and specialized optical fibers. In subsequent work, I have derived the analytical model for decoherence of an entangled state in an optical fiber to show that such a decoherence causes loss of entanglement. I also showed that such states can be preserved with DD.

In Chapter 1, I have introduced the subject of a quantum computer and its relation to quantum communication. I give a brief overview of fundamental concepts and tools required to understand the subject matter.

In Chapter 2, I discuss optical fibers from the perspective of the electromagnetic wave in a waveguide and explain the modes in an optical fiber. Later, I explain about the sources of noise or refractive index fluctuation in an optical fiber and show how to numerically reproduce a model of an optical fiber.

In Chapter 3, I introduce the topic of quantum decoherence and discuss in detail an open-loop control technique called Dynamical Decoupling, that is applied to the system to minimize decoherence. I discuss ideal and nonideal pulse sequences used for suppressing decoherence.

In Chapter 4, I derive the analytical model for decoherence of a polarization qubit in a single-mode, multi-mode fiber, and decoherence OAM qudit in specialized multi-mode fiber.

In Chapter 5, I introduce the topic of entanglement for the bipartite system and multi-partite system, and a measure called concurrence to quantify the entanglement. I then derive the analytic model for decoherence of a pure entangled state and show that decoherence causes loss of entanglement for the case of a pure and mixed Werner-like state.

In Chapter 6, I discuss the method of numerical simulation and show by numerical simulation that polarization qubit, OAM qudit and entanglement of polarization qudit can be preserved with dynamical decoupling in an optical fiber.

In Chapter 7, I have summarized the results and discuss the scope of future work.

In the appendix, I have included additional research work not directly related to the current topic of decoherence in an optical fiber.

To summarize my research, I have derived a model for decoherence and then numerically showed that a polarization qubit can be preserved in a single mode and multi-mode optical fiber. I also show that an OAM qudit can be preserved for a certain maximum value of quantum number l. Finally, I show that entanglement of pure and Werner mixed states can be preserved.

Chapter 1
Introduction and Outline

1.1 Introduction

Tremendous progress has been made theoretically and experimentally in the develop -ment of a quantum computer since the time it was proposed by Feynman in 1980 such a machine could use interference of many-particle quantum wave function to solve computationa -lly hard problems. It is a machine that could use quantum mechanical effects to solve problems for which there exist no classically efficient known algorithms to solve on a classical computer. To clarify it a little further, a good analogy would be the comparison of a light bulb to the laser. Light bulb emits an incoherent light that is electromagnetic waves emitted by a source at random times with respect to each other, whereas a laser is a quantum mechanical device engineered to produce coherent light where the sources emit the electromagnetic waves in phase. The purpose of the two sources of light is different, a laser is not a replacement of light bulb but its use is rather for a different application.

The initial set of algorithms that motivated the development of a quantum computer are factoring, comparing functions, unstructured search and quantum simulation and they were shown to be advantageous over classical known algorithms. These algorithms can be categorized into three main classes. First, this class of algorithms are based on the quantum version of Fourier transform, and examples of this type of algorithm are Deutsch-Jozsa algorithm to determine if a function is constant or balanced and Shor's algorithm for factoring. The second class of algorithm is search algorithm and example is Grover quantum search algorithm. The third class of algorithm is the quantum simulation, where the quantum computer is used to simulate a quantum system; an example for this would be simulating the behavior of a moderately sized molecule under certain constraints in quantum chemistry.

Several approaches have been pursued by researchers over a period of two decades to physically realize a quantum computer: Superconductor-based quantum computer, Trapped ion quantum computer, Quantum dot based quantum computer, Nuclear magnetic resonance based quantum computer, cavity quantum electrodynamics based quantum com -puter, Diamond-based quantum computer, Linear optical quantum computer, etc. Each of the approaches have some advantages and drawbacks; it may happen that the final realization would be a combination of different technologies.

For any quantum information processing task the basic unit of quantum information, i.e. a qubit, would have to be transported between nodes of the quantum computer for processing. The nodes could be located locally or at a distant location as in the case of quantum networks. An important physical system for encoding information for long distance quantum communication is an optical photon, where the quantum information can be encoded in the spin or angular momentum degree of freedom. The properties that make photons such an important candidate for communication are that they do not interact strongly with each other or with the surrounding matter. They can travel long distances in optical fibers with very low transmission loss; with current technological advancement the losses are as low as ≈ 0.16db/km($\approx 3.6\%$). They can be easily delayed with phase shifters and can be switched with mirrors and beam splitters.

Quantum communication research promises much more than a quantum computer. It allows for the distribution of secret information between two parties with security guaranteed by the laws of physics. It allows for an enhanced communication capacity as in the case of super-dense coding, in which two parties who initially share an entangled bit can send two bit of classical information by sending a single qubit [4, 5]. Optical fibers that preserve a quantum state with high fidelity can be used to make quantum memories and quantum delay lines.

1.1.1 Communication System

A communication system is used for transmitting information or data from one point to another. A general block diagram for visulalizing such a system is shown in Figure. 1.1. It consists of a source that generates data in the form of messages represented by M_A, that could be a voice wave form, a sequence of binary digits or output from probe sensors. The channel could be high-frequency radio link, a storage medium or an optical fiber. The channel is generally subjected to various types of noise caused by time-varying frequency response, thermal noise, cross talk or switching noise. The encoder does any pre-processing required on the message message M_A before transmission that might include any combination of modulation, data compression and redundancy insertion for combating noise in the channel. The decoder does an inverse processing on the output of the channel to reproduce an approximation of the source data represented by M_B.

Figure 1.1: A classical communication system. M_A and M_B represent the message sent by Alice and decoded by Bob respectively [1].

In a noisy channel, the output probability depends upon the input, channel characteristic, and channel structure [6]. The characteristic of the channel is the underlying conditional probability distribution for the output given the input and the structure of the channel, that represents the presence of feedback. For a given channel the capacity is defined as the maximum rate at which a sender can transmit information over a given channel such that the receiver can recover the information at the output of the channel with an arbitrarily small error in the limit of many channel uses. The capacity represents the thin line between the communication rates which are achievable and those which are not.

Classically, the basic unit of information is a 'bit', which are represented by a physical system that has macroscopic states denoted by 0 and 1. These bits are used to encode classical information generated by the source and transmitted through a noisy channel to the receiver.

1.2 Fundamental Concepts

We first review some of the fundamental concepts and tools required for understanding the subject of quantum communication.

1.2.1 Quantum Bit

The basic unit of quantum information is called the qubit. It is a quantum mechanical analogue of a classical bit, but unlike a classical bit, it can be in state 0, 1 or a superposition. The qubit can be represented as a two-dimensional quantum system, which means that the state of the system lives in a complex two-dimensional Hilbert space H. We define a standard basis $\{|0\rangle, |1\rangle\}$, called the computational basis, which is used for preparation and measurement of quantum information [7, 8, 9]. The choice of physical system to represent a qubit can be a spin of a particle, polarization of light or any other quantum mechanical degree of freedom of a system. The matrix representation in computational basis is written as

$$|1\rangle = \begin{pmatrix} 0 \\ 1 \end{pmatrix} \quad \text{and} \quad |0\rangle = \begin{pmatrix} 1 \\ 0 \end{pmatrix} \tag{1.1}$$

1.2.2 Bloch Sphere

A general qubit state in the computational basis can be represented as

$$|\psi\rangle = \alpha|0\rangle + \beta|1\rangle, \quad \text{where } |\alpha|^2 + |\beta|^2 = 1. \tag{1.2}$$

We can rewrite the equation (1.2) as

$$|\psi\rangle = e^{i\gamma}\left(\cos\frac{\theta}{2}|0\rangle + e^{i\phi}\sin\frac{\theta}{2}|1\rangle\right), \tag{1.3}$$

where θ, ϕ and γ are real numbers. We can ignore the factor $e^{i\gamma}$ because it has no observable effect and it can be further rewritten as

$$|\psi\rangle = \cos\frac{\theta}{2}|0\rangle + e^{i\phi}\sin\frac{\theta}{2}|1\rangle. \tag{1.4}$$

The number θ and ϕ define a point on a unit three-dimensional sphere as shown in the Figure 1.2 and this sphere is called the *Bloch sphere*. It provides a visual picture of single qubit state. Many of the operations on single qubit state can be approximated as a sequence of rotations about a given axis. This visualization of Bloch sphere is limited to a single qubit and cannot be extended for a multi-qubit system or multi-level system.

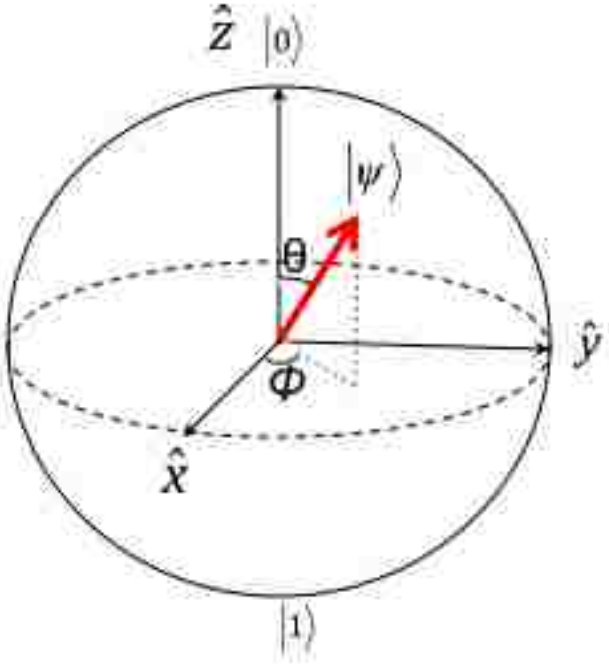

Figure 1.2: Bloch sphere for visualizing the state of a single qubit. The parameter θ varies in the range $[0, \pi]$ and the relative phase ϕ varies in the range $[0, 2\pi]$.

1.2.3 Rotation Operator

Rotations affect physical systems and the state ket corresponding to the rotated system is different from the original state ket of unrotated system [10]. Given a rotation operation R, characterized by a 3×3 orthogonal matrix, we associate an operator $\mathscr{D}(R)$ for an

appropriate ket such that

$$|\alpha\rangle_R = \mathscr{D}(R)|\alpha\rangle \tag{1.5}$$

where the ket $|\alpha\rangle_R$ and $|\alpha\rangle$ corresponds to the state of the rotated and unrotated system respectively. Classically, for the case of a three-dimensional system, a 3×3 matrix acts on column matrix corresponding to the three components of a classical vector, while the operator $\mathscr{D}$ acts on a state vector in ket space. The matrix for $\mathscr{D}(R)$ depends on the dimensionality N of the particular ket space. For $N = 2$, a 2×2 matrix is appropriate for describing a spin $\frac{1}{2}$ system with no other degree of freedom; for $N = 3$, a 3×3 matrix is appropriate for describing a spin 1 system and similarly for other dimensions.

We know from classical mechanics that angular momentum is the generator of rotations in the same way that momentum and Hamiltonian are the generators of translation and time evolution. We can write any approximate infinitesimal operator as

$$U_\epsilon = 1 - iG\epsilon, \tag{1.6}$$

where G is a Hermitian operator. Using this fact, we define the angular momentum operator J_k, such that the operator for an infinitesimal rotation around k^{th} axis by an angle $d\phi$ can be obtained by letting

$$G \to \frac{J_k}{\hbar}, \epsilon \to d\phi, \tag{1.7}$$

where J_k is assumed to be Hermitian. The infinitesimal rotation operator is unitary and it reduces to the identity operator in the limit $d\phi \to 0$. More generally, we have

$$\mathscr{D}(\hat{\mathbf{n}}, d\phi) = 1 - i\left(\frac{\mathbf{J} \cdot \hat{\mathbf{n}}}{\hbar}\right) d\phi \tag{1.8}$$

for rotation by an angle $d\phi$ about the direction given by unit vector $\hat{\mathbf{n}}$.

A finite rotation can be generated by compounding infinitesimal rotations successively about the same axis. A finite rotation by an angle ϕ about z-axis is given by

$$\begin{aligned}\mathscr{D}(\phi) &= \lim_{N\to\infty}\left[1 - i\left(\frac{J_z}{\hbar}\right)\left(\frac{\phi}{N}\right)\right]^N \\ &= \exp\left(\frac{-iJ_z\phi}{\hbar}\right) \\ &= 1 - \frac{iJ_z\phi}{\hbar} - \frac{J_z^2\phi^2}{2\hbar^2} + \cdots \end{aligned} \tag{1.9}$$

and similarly rotation about x-axis and y-axis can be defined. The operator $\mathscr{D}(R)$ has the following properties:

$$\text{Identity :} \qquad \mathscr{D}(R)\cdot 1 = \mathscr{D}(R) \tag{1.10}$$

$$\text{Closure :} \qquad \mathscr{D}(R_1)\mathscr{D}(R_2) = \mathscr{D}(R_3) \tag{1.11}$$

$$\text{Inverse :} \qquad \mathscr{D}(R)\mathscr{D}^{-1}(R) = 1 \tag{1.12}$$

$$\mathscr{D}^{-1}(R)\mathscr{D}(R) = 1$$

$$\begin{aligned}\text{Associativity : } \mathscr{D}(R_1)[\mathscr{D}(R_2)\mathscr{D}(R_3)] &= [\mathscr{D}(R_1)\mathscr{D}(R_2)]\mathscr{D}(R_3) \\ &= \mathscr{D}(R_1)\mathscr{D}(R_2)\mathscr{D}(R_3).\end{aligned} \tag{1.13}$$

We know from the classical commutation relation that$R_x(\epsilon)R_y(\epsilon) - R_y(\epsilon)R_x(\epsilon) = R_z(\epsilon^2) - 1$ and analogous to it, we derive the operator commutation relation using the equation (1.9)

$$\begin{aligned}&\left(1 - \frac{iJ_x\epsilon}{\hbar} - \frac{J_x^2\epsilon^2}{2\hbar^2}\right)\left(1 - \frac{iJ_y\epsilon}{\hbar} - \frac{J_y^2\epsilon^2}{2\hbar^2}\right) \\ &\qquad - \left(1 - \frac{iJ_y\epsilon}{\hbar} - \frac{J_y^2\epsilon^2}{2\hbar^2}\right)\left(1 - \frac{iJ_x\epsilon}{\hbar} - \frac{J_x^2\epsilon^2}{2\hbar^2}\right) = 1 - \left(1 - \frac{iJ_z\epsilon}{\hbar} - \frac{J_z^2\epsilon^2}{2\hbar^2}\right).\end{aligned} \tag{1.14}$$

First order ϵ terms cancel out and equating ϵ^2 terms on both sides of equation, we obtain

$$[J_x, J_y] = i\hbar J_z. \tag{1.15}$$

Similarly, we obtain the rotation operator about other axis and we also obtain the following fundamental commutation relationship of angular momentum.

$$[J_i, J_j] = i\hbar\epsilon_{ijk}J_k. \tag{1.16}$$

1.2.4 Spin $\frac{1}{2}$ Systems

For spin $\frac{1}{2}$ systems, we know that the ket space is spanned by $|+\rangle, |-\rangle$ and the angular momentum operator are S_x, S_y, S_z. The matrix representation of kets and angular momentum operator are

$$|+\rangle = \begin{pmatrix} 1 \\ 0 \end{pmatrix}, \quad |-\rangle = \begin{pmatrix} 0 \\ 1 \end{pmatrix} \tag{1.17}$$

$$S_x = \frac{\hbar}{2}\begin{pmatrix} 0 & 1 \\ 1 & 0 \end{pmatrix}, \quad S_y = \frac{\hbar}{2}\begin{pmatrix} 0 & -i \\ i & 0 \end{pmatrix}, \quad S_z = \frac{\hbar}{2}\begin{pmatrix} 1 & 0 \\ 0 & -1 \end{pmatrix}. \tag{1.18}$$

The operators S_x, S_y and S_z given earlier satisfy the angular momentum commutation relations

$$[S_i, S_j] = i\hbar\epsilon_{ijk}S_k. \tag{1.19}$$

In 1926, W. Pauli introduced the spinor formalism to make the manipulation with state ket easy for $\frac{1}{2}$ systems. He defined *Pauli matrices* σ_k, such that matrix elements of $\langle\pm|S_k|+\rangle$ and $\langle\pm|S_k|-\rangle$ are equal to $\hbar/2$ times the matrix elements of σ_k. Explicitly the Pauli matrices are give as

$$\sigma_x = \begin{pmatrix} 0 & 1 \\ 1 & 0 \end{pmatrix}, \quad \sigma_y = \begin{pmatrix} 0 & -i \\ i & 0 \end{pmatrix}, \quad \sigma_z = \begin{pmatrix} 1 & 0 \\ 0 & -1 \end{pmatrix}. \tag{1.20}$$

The anticommutation and commutation relations of Pauli matrices are

$$\{\sigma_i, \sigma_j\} = 2\,\delta_{ij}, \tag{1.21a}$$

$$[\sigma_i, \sigma_j] = 2\,i\epsilon_{ijk}\sigma_k. \tag{1.21b}$$

These relations are similar to angular momentum commutation relations (1.18). The other useful properties of Pauli matrices are

$$\sigma_i^\dagger = \sigma_i, \tag{1.22a}$$

$$\det(\sigma_i) = -1, \tag{1.22b}$$

$$\mathrm{Tr}\,(\sigma_i) = 0. \tag{1.22c}$$

There is another important property that we will need to reduce the expression for rotation operator

$$(\sigma \cdot \mathbf{a})(\sigma \cdot \mathbf{b}) = \mathbf{a} \cdot \mathbf{b} + i\,\sigma \cdot (\mathbf{a} \times \mathbf{b}) \tag{1.23}$$

Using the formalism discussed above we now write a rotation operator for a spin $\frac{1}{2}$ system. The 2×2 matrix represents a rotation by an angle ϕ about an axis $\hat{n}$ and it is given by

$$\mathscr{D}(\hat{\mathbf{n}}, \phi) = \exp\left(\frac{-i\mathbf{S} \cdot \hat{\mathbf{n}}\phi}{\hbar}\right) = \exp\left(\frac{-i\sigma \cdot \hat{\mathbf{n}}\phi}{2}\right). \tag{1.24}$$

Using the relation

$$(\sigma \cdot \hat{\mathbf{n}})^2 = \begin{cases} 1 & \text{for } n \text{ even}, \\ \sigma \cdot \hat{\mathbf{n}} & \text{for } n \text{ odd}\ , \end{cases} \tag{1.25}$$

that follows from (1.23), we can rewrite the rotation operator as

$$\mathscr{D}(\hat{\mathbf{n}},\phi)=\exp\left(\frac{-i\sigma\cdot\hat{\mathbf{n}}\phi}{2}\right)=\left[1-\frac{(\sigma\cdot\hat{\mathbf{n}})^2}{2!}\left(\frac{\phi}{2}\right)^2+\frac{(\sigma\cdot\hat{\mathbf{n}})^4}{4!}\left(\frac{\phi}{2}\right)^4-\cdots\right]$$
$$-i\left[\frac{(\sigma\cdot\hat{\mathbf{n}})}{1!}\left(\frac{\phi}{2}\right)-\frac{(\sigma\cdot\hat{\mathbf{n}})^3}{3!}\left(\frac{\phi}{2}\right)^3+\cdots\right]$$
$$=\mathbf{1}\cos\left(\frac{\phi}{2}\right)-i\,\sigma\cdot\hat{\mathbf{n}}\sin\left(\frac{\phi}{2}\right). \tag{1.26}$$

The rotation operator obtained in equation (1.26) is used to rotate a ket on Bloch sphere.

1.2.5 Distance Measures

A distance measure in information theory gives a quantitative answer to the question of how one state is different from the other or how well the information is preserved by a physical process. The distance measures can be broadly classified in two categories: *static measures* and *dynamic measures* [5].

In classical information theory the information source is usually modeled as random variable with a probability distribution over some source alphabet. Hence the question of distance measure becomes, how the two probability distributions p_x and q_x representing the two sources are similar? The two static measures used to answer this questions are *trace distance*, also called *Kolmogorov distance*, and *fidelity*. If the random variable X with probability p_x is sent through a noisy channel whose output is random variable Y with probability distribution q_x then we use dynamic measure of distance to quantify the closeness of two distributions. Dynamic measure is a special case of static trace distance.

The quantum generalization for closeness of two quantum states is an extension of classical notions of trace distance and fidelity. The *trace distance* between the two quantum states ρ and σ is defined as

$$D(\rho,\sigma)=\frac{1}{2}\operatorname{Tr}|\rho-\sigma|, \tag{1.27}$$

where $|A|=\sqrt{A^\dagger A}$ is defined to be a positive square root of $A^\dagger A$. Trace distance can be

understood more clearly by generalizing the classical notion of trace distance:

$$D(\rho, \sigma) = \max_P \mathrm{Tr}(P(\rho - \sigma)), \tag{1.28}$$

where the maximization is taken over all projectors P, such that P is positive operator and $P \leq I$. It is the difference in probabilities of a measurement outcome of a POVM P on the states ρ and σ, maximized over all such possible positive operator valued measurement (POVM) P.

Since trace distance is a metric on the space of density operators, it satisfies certain properties:

$$\text{Invariance :} \qquad D\big(U\rho U^\dagger, U\sigma U^\dagger\big) = D(\rho, \sigma) \tag{1.29a}$$

$$\text{Symmetric :} \qquad D(\rho, \sigma) = D(\sigma, \rho), \tag{1.29b}$$

$$\text{Contractive :} \qquad D(\varepsilon(\rho), \varepsilon(\sigma)) \leq D(\rho, \sigma), \tag{1.29c}$$

$$\text{Triangle inequality :} \qquad D(\rho, \tau) \leq D(\rho, \sigma) + D(\sigma, \tau), \tag{1.29d}$$

$$\text{Strong convexity :} \qquad D\left(\sum_i p_i\rho_i, \sum_i q_i\sigma_i\right) \leq D(p_i, q_i) + \sum_i p_i D(\rho_i, \sigma_i). \tag{1.29e}$$

Trace distance $D(\rho, \sigma) = 0$ if and only if $\rho = \sigma$. It is symmetric function of its input and invariant under unitary transform. Trace preserving quantum operation ε representing a physical process never increases the distance between two quantum states. Trace distance is strongly convex in its inputs.

Fidelity is another measure of distance distance between two quantum states. It is not an actual metric on density operators but has useful properties for being a measure. It is defined for states ρ and σ as

$$F(\rho, \sigma) = \mathrm{Tr}\,\sqrt{\rho^{1/2}\sigma\rho^{1/2}}. \tag{1.30}$$

When the two quantum state commute, that is, they are diagonal in same basis,

$$\rho = \sum_i r_i |i\rangle\langle i| \quad \text{and} \quad \sigma = \sum_i s_i |i\rangle\langle i|, \tag{1.31}$$

then it can be simplified further as

$$\begin{aligned} F(\rho, \sigma) &= \mathrm{Tr}\left(\sum_i \sqrt{r_i s_i} |i\rangle\langle i| \right) \\ &= \sum_i \sqrt{r_i s_i}. \end{aligned} \tag{1.32}$$

The fidelity satisfies many of the same properties as trace distance

$$\text{Invariance :} \qquad F\big(U\rho U^\dagger, U\sigma U^\dagger\big) = F(\rho, \sigma) \tag{1.33a}$$

$$\text{Symmetric :} \qquad F(\rho, \sigma) = F(\sigma, \rho), \tag{1.33b}$$

$$\text{Monotonicity :} \qquad F(\varepsilon(\rho), \varepsilon(\sigma)) \geq F(\rho, \sigma), \tag{1.33c}$$

$$\text{Strong concavity :} \qquad F\left(\sum_i p_i \rho_i, \sum_i q_i \sigma_i \right) \geq \sum_i \sqrt{p_i q_i} F(\rho_i, \sigma_i). \tag{1.33d}$$

Fidelity of two pure states $\rho = |\psi\rangle\langle\psi|$ and $\sigma = |\phi\rangle\langle\phi|$ can be written as

$$\begin{aligned} F(\rho, \sigma) &= \mathrm{Tr} \sqrt{|\psi\rangle\langle\psi||\phi\rangle\langle\phi|} \\ &= |\langle\psi|\,\phi\rangle|. \end{aligned} \tag{1.34}$$

1.3 Thesis Outline

We have discussed the fundamentals required to understand the representation of photonic qubit. In the rest of the chapters we will use these fundamental concepts to understand the decoherence process of photonic qubits in an optical fiber.

Chapter 2 explains the noise in different kinds of optical fiber and shows how to model the noise, caused by index fluctuation, in different kinds of optical fibers. Chapter 3 details

theoretically one of the methods for minimizing dephasing error in an open quantum system. In Chapter 4 a model for decoherence has been derived for a polarization qubit and a OAM qudit in optical fiber. In Chapter 5, we derive a decoherence model for the case when the qubits are entangled and show how decoherence causes loss of entanglement. Chapter 6 details the method and results of numerical simulation. Finally we conclude in Chapter 7 detailing the implications of our result and future research work. Appendix A contains additional research work not directly related to the thesis topic.

Chapter 2
Modeling Noise in Optical Fiber

2.1 Introduction

Optical fibers have been proven to be a superior medium for high bandwidth communica -tion over long distances. The key characteristics that enable their performance are its low power loss as the signal propagates along the length of the optical fiber. Optical fibers are waveguides that are made up of low loss materials such as pure silica glass. They are cylindrical in structure with a central core through which the light is guided, embedded in an outer cladding of a slightly smaller refractive index. The Figure 2.1 depicts the structure of an optical fiber. The light incident on the core-cladding boundary at an angle greater than critical angle goes through a total internal reflection and are guided through the core.

Light propagates in waveguides in the form of modes. Each mode travels along the axis of the waveguide with a distinct propagation constant and group velocity in order to preserve the spatial and polarization profile. A fiber is called single-mode when the core diameter is small and only one mode is permitted in the fiber. If the core diameter is large and many modes are allowed then it is called a multimode fiber.

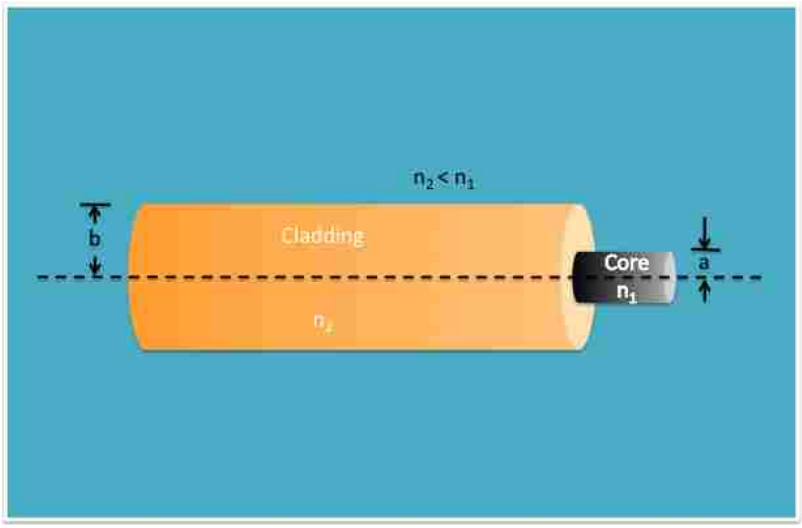

Figure 2.1: Optical fiber: A cylindrical dielectric waveguide.

One problem associated with classical light propagation in multimode waveguide is modal dispersion where different modes travel with different group velocities. This results in broadening light pulses, which limits the speed at which adjacent pulses can be sent without overlapping and therefore limits the bandwidth of fiber-optic communication. Modal dispersion can be minimized by varying the refractive index of the fiber from a maximum value at the center to a minimum value at the core-cladding boundary. Such a fiber is called graded-index fiber; otherwise, it is called step-index fiber in which the core and cladding refractive index are constant. Varying the refractive index causes the light at the center to travel slowly in comparison to the light traveling at the core-cladding boundary. This averages the time of travel and reduces the broadening of light pulse.

Another problem in multimode waveguide is modal noise or speckle, where each mode undergoes a random phase, so that the sum of the complex amplitudes of the modes has a random intensity. This modal noise is caused by uncontrollable imperfections, strains, and temperature fluctuations.

In this chapter we will be studying a similar effect that causes the dephasing of photons that are in a superposition of two states.

2.2 Light Propagation in Wave Guide

We now review the propagation of monochromatic light in step-index fibers using electromagnetic theory. We apply the boundary condition, imposed by cylindrical dielectric inside the core and cladding, on Maxwell's equations to determine the electric and magnetic field of guided wave. The special solutions that obey the boundary conditions are called modes, and each mode has a distinct propagation constant, a characteristic distribution of field in transverse plane and two independent polarization states.

Electric and magnetic fields components must satisfy the Helmholtz equation, $\nabla^2 U + n^2 k_0^2 U = 0$, in the core $r < a$ where $n = n_1$ and in the cladding $r > a$ where $n = n_2$ with condition $k_0 = 2\pi/\lambda$. To study the field propagation inside the core and at the core-cladding boundary we assume that the radius of cladding b is sufficiently large and

can be assumed to be infinite. The Helmholtz equation in cylindrical coordinates in given as

$$\frac{\partial^2 U}{\partial r^2} + \frac{1}{r}\frac{\partial U}{\partial r} + \frac{1}{r^2}\frac{\partial^2 U}{\partial \phi^2} + \frac{\partial^2 U}{\partial z^2} + n^2 k_0^2 U = 0, \tag{2.1}$$

where complex amplitude $U = U(r, \phi, z)$ represents the Electric and magnetic field compo -nents in cylindrical coordinates. Now we seek solutions of wave traveling in z direction such that z dependence of U has the form $e^{-i\beta z}$, where β is the propagation constant. U should be periodic in ϕ with a period of 2π; hence we assume ϕ is harmonic with form $e^{-il\phi}$, where l is an integer. U has the following form

$$U(r, \phi, z) = u(r)e^{-il\phi}e^{-i\beta z}, \quad l = 0, \pm 1, \pm 2, \cdots . \tag{2.2}$$

We substitute U in the equation 2.1 to obtain differential equation $u(r)$:

$$\frac{d^2 u}{dr^2} + \frac{1}{r}\frac{du}{dr} + \left(n^2 k_0^2 - \beta^2 - \frac{l^2}{r^2}\right)u = 0. \tag{2.3}$$

For guided wave the propagation constant should be smaller than wave number in the core $\beta < n_1 k_0$ and greater than the wave number in the cladding $\beta > n_2 k_0$. For notational convenience we define

$$k_T^2 = n_1^2 k_0^2 - \beta^2 \quad \text{and} \quad \gamma^2 = \beta^2 - n_2^2 k_0^2, \tag{2.4}$$

where k_T^2 and γ^2 are positive and k_T and γ are real. The ordinary differential equation in (2.3) can be written for core and cladding separately using the conditions for guided wave as

$$\frac{d^2 u}{dr^2} + \frac{1}{r}\frac{du}{dr} + \left(k_T^2 - \frac{l^2}{r^2}\right)u = 0, \quad r < a \text{ (core)}, \tag{2.5}$$

$$\frac{d^2 u}{dr^2} + \frac{1}{r}\frac{du}{dr} - \left(\gamma^2 + \frac{l^2}{r^2}\right)u = 0, \quad r > a \text{ (cladding)}. \tag{2.6}$$

These differential equations have known solutions, a family of Bessel functions, and the bounded solutions are:

$$u(r) \propto \begin{cases} J_l(k_T r), & r < a \text{ (core)}, \\ K_l(\gamma r), & r > a \text{ (cladding)}, \end{cases} \tag{2.7}$$

where $J_l(x)$ is the Bessel function of the first kind and order l, and $K_l(x)$ is the modified Bessel function of the second kind and order l.

The only unknown is the constant of proportionality in equation (2.7); hence we apply boundary conditions to determine it. We first start by writing the electric and magnetic field complex amplitudes E_z and H_z in the form of equation (2.2). We use the condition that electric and magnetic field components should be continuous at the core-cladding boundary $r = a$, to determine the coefficients of proportionality. The remaining four components E_ϕ, H_ϕ, E_r and H_r are determined with the help of Maxwell's equations. Continuity of E_ϕ, H_ϕ at $r = a$ gives two more equations. One equation relates the coefficients of proportionality in E_z and H_z and the other equation gives the condition that the propagation constant β must satisfy. This condition is called dispersion relation and it is an equation for β with ratio a/λ_0 and the fiber indices n_1 and n_2.

For each azimuthal index l, the dispersion relation has multiple solutions yielding discrete propagation constants β_{lm}, $m = 1, 2, \cdots$, each solution represents a distinct mode. The corresponding k_{Tlm} and γ_{lm} governs the spatial distribution in the field and cladding. Therefore a mode characterizes the azimuthal and radial distribution in the fiber. For each mode there are two independent configurations of E and H vector corresponding to two states of polarization [11].

2.2.1 Single Mode Fiber

A single mode fiber supports a single mode of propagation by using a small core diameter and small numerical aperture. The fundamental mode has a bell-shaped distribution

similar to a Gaussian distribution. This mode provides the highest confinement of the light power within the core and hence used is for long distance communication.

2.2.2 Polarization Maintaining Fiber

A fiber with circular cross section has many allowed modes and each mode can exist in two independent states of polarization with the same propagation constant. In a single-mode fiber the mode can be in one of the two polarization state H or V for which the propagation constants and group velocities are the same. Ideally the power delivered in input polarization state should remain in that polarization state at the receiver and there should be no power exchange between the polarization states. Such ideal fibers have constant circular cross section; these are difficult to manufacture. They are called low-birefringence polarization maintaining fiber. In reality the stress and strain in the fiber causes a random transfer of power between the two polarization modes thus the linear polarized input state is transforms into elliptically polarized state at the output. This problem is fixed by polarization maintaining fiber, which is a specialty fiber with a strong built-in high-birefringence.

In a polarization maintaining fiber, if the polarization of the light launched in to the fiber and it is aligned with one of the birefringent axes then the light polarization is preserved even if the there is a strain in the fiber. The propagation constant for the two modes are so different that the slowly varying disturbance in the fiber do not couple the polarization modes.

2.3 Asymmetry in Optical Fiber

The electromagnetic polarization represents, how the electric field component orientation varies in a plane perpendicular to the direction of propagation. For an electromagnetic wave propagating along z axis, it may be represented as superposition of two partial waves with mutually orthogonal linear polarization with same frequency. The field $E = E_x + E_y$, where E_x and E_y are components of electric field oscillating along x and y axis respectively. These two vectors may be assigned to two polarization modes of circular dielectric waveguide.

Assuming a lossless medium the field components can be represented as

$$E_x(z,t) = E_{0,x}\cos(kz - \omega t + \phi_x),$$
$$E_y(z,t) = E_{0,y}\cos(kz - \omega t + \phi_y), \tag{2.8}$$

where $E_{0,x}, E_{0,y}$ are field amplitudes, ω is the field angular frequency, t is the time, ϕ_x, ϕ_y are the phases of wave and k is the wave vector. The ratio of amplitudes $E_{0,x}$ and $E_{0,y}$ and the phase difference $\Delta\phi = \phi_x - \phi_y$ determines the state of polarization of the resulting wave.

When the amplitudes are equal $E_{0,x} = E_{0,y}$ and $\Delta\phi = 0$, the orthogonal waves are in phase and we obtain a linearly polarized light by their superposition. Its direction of polarization is 45° to y axis or -45° to x axis. If $E_{0,x} = E_{0,y}$ and $\Delta\phi = \pm\pi/2$ the resultant field has circular polarization, since the end point of the vector E traces a circle. If $E_{0,x} \neq E_{0,y}$ and $\Delta\phi \neq 0, \pm\pi/2$ then we obtain an elliptically polarized wave. The end point of vector E traces an ellipse.

In an isotropic medium the refractive index is constant and it is independent of direction; hence the wave propagation velocity remains constant independent of direction of propagation. The wave phase velocity $v_p = n/c$, where n is the refractive index of the medium and c is the wave velocity in vacuum. However if the medium is anisotropic then the phase velocity depends on the direction of propagation of a particular polarization. This effect is observed in birefringent materials. If the wave is polarized between the x and y axes then the velocity of the wave is determined by the refractive indices n_x and n_y and a phase shift occurs between the orthogonal components of the field. This occurs due to the difference in propagation velocities of the components and the resulting state polarization depends on the total phase difference $\Delta\phi$, which is a function of propagation length in the birefriengent medium.

2.3.1 Linear Birefringence

In a single-mode optical fiber with circular core cross-section two orthogonally polarized state may exist and the superposition of these two modes results in the wave propagating in the fiber. The amplitude ratio and phase relation of these two modes determines the polarization state of the wave in the fiber. The propagation constants of the two orthogonal modes in the fiber are given by $\beta_x = \frac{\omega n_x}{c}$ and $\beta_y = \frac{\omega n_y}{c}$, where ω is the angular frequency, n is the refractive index and c is the speed of light in vacuum. An ideal single mode fiber made from isotropic material with circular symmetry along the length of fiber has the same refractive index for both the modes and hence $\beta_x = \beta_y$. A non-ideal fiber has some asymmetry due to manufacturing imperfections or stress on the fiber due to deployment in the field. The asymmetry in the fiber breaks the degeneracy of two orthogonal modes and fiber behaves as a birefringent medium with different refractive indices n_x and n_y. It results in difference in phase velocity and propagation constants β_x and β_y for two modes. We designate propagation constant β_y and β_x as fast mode and slow mode respectively [12]. The birefringence can be circular or linear but circular birefringence is negligible in common single-mode fibers.

For a short section of fiber, linear birefringence can be considered to be uniform. The difference between the propagation constant of slow and fast modes can be expressed as

$$\Delta\beta = \frac{\omega n_s}{c} - \frac{\omega n_f}{c} = \frac{\omega \Delta n}{c} \tag{2.9}$$

where ω is the angular frequency, c is the speed of light, and $\Delta n = n_s - n_f$ is the differential effective refractive index between slow (s) and fast (f) modes [13].

When a linearly polarized wave (such as 45°) polarization is launched into the fiber, the asymmetry in the fiber causes a phase shift between the two orthogonal modes. This occurs because these two modes travel with different phase velocities and acquire a relative phase shift that is a function of propagation length in the birefringent fiber. As a consequence, the

state of polarization (SOP) evolves in a cyclic fashion as the light propagates down the fiber (i.e., from linear to elliptical to circular and back through elliptical to linear state that is orthogonal to the initial state). The output mode will not be stable as environmental factors such as stress and ambient temperature changes will change the birefringent properties of fiber. This complicates the utilization of single-mode fiber in applications such as quantum cryptography and quantum communication where polarization modes need to be preserved.

The birefringence in optical fiber is characterized by the beat length l_b. It is the length of fiber over which the total phase shift between the two orthogonal modes is $\Delta\phi = 2\pi$ and mathematically defined as

$$l_b = \frac{2\pi}{\beta_x - \beta_y} = \frac{\lambda}{n_x - n_y} = \frac{\lambda}{\Delta n}, \tag{2.10}$$

where β_x and β_y are the propagation constants for the slow and fast modes, Δn is the difference of refractive indices and λ is the wavelength of light. Standard telecommunica -tion-type fibers have beat lengths of $10m$ with $\Delta n \approx 10^{-7}$ on the other hand, polarization -maintaining fibers are manufactured to have large Δn and beat length of 3mm.

2.4 Imperfection in Optical Fiber

Birefringence in an optical fiber can result from both intrinsic and extrinsic perturba -tions. Intrinsic perturbation can originate during the manufacturing process and is perma -nent. Form (geometric) birefringence can arise due to non-circular waveguides and stress birefringence is due to forces set up by asymmetry of the core. Extrinsic perturbation can be caused by spooling the fiber or embedding the fiber in the ground, lateral stress, bending, or twisting. These perturbations create linear birefringence and can change as the fiber's external environment changes [14, 15].

- **Elliptical fiber core**

The linear birefringence may be intrinsic or extrinsic in nature but the main cause of intrinsic linear birefringence is manufacturing imperfection. The core cross-section of the fiber is not circular but slightly elliptical as shown in Figure 2.2.

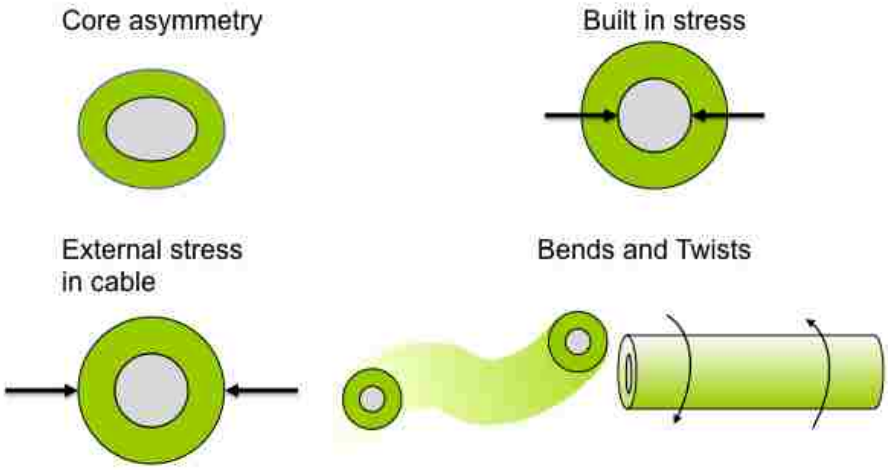

Figure 2.2: Intrinsic and extrinsic noise sources in Optical fiber.

- **Stress Induced linear birefringence**

The linear birefringence is caused by the stress induced by the cladding on the core.

2.5 Modeling Noise in Optical Fiber

Optical phase difference between the two modes due to refractive index fluctuation in the short-length regime is deterministic because birefringence is inherently additive, but today's optical fiber transmission systems are 100s and 1000s of km long and birefringence is no longer additive. The birefringence axis changes randomly along the fiber from segment to segment causing polarization mode coupling, where the polarization from one segment decomposes into both fast and slow modes of the next segment. This coupling results from the localized stress formed during manufacturing, spooling, cabling and deployment. Long fibers are typically modeled as concatenated segments of birefringent segments whose birefringence changes randomly along the fiber as shown in Figure 2.3 [16]. The refractive

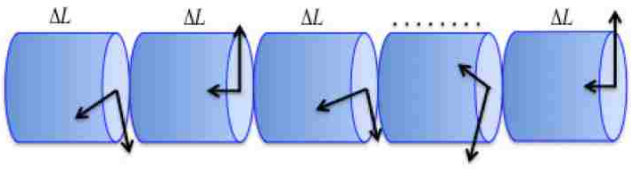

Figure 2.3: The fiber is modeled as concatenated segments of fiber of length ΔL with constant birefringence Δn.

index fluctuation across these segments follows a distribution which can be either a Gaussian distribution or Rayleigh distribution [17] depending on the type of optical fiber under consideration. For our work we model three different types of optical fiber: polarization maintaining fiber, single mode fiber and multimode fiber.

2.5.1 Polarization Maintaining Fiber

An ideal single mode fiber with symmetrical circular core has two orthogonally polarized modes; these two modes have the same group velocity and hence the state of polarization is preserved. However, in reality, fibers have some amount of asymmetry caused due to intrinsic and extrinsic perturbations. This asymmetry breaks the degeneracy of two orthogonally polarized modes, resulting in birefringence along the length of the fiber. A small birefringence causes evolution of the polarization state as the light propagates through the fiber. To control this state evolution, special fibers are made with very high birefringence and very small beat length such that total acquired phase is 2π such that mode coupling is minimized and state of polarization is preserved. Such optical fibers are called polarization maintaining optical fiber or PM fibers.

A polarization maintaining fiber is a special type of single-mode fiber that preserves the two polarization states. These fibers have large linear birefringence. Since the core radius is very small for such fibers, the index fluctuation along the radial direction is very small and hence it is safely assumed to be constant.

We model the refractive index fluctuation in PM optical fiber of length L by representing it as concatenated, homogeneous segments of length ΔL with constant birefringence $\Delta\beta = \frac{\omega\left(n_s - n_f\right)}{c}$ [18, 2]. The birefringence fluctuation across these segments is modeled using a

random number generator that uses a Gaussian distribution with zero mean and standard deviation. The probability density function is given as

$$f(x,\sigma) = \frac{1}{\sigma\sqrt{2\pi}} \exp\left[-x^2/\left(2\sigma^2\right)\right]. \tag{2.11}$$

We numerically simulate the birefringence in a polarization maintaining fiber of length 500 meter. The standard deviation for the zero mean Gaussian distribution is $\sigma\beta = 100$ radians/meter. The result of numerical simulation is shown in Figure 2.4.

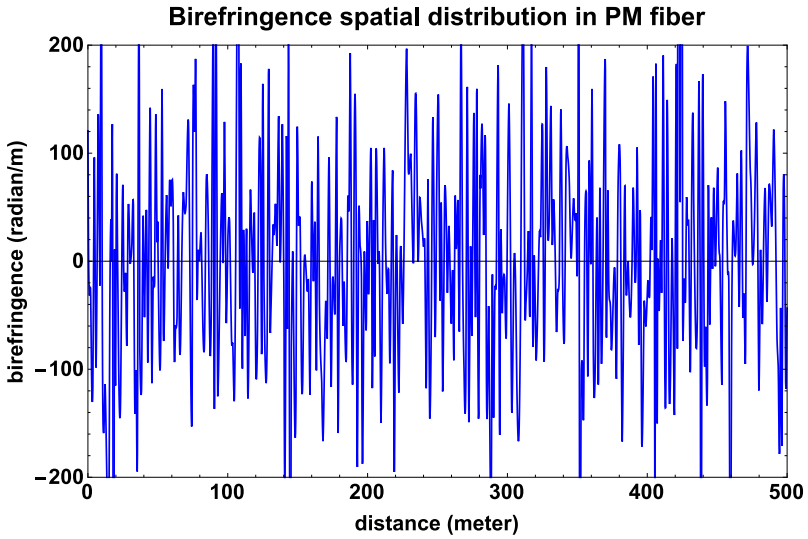

Figure 2.4: Numerically simulated birefringence in a polarization maintaining fiber with a zero mean Gaussian distribution and $\sigma\beta = 100$ radian/m [2].

The numerical simulation is done using Mathematica and the function for generating the noise profile in polarization maintaining fiber is given in the Figure 2.5.

2.5.2 Single Mode Fiber

Single-mode fibers are waveguides with only one propagation mode for each polarization; they are also called telecommunication fibers. Single-mode fibers with circular core have small $\Delta n \approx 10^{-7}$ and beat length of ≈ 10m.

We model the refractive index fluctuation in single-mode optical fiber of length L by representing it as concatenated, homogeneous segments of length ΔL with constant

```
We characterize our system by
ΔL = 0.3 and Δϕ = 100. This is sufficient to build our profile with Length L

BuildProfile[ΔL_, Δϕ_, L_] := Block[{x, ref, profile},
   x = 0;
   profile = {};
   While[x < L,
    AppendTo[profile, {x, RandomReal[NormalDistribution[0.0, Δϕ]]}];
    x += RandomReal[NormalDistribution[1, ΔL]];
   ];
   AppendTo[profile, {L, RandomReal[NormalDistribution[0.0, Δϕ]]}];
   Return[Interpolation[profile]];
  ];
```

Figure 2.5: Mathematica function for simulating the birefringence in a polarization maintaining fiber. L is the length of fiber, ΔL is segment size and $\Delta\phi$ is the standard deviation for the Gaussian distribution.

birefringence $\Delta\beta = \frac{\omega(n_s - n_f)}{c}$ [18, 2]. The birefringence fluctuation across these segments is modeled by generating a set of values according to the Rayleigh distribution, whose probability density function is given as

$$f(x, \sigma) = \frac{x}{\sigma^2} e^{-x^2/(2\sigma^2)}, \; x \geq 0 \tag{2.12}$$

where $\sigma \geq 0$, is the scale parameter of the distribution, and x is the distance along the fiber [17, 2]. A noise profile of the fiber is extrapolated from these phase error values. Here we assume that the fiber only exhibits linear index fluctuation as the radial dimension of the fiber is very small.

Our model of noise closely represents the experimentally measured spatial distribution of birefringence in a single-mode fiber [2]. It represents the birefringence in different types of fibers: standard step-index and dispersion shifted fibers. In general, axially varying birefringent dephasing in an optical fiber of length L can be represented by a series of concatenated, homogeneous segments of length ΔL with constant Δn, as illustrated in Figure 2.6. The birefringence across these segments follows a Rayleigh distribution [17]. Here we assume that the fiber only exhibits linear birefrengence.

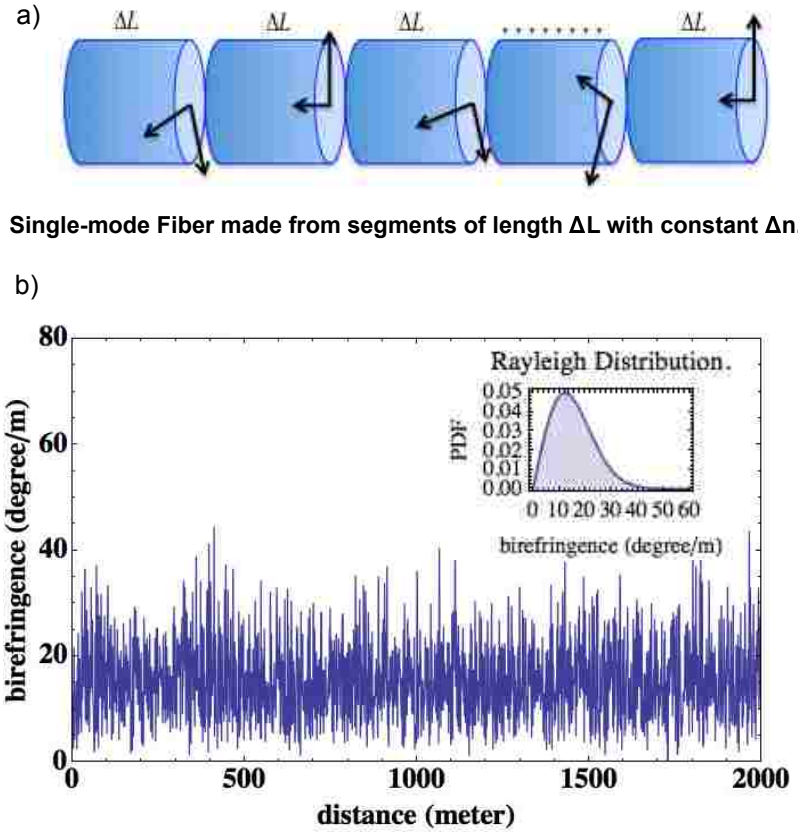

Figure 2.6: Model of a single-mode optical fiber. a) The fiber is modeled as concatenated segments of fiber of length ΔL with constant birefringence Δn. b) Numerically reproduced birefringence in a single-mode fiber, where the scale parameter for Rayleigh distribution is $\sigma\beta = 12.6$ degree/m [2].

The numerical simulation is done using Mathematica and the function for generating the noise profile in a single-mode fiber is given in the Figure 2.7.

2.5.3 Multimode Fiber

We simulate special type of multimode fiber that preserves the orbital angular momen -tum modes for the photon. The fiber of length L is again modeled as before by representing it as concatenated, homogeneous segments of length ΔL with constant fluctuation of refractive index $\Delta\beta = \frac{\omega(n_l - n_{-l})}{c}$. The result of numerical simulation is shown in Figure 2.8.

```
(*** Rayleigh Noise Profile Function ***)
RayleighNoiseProfile[L_, ΔL_, σβ_] := Block[{x, ref, profile},
   x = 0;
   profile = {};
   While[x < L,
    AppendTo[profile, {x, RandomReal[RayleighDistribution[σβ]]}];
    x += ΔL;
    (*x+=RandomReal[NormalDistribution[1,ΔL]];*)
   ];
   AppendTo[profile, {L, RandomReal[RayleighDistribution[σβ]]}];
   Return[Interpolation[profile]];
  ];
```

Figure 2.7: Mathematica function for simulating the birefringence in a single-mode fiber. L is the length of fiber, ΔL is segment size and $\sigma\beta$ is the standard deviation for the Gaussian distribution.

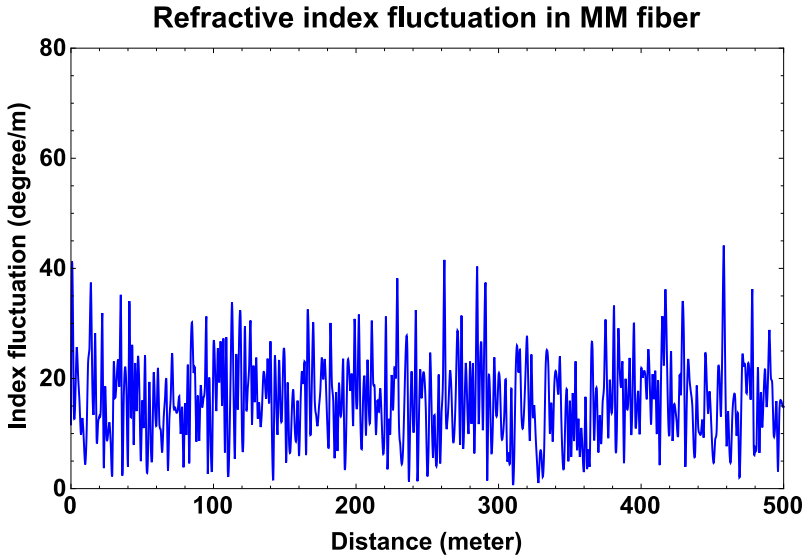

Figure 2.8: Numerically simulated index fluctuation in a multi-mode fiber, where the scale parameter for Rayleigh distribution is $\sigma\beta = 12.6$ degree/m [2].

2.6 Summary

To summarize, we discussed in short the propagation of plane wave in a circular wave guide using Maxwell's equations. From the derivation we uncovered the properties of a polarization maintaining fiber, single-mode fiber and multi-mode fiber. We later talked about the different sources of index fluctuation in optical fiber and how they can be

numerically modeled. Specifically we numerically simulated the model of polarization maintaining fiber, single-mode fiber, and multi-mode fiber. We will use this noise model to simulate the decoherence of qubit and qudit photons in optical fiber in the forthcoming chapters.

Chapter 3
Decoherence and Dynamical Decoupling

3.1 Introduction

A realistic quantum system is never isolated, instead it is always immersed in surrounding environment, where it continuously interacts with the environment. The system can be in a superposition of internal states but the interaction of the system with the uncontrollable degree of freedom of the environment results in the formation of quantum correlation between the internal system states and environment. This causes the system to lose the phase relationship between preferred states, selected by the environment. The linear superposition of states is destroyed and the density matrix of the system transits from a pure to a mixed state.

In the literature several strategies have been developed to minimize decoherence, where notable ones are quantum error-correction (QECC) and decoherence-free subspace (DFS) [19, 20, 21, 22]. The two techniques rely on careful encoding of the quantum state with the redundant ancilla into a bigger Hilbert space. The drawback of this strategy is that it requires large amount of resources for encoding, decoding, measurement and error correction. Alternative approaches have been developed which avoid using ancilla space and encoding and decoding and can be divided in two main categories: closed-loop techniques and open-loop control as shown in Figure 3.1. In closed-loop control technique, appropriate measurements are made on the system and based on the results of the measurement system dynamics are corrected in real time. In open-loop system no such measurements are done on the system; instead an external suitably tailored, time-dependent pulse is applied to the system. The control pulses are designed such that any undesired effect of environment such as decoherence can be eliminated if the pulses are applied faster than the correlation time of the environment.

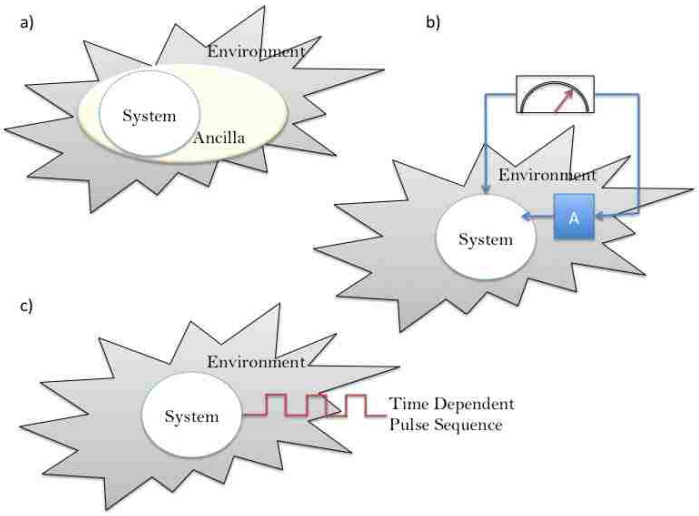

Figure 3.1: Three strategies to minimize decoherence. a) System encoded with ancilla immersed in environment. b) Closed-loop technique where measurement is done on the system and in real time a corrective action is applied to the system. c) Open-loop control, where a tailored time dependent pulse is applied to system.

The input state with encoded information can usually be prepared with high accuracy in a laboratory. Maintaining that state along the optical communication channel, however, is much more demanding due to the presence of refractive index fluctuation. One technique to preserve the coherence of polarization qubit against the detrimental effects of noise encountered in the communication channel is *open-loop* control, where the system is subjected to external, suitably tailored, space-dependent pulses which do not require measurement. This control technique minimizes the undesired interaction of system with the environment if the control pulses are applied faster than the correlation length of environment and is called *dynamical decoupling* (DD) [23, 24, 25]. The advantage of DD is that it requires modest resources and no additional resource for information encoding, error correction, measurement, or feedback. The physical idea behind this scheme comes from the refocusing technique of nuclear magnetic resonance (NMR), where time dependent, rapid, and strong pulses known as bang-bang controls are applied to the system to suppress decoherence [26].

3.2 Dynamical Decoupling

Dynamical Decoupling (DD) is an open-loop control technique to decouple the system from environmental interaction. One important aspect of this technique is that one can effectively control the dynamical evolution of the system while still eliminating the effects of environment. Even though the environment makes it impossible to achieve an arbitrary unitary evolution of the system, an effective dynamical evolution of the system can still be constructed with this technique.

This technique is inspired by the nuclear magnetic resonance technique where tailored time dependent perturbations are used to control the system evolution. In DD, we apply a sequence of pulses to the system, which is faster than the shortest time scale accessible to the reservoir degree of freedom, such that system-bath coupling is averaged to zero during the evolution. This procedure is conceptually different from NMR, because any decoupling action is only applied to system variable.

To apply the formalism of DD, we consider a system S coupled to a bath B, which together form a closed system defined by Hilbert space $\mathcal{H} = \mathcal{H}_S \otimes \mathcal{H}_B$, where $\mathcal{H}_S$ and $\mathcal{H}_B$ denotes the system and bath Hilbert spaces respectively. The overall Hamiltonian is rewritten in an explicit form as

$$H_0 = H_S \otimes \mathbb{I}_B + \mathbb{I}_S \otimes H_B + H_I \tag{3.1}$$

where $\mathbb{I}$ is the identity operator and H_I is the interaction Hamiltonian. The bath operator couples the polarization qubit to the noise bath and causes decoherence. To decouple the system from the environment, we introduce time-dependent perturbing Hamiltonian which rotates the qubit around a given axis on the Bloch sphere [24, 27]. The Hamiltonian with added decoupling perturbation is given as

$$H(t) = H_0 + H_1(t) \otimes \mathbb{I}_B. \tag{3.2}$$

The initial state over $\mathcal{H}$ is represented by the density matrix $\rho_{\text{tot}}(0) = \rho_S(0) \otimes \rho_B(0)$, and the state after the coarse-grained dynamics results in open-system evolution defined by $\rho_S(0) \to \rho_S(t) = \text{Tr}_B\{\rho_{\text{tot}}(t)\}$, where Tr_B denotes the partial trace over H_B. In the case of the polarization qubit in an optical fiber we assume that the relaxation dynamics for $\rho_S(t)$ involves only the decoherence mechanisms represented by coupling operators. The irreversible loss of quantum coherence is caused by presence of exponential decay in the off diagonal term of the output density matrix.

The decoupling field is made to be cyclic and the decoupling operator $U_1(t)$ that is periodic over some cycle time $T_c > 0$ is given as

$$U_1(t) \equiv T \ \exp\left\{-i \int_0^t dt^{'} H_1(t^{'})\right\} = U_1(t + T_c) \tag{3.3}$$

In the interaction picture, the state after the perturbation due to $H_I(t)$ is defined by $\rho_{\text{tot}}(t) = U_1(t)\tilde{\rho}_{tot}(t)U_1^{\dagger}(t)$ and the evolution is defined by a time-varying Hamiltonian,

$$\tilde{H}(t) = U_1^{\dagger}(t)H_0U_1(t). \tag{3.4}$$

The decoupling pulse sequence representing the control field is chosen in such a way that $U_1(T_c) = \mathbb{I}_S$ and the integral term $\int_0^t dt H_I(t)$ averages to zero, as a consequence decoherence is minimized.

3.3 DD Pulse Sequence

3.3.1 Carr-Purcell-Meiboom-Gill

To preserve the polarization qubit from decoherence, a series of stroboscopic control pulses are applied to the system repeatedly with cycles of period T_c. Over that period, the time average interaction is described by an effective Hamiltoninan and the goal of DD is to effectively reverse this interaction. This method of applying pulse sequence was first pioneered by Hahn in his spin-echo experiment, where he applied π-pulse to the spin system

after it was allowed to evolve for a period of τ in the magnetic field. This pulse effectively changes the sign of system-environment interaction and echo is seen after the refocusing or reverse evolution period of same duration τ. If the magnetic field is static then the interaction is completely reversed and initial state is recovered. However, if magnetic field is fluctuating then its effect can not be completely reversed and echo amplitude decays as a function of the refocusing time. The decay contains information about the time-dependence of the environment.

To reduce the decay rate of the echo caused by the time dependent environment, Carr and Purcell (CP) introduced a variant of Hahn-echo pulse sequence, where the single π-pulse is replaced by a series of π-pulse separated by intervals of duration τ. This CP sequence reduces the effect of time varying environment if the pulse intervals are shorter than correlation time of the environment. However, the pulse error tend to accumulate as number of pulses applied to the system increases. This destroys the state of the system instead of preserving it against the effect of the environment.

Meiboom and Gill (MG) noticed this and proposed a modification to CP sequence for compensating pulse errors and it is called CPMG sequence. This pulse sequence is composed of two π-pulse, in which the system is allowed to free evolve for a period of τ, then first π-pulse is applied, again system is allowed to free evolve for a period of 2τ, second π-pulse is applied and system is allowed to free evolve for a period of τ.

For minimizing decoherence of polarization qubit in optical fiber, we select the simplest CPMG pulse sequence which is made up of two π-pulse separated as shown in Figure 3.2. This sequence is implemented in optical fiber using half wave-plate and it achieves a fidelity of 99% in preserving the state of the qubit.

3.3.2 Knill Dynamical Decoupling

The goal of DD is to time reverse the system-bath interaction by applying series of stroboscopic pulses in cycles of period T_c. If the pulse is instantaneous and perfect, then the dynamics of the system is completely time reversed, and the initial state of the system

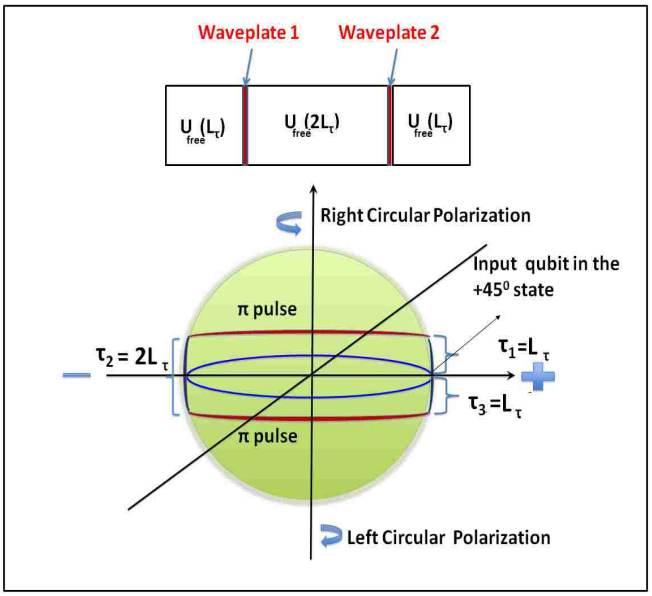

Figure 3.2: Top: CPMG sequence implemented with half-wave plates in the diagonal basis along the fiber; U_{free}'s are the propagators corresponding to the free propagations through the dephasing segments. Bottom : Free propagations and π rotations caused by the waveplates for the input qubit in the $+45°$ state are shown on the Bloch sphere.

is recovered. However, if the pulses are finite and have errors, then the system dynamics cannot be completely reversed, and these errors accumulate, and the initial state is lost. In reality, the pulses have finite length and errors and if the number of applied pulses are large and the design of the pulse sequence does not incorporate error compensation, then these errors accumulate and lead to decoherence of the system more severe than due to system environment interaction.

One type of non-ideal pulse has finite length, which imposes limits on the achievable cycle time for the sequence. The constraint on cycle time imposes an upper bound on the maximum achievable DD performance. Another type of non-ideal pulse, which can be more detrimental, is due to rotation error, which is caused by deviation in the control pulse strength. The rotation error can be attributed to rotations about a non ideal axis or deviation in rotation angle.

Several approaches have been proposed [28, 29] to make DD insensitive to pulse imperfec -tions and one of the approaches focuses on the design of pulses which are inherently robust or insensitive to imperfect rotation. Rotation about an axis can be achieved either by one single pulse about a given axis or by using a sequence of pulses which are inherently robust against classes of imperfections and generate a rotation close to ideal rotation even in the presence of these errors. In NMR literature, such pulse sequences are called composite pulses [30].

If DD sequence are made up of only π-rotations, then replacing the π-rotation with a composite sequence which can achieve a near-ideal rotation in case of imperfection should improve DD performance. KDD sequence uses this design principle and is given as

$$\begin{aligned} KDD_{\phi} =& f_{\tau/2} - (\pi)_{\pi/6+\phi} - f_{\tau} - (\pi)_{\phi} - f_{\tau} - (\pi)_{\pi/2+\phi} \\ & - f_{\tau} - (\pi)_{\phi} - f_{\tau} - (\pi)_{\pi/6+\phi} - f_{\tau/2}, \end{aligned} \tag{3.5}$$

where the notation $f_{\tau/2}$ represents free evolution for a period of $\tau/2$ and $(\pi)_{\pi/6+\phi}$ is π rotation about an axis $\pi/6+\phi$. It is a 20-pulse, self correcting sequence that is created by combining 5-pulse blocks shifted in phase by $\pi/2$ to form $[KDD_{\phi} - KDD_{\phi+\pi/2} - KDD_{\phi+\pi} - KDD_{\phi+3\pi/2}]$ [3].

We preserve the polarization qubit in a single-mode fiber from birefringent dephasing by implementing the KDD pulse sequence in space by introducing half-wave plate at specified distances in the fiber as shown in Fig. 3.3.

The impact of pulse imperfections on fidelity in the absence of environment have been analyzed previously and it was found that the KDD sequence is least susceptible to pulse imperfections when compared with other sequences [3].

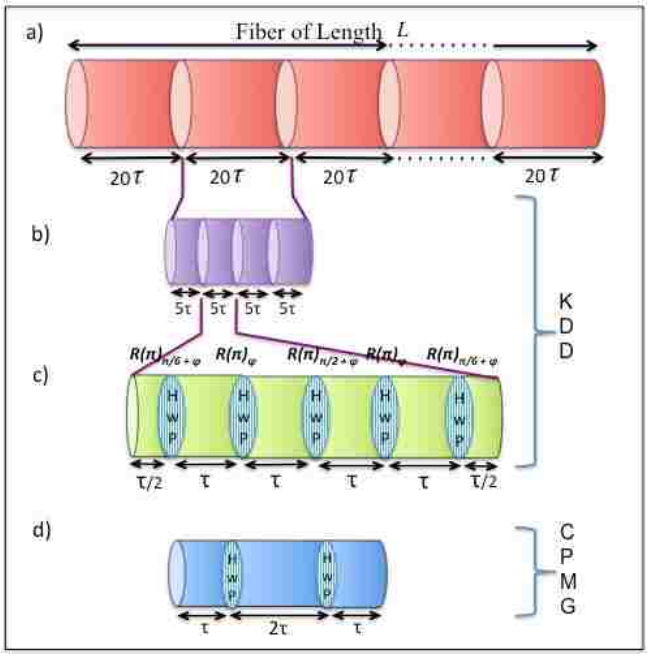

Figure 3.3: A 20 pulse sequence created by combining 5-pulse block shifted in phase by $\pi/2$. The cyclic repetition of these 20 pulse sequence is referred to as KDD [3]. a) Single-mode fiber of length L divided in to blocks of length 20 τ. b) each block is then divided in four parts of length 5 τ. c) In each part a KDD block is implemented by introducing 5 half-wave plate at specified distances. d) CPMG pulse implemented using half-wave plate.

3.4 Summary

To summarize, we discussed different strategy available to minimize decoherence. In particular, we reviewed dynamical decoupling and talked about ideal and non-ideal pulse sequence.

Chapter 4
Decoherence of qubit and qudit states in Fiber

4.1 Introduction

The storage of quantum states and its distribution over long distances is essential for emerging quantum technologies such as quantum networks and long distance quantum cryptography. Quantum networks and quantum cryptographic systems [31, 32] use photonic qubits as information carriers because of their quantum nature and low-loss coefficient pertaining to transmission, both in optical fiber [33] and in free space [34]. Nevertheless, the losses become significant when we envision transmission over hundreds of kilometers or more and is accompanied by decoherence. In classical telecommunication the issue of signal loss is overcome by use of amplifiers (also called repeaters) that amplify the signals. Unfortunately this option of signal amplification is forbidden in quantum communication because of the no-cloning theorem [35, 36] unless one restricts oneself to an orthogonal set of states; in fact a quantum protocol such as quantum key distribution arises precisely due to existence of non-orthogonal states.

The problem of signal amplification in quantum communication can be overcome with the use of sophisticated entanglement-based scheme known as a quantum repeater [37]. Entanglement has a special property that it can be swapped. Given a entangled state between A and B and another between C and D, it is possible to create entanglement between A and D by performing a joint measurement in the basis of entangled states, followed by classical communication of the result to the location A and/or D. The states at A and D need to be preserved in a quantum memory for the period of time in which the classical result are communicated for the teleportation protocol to be successful [38]. Current schemes [39, 40, 37] suggest use of atomic states to preserve the state of qubit, but

it would be beneficial if the qubit state can be preserved in an all optical quantum memory so that all optical implementation of quantum repeater device is feasible [41].

Another issue faced by any quantum repeater scheme[37, 39, 42] is decoherence of the qubit (or qdit) caused by the interaction of a photon qubit with the environment, such as in the case of single-mode and multi-mode fiber. Typically, the information is encode in one or multiple degrees of freedom of photon. The interaction of the photons with the noisy environment of an optical fiber makes secure, long-distance communication difficult because the refractive index fluctuation in fiber randomizes the phase of the photon, leading to a loss of coherence and subsequently loss of information. This effect is called decoherence and it limits the distance over which quantum information can be stored and transmitted and it is one of the obstacle in physical realization of any quantum repeater scheme that uses optical communication of qubit state. The input state with encoded information can usually be prepared with high accuracy in a laboratory. Maintaining that state along the communication channel, however, is much more demanding due to the presence of refractive index fluctuation.

In this chapter we derive the analytic model for decoherence of polarization qubit and OAM qudit in optical fiber.

4.2 Polarization Qubit in Single Mode Fiber

Decoherence of the polarization qubit has its origin in optical birefringence of the fiber. A telecommunication fiber is often called a single-mode fiber, although it supports two orthogonal polarization modes due to its circular symmetry. In a perfect fiber, these two modes have the same phase velocity, but real fibers have some asymmetry due to manufacturing imperfections or stress on the fiber due to deployment in the field. The asymmetry in the fiber breaks the degeneracy of two orthogonal modes, which results in birefringence: a difference in phase velocity of the two modes.

Birefringence in an optical fiber can result from both intrinsic and extrinsic perturbations. Intrinsic perturbation can originate during the manufacturing process and is permanent.

Form (geometric) birefringence can arise due to non-circular waveguides and stress birefringence is due to forces set up by asymmetry of the core. Extrinsic perturbation can be caused by spooling the fiber or embedding the fiber in the ground, lateral stress, bending, or twisting. These perturbations create linear birefringence and can change as the fiber's external environment changes [14, 15].

For a short section of fiber, birefringence can be considered to be uniform. The difference between the propagation constant of slow and fast modes can be expressed as

$$\Delta\beta = \frac{\omega n_s}{c} - \frac{\omega n_f}{c} = \frac{\omega \Delta n}{c} \tag{4.1}$$

where ω is the angular frequency, c is the speed of light, and $\Delta n = n_s - n_f$ is the differential effective refractive index between slow (s) and fast (f) modes [13].

When a linearly polarized wave (such as 45^0) polarization is launched into the fiber, the asymmetry in the fiber causes a phase shift between the two orthogonal modes. This occurs because these two modes travel with different phase velocities and acquire a relative phase shift that is a function of propagation length in the birefringent fiber. As a consequence, the state of polarization (SOP) evolves in a cyclic fashion as the light propagates down the fiber (i.e., from linear to elliptical to circular and back through elliptical to linear state that is orthogonal to the initial state). The output mode will not be stable as environmental factors such as stress and ambient temperature changes will change the birefringent properties of fiber. This complicates the utilization of single-mode fiber in applications such as quantum cryptography and quantum communication where polarization modes need to be preserved.

4.2.1 Analytic Model of Decoherence

Let us consider the following pure input state that is in superposition of horizontal and vertical polarization:

$$|\psi\rangle = \alpha|H\rangle + \beta|V\rangle, \tag{4.2}$$

where α and β are complex numbers such that $\alpha^2 + \beta^2 = 1$. For the above input state the density matrix is given by

$$\hat{\rho}_{\text{in}} = |\psi\rangle\langle\psi| = \begin{pmatrix} |\alpha|^2 & \alpha\beta^* \\ \alpha^*\beta & |\beta|^2 \end{pmatrix}. \tag{4.3}$$

When the photon travels through the j^{th} segment, the rotation operator $\mathbb{M}_z(\delta\phi_j)$ given by

$$\begin{aligned} \mathbb{M}_z(\delta\phi_j) &= \begin{pmatrix} \mathrm{e}^{i\frac{\delta\phi_j}{2}} & 0 \\ 0 & \mathrm{e}^{-i\frac{\delta\phi_j}{2}} \end{pmatrix} \\ &= \cos\left(\frac{\delta\phi_j}{2}\right)\mathbb{I} + i\sin\left(\frac{\delta\phi_j}{2}\right)\sigma_z \\ &= \mathrm{e}^{i\frac{\delta\phi_j}{2}\sigma_z} \\ &= \mathbb{R}_z(\delta\phi_j) \end{aligned} \tag{4.4}$$

where $\delta\phi_j = \Delta\beta_j\Delta L$ is the phase angle acquired due to propagation through the j^{th} segment of fiber. The rotation operator acts on the photon and rotates the polarization degrees of freedom. The output density matrix is given by

$$\begin{aligned} \hat{\rho}_{j_{\text{out}}} &= \mathbb{M}_z(\delta\phi_j)\rho_{in}\mathbb{M}_z(\delta\phi_j)^\dagger \\ &= \begin{pmatrix} |\alpha|^2 & \alpha\beta^*\mathrm{e}^{i\delta\phi_j} \\ \alpha^*\beta\mathrm{e}^{-i\delta\phi_j} & |\beta|^2 \end{pmatrix}. \end{aligned} \tag{4.5}$$

After passing through the fiber with n homogeneous concatenated segments the output density matrix is

$$\hat{\rho}_{\text{out}} = \begin{pmatrix} |\alpha|^2 & \alpha\beta^* \prod_{j=1}^{n} \mathrm{e}^{i\delta\phi_j} \\ \alpha^*\beta \prod_{j=1}^{n} \mathrm{e}^{-i\delta\phi_j} & |\beta|^2 \end{pmatrix}. \tag{4.6}$$

We model the set of acquired phases $\{\delta\phi_1, \delta\phi_2, ..., \delta\phi_n\}$ as random variable $\hat{\phi}$ with a mean $\left\langle \hat{\phi} \right\rangle = \phi$ and a nonzero variance $\left\langle \Delta\hat{\phi}^2 \right\rangle = \Delta\phi^2$. Here ϕ is proportional to n but $\Delta\phi^2$ is independent of n.

$$\begin{aligned} \prod_{j=1}^{n} \mathrm{e}^{\pm i\delta\phi_i} &= \exp\left[\sum_{j=1}^{n} (\pm i\delta\phi_i)\right] \\ &= \exp\left[\pm i\left\langle \hat{\phi} \right\rangle \pm i\Delta\hat{\phi}\right] \\ &= \exp\left[\pm i\left\langle \hat{\phi} \right\rangle\right] \exp\left[\pm i\Delta\hat{\phi}\right]. \end{aligned} \tag{4.7}$$

We Taylor expand the factor $\exp\left[\pm i\Delta\hat{\phi}\right]$ of Eq.4.7 and take the average to obtain

$$\begin{aligned} \left\langle \exp\left[\pm i\Delta\hat{\phi}\right] \right\rangle &= \left\langle 1 \pm i\Delta\hat{\phi} - \frac{1}{2}\Delta\hat{\phi}^2 + \cdots \right\rangle \\ &= 1 \pm i\left\langle \Delta\hat{\phi} \right\rangle - \frac{1}{2}\left\langle \Delta\hat{\phi}^2 \right\rangle + \cdots \end{aligned} \tag{4.8}$$

Since the mean of variance is zero in Eq.4.8 and average of the variance is $\left\langle \Delta\hat{\phi}^2 \right\rangle = \Delta\phi^2$, hence we obtain the expression

$$\left\langle \exp\left[\pm i\Delta\hat{\phi}\right] \right\rangle = 1 - \frac{1}{2}\Delta\phi^2 + \cdots \qquad \approx \mathrm{e}^{-\frac{1}{2}\Delta\phi^2}. \tag{4.9}$$

Using Eq.4.9, we can write Eq.4.7 as

$$\left\langle \prod_{j=1}^{n} \mathrm{e}^{\pm i\delta\phi_i} \right\rangle = \left\langle \exp\left[\pm i\left\langle \hat{\phi} \right\rangle\right] \right\rangle \left\langle \exp\left[\pm i\Delta\hat{\phi}\right] \right\rangle$$
$$= \mathrm{e}^{\pm i\phi}\mathrm{e}^{-\frac{1}{2}\Delta\phi^2}. \tag{4.10}$$

Using the expression in Eq.4.10, the density matrix in Eq.4.6 can be rewritten as

$$\hat{\rho}_{\mathrm{out}} = \begin{pmatrix} |\alpha|^2 & \alpha\beta^*\mathrm{e}^{i\phi}\mathrm{e}^{-\frac{1}{2}\Delta\phi^2} \\ \alpha^*\beta\mathrm{e}^{-i\phi}\mathrm{e}^{-\frac{1}{2}\Delta\phi^2} & |\beta|^2 \end{pmatrix}. \tag{4.11}$$

The state represented by $\hat{\rho}_{\mathrm{out}}$ is no longer pure due to presence of $\mathrm{e}^{-\frac{1}{2}n^2\Delta\phi^2}$ in the off-diagonal terms [43].

4.3 Orbital Angular Momentum State in Fiber

For the past few years the quantum information community has been putting a great deal of effort into boosting the bit rate for photonic quantum state transmission by encoding more than one bit per photon. This is done by exploiting multiple temporal, spatial, polarization, and frequency modes of the single photon and then preparing a single photon in a superposition of those modes as a qudit. The number of bits then is $\log_2 d$, where d is the dimension of the qudit. The focus has been on using orbital angular momentum (OAM) modes of the photon, particularly in multimode optical fiber, as a road to high bit rate.

Photons that are OAM eigenstates, originate as a consequence of spatial distribution of optical field intensity and phase [44, 45]. The photon carries an azimuthal phase term $\exp(il\theta)$ and l units orbital angular momentum [46]. Such phase dependence is characteristic of either Laguerre-Gaussian or Bessel modes and each of these mode families provides a higher dimensional state space. The most immediate advantage of a large state space is the large alphabet size for quantum communication and hence considerable increase in data capacity. Higher dimensional systems have been known to improve security in quantum

cryptography [47] and are required by some quantum network protocols [48] and quantum computation schemes [49] to efficiently solve problems like Byzantine agreement problem [50] and quantum coin tossing [51].

There are several protocols that encode quantum information in the two-dimensional Hilbert space of the photon's spin and exploit the polarization or time-bin degrees of freedom [31, 52]. Physical implementations of one such protocol for quantum key distribution has shown that such a encoding is not optimal for practical applications due to a low bit rate [53]. Information encoding based on the two-dimensional Hilbert space of photon polarization (or SAM) imposes a limitation on the rate of optical communication. To overcome such limitations the orbital angular momentum (OAM) of light has been proposed that uses the photon's spatial mode structure and allows use of higher-dimensional Hilbert space, or a "qudit" encoding of a photon [54]. This leads to an increased alphabet size and subsequently, increased rate of communication [55, 56, 57]. Recent experiments have shown that the classical data-carrying capacity of a terabit per second can be achieved using OAM states of light in an optical fiber [58]. The potential of higher dimensional encoding of quantum information to achieve a higher bit rate can only be achieved if the photon can be protected from the decohering effect of optical index of refraction fluctuation in an optical fiber.

Here we derive an analytic model for decoherence caused by the refractive index fluctuation in a multi-mode fiber for an OAM photon state. We show that rate of decoherence is faster for large values of l and it scales exponentially with l^2, where l is azimuthal mode number.

4.3.1 Analytic Model of Decoherence

The transverse spatial wave function of a paraxial beam is an eigenstate of OAM and it can be written in cylindrical coordinates as

$$\varphi_{pl}(r,\theta) = \frac{1}{\sqrt{2\pi}} R_{p,l}(r) \exp\left(i\, l\, \theta\right). \tag{4.12}$$

The functions $R_{p,l}(r)$ are a basis for the radial dependence, such as the Laguerre-Gauss functions. They are defined in free space as

$$R_{p,l}(r) = \frac{A}{w(z)}\left(\frac{\sqrt{2}r}{w(z)}\right)^{|l|} L_p^{|l|}\left(\frac{2r^2}{w(z)^2}\right) \times e^{ikr^2/[2R(z)]}\mathrm{e}^{i(2p+|l|+1)\tan^{-1}(z/z_R)}, \tag{4.13}$$

where $w(z) = w_0\sqrt{1+(z/z_R)^2}$ is the beam width, $R(z) = z[1+(z_R/z)^2]$ is the radius of wave-front curvature, and $z_R = \frac{1}{2}kw_0^2$ is the Rayleigh range. The quantity $\tan^{-1}(z/z_R)$ is known as the Gouy phase. These $R_{p,l}(r)$ functions are modified slightly inside fiber.

Optical fibers have other complex spatial modes but for simplicity, we consider here an OAM photon that is launched in to a multimode optical fiber that is in superposition of l and $-l$ states and has the following ket representation

$$|\psi_{pl}\rangle = \frac{1}{\sqrt{2\pi}}R_{p,l}(r)[\exp(i\,l\,\theta)|p,l\rangle + \exp(-i\,l\,\theta)|p,-l\rangle]. \tag{4.14}$$

For example, such a state could be used as one code letter of a four-letter code for the BB84 protocol [31]. The other letters would be the negative superposition and the individual $\pm l$ states. The density matrix for the above input state can be written as

$$\hat{\rho}_{\mathrm{in}} = |\psi_{pl}\rangle\langle\psi_{pl}| = |R_{p,l}(r)|^2\begin{pmatrix} 1 & \mathrm{e}^{i\,2l\theta} \\ \mathrm{e}^{-i\,2l\theta} & 1 \end{pmatrix}. \tag{4.15}$$

In general, the index of refraction fluctuation in an optical fiber can be represented by a series of concatenated, homogeneous segments of length ΔL with constant index fluctuation $\Delta\beta = \frac{\omega(n_l - n_{-l})}{c}$ [18, 2]. When a photon that is in superposition of $+l$ and $-l$

propagates through the fiber in z direction the E-fields see a slightly different refractive index profile due to the corkscrew nature of the OAM photon. The photon acquires a phase proportional to the azimuthal mode number l, since the number of helix surfaces in a fixed volume of fiber is proportional to the helix step length $\lambda/|l|$. The two independent index of refraction fluctuations interact with the orbital angular momentum degree of freedom of the photon. The noise operator is given by

$$\begin{aligned}\mathbb{M}_z(\delta\phi_j) &= \begin{pmatrix} \mathrm{e}^{i\,l\,\frac{\delta\phi_j}{2}} & 0 \\ 0 & \mathrm{e}^{-i\,l\,\frac{\delta\phi_j}{2}} \end{pmatrix} \\ &= \cos\left(l\,\frac{\delta\phi_j}{2}\right)\mathbb{I} + i\sin\left(l\,\frac{\delta\phi_j}{2}\right)\hat{L}_z \\ &= \mathrm{e}^{i\,l\,\frac{\delta\phi_j}{2}\hat{L}_z} \\ &= \mathbb{R}_z(l\,\delta\phi_j) \end{aligned} \tag{4.16}$$

where $\delta\phi_j = \Delta\beta_j\Delta L$ is the phase angle acquired due to propagation through the j^{th} segment of fiber and $\hat{L}_z = -i\frac{\partial}{\partial\theta}$ is orbital angular momentum operator that generates rotation about z axis. Laguerre-Gaussian beams are eigenfunction of orbital angular momentum operator $\hat{L}_z$. The output density matrix after the interaction in the j^{th} segment is given by

$$\begin{aligned}\hat{\rho}_{j_{\mathrm{out}}} &= \mathbb{M}_z(\delta\phi_j)\hat{\rho}_{in}\mathbb{M}_z(\delta\phi_j)^\dagger \\ &= |R_{p,l}(r)|^2 \begin{pmatrix} 1 & \mathrm{e}^{i\,(2\,l\,\theta + l\,\delta\phi_j)} \\ \mathrm{e}^{-i\,(2\,l\,\theta + l\,\delta\phi_j)} & 1 \end{pmatrix}. \end{aligned} \tag{4.17}$$

Now, if we assume that cross-talk between OAM modes is negligible [58], which is a good approximation for linear interactions, then the above density matrix can be rewritten as:

$$\hat{\rho}_{j_{\mathrm{out}}} = |R_{p,l}(r)|^2 \begin{pmatrix} 1 & \mathrm{e}^{i\,l(2\,\theta + \delta\phi_j)} \\ \mathrm{e}^{-i\,l(2\,\theta + \delta\phi_j)} & 1 \end{pmatrix}. \tag{4.18}$$

After passing through the fiber with n homogeneous concatenated segments the output density matrix is

$$\hat{\rho}_{j_{\text{out}}} = |R_{p,l}(r)|^2 \begin{pmatrix} 1 & \mathrm{e}^{i\,(2\,l\,\theta)} \prod_{j=1}^{n} \mathrm{e}^{i\,(l\,\delta\phi_j)} \\ \mathrm{e}^{-i\,(2\,l\,\theta)} \prod_{j=1}^{n} \mathrm{e}^{-i\,(l\,\delta\phi_j)} & 1 \end{pmatrix}. \tag{4.19}$$

We model the sum of acquired phases $\{\delta\phi_1, \delta\phi_2, ..., \delta\phi_n\}$ as random variable $\hat{\phi}$ with a mean $\left\langle \hat{\phi} \right\rangle = \phi_0$ and a nonzero variance $\left\langle \Delta\hat{\phi}^2 \right\rangle = \Delta\phi^2$. Here ϕ_0 is proportional to n but $\Delta\phi^2$ is independent of n. The factor $\prod_{j=1}^{n} \mathrm{e}^{\pm i\,l\,\delta\phi_i}$ in the off-diagonal term of Eq.4.19 can be expressed in terms of mean and variance of random variable $\hat{\phi}$

$$\begin{aligned} \prod_{j=1}^{n} \mathrm{e}^{\pm i\,l\,\delta\phi_i} &= \exp\left[\sum_{j=1}^{n} (\pm i\,l\,\delta\phi_i)\right] \\ &= \exp\left[\left(\pm i\,l\left\langle \hat{\phi} \right\rangle \pm i\,l\,\Delta\hat{\phi}\right)\right] \\ &= \exp\left[\pm i\,l\left\langle \hat{\phi} \right\rangle\right] \exp\left[\pm i\,l\,\Delta\hat{\phi}\right]. \end{aligned} \tag{4.20}$$

We then Taylor expand the factor $\exp\left[\pm i\,l\,\Delta\hat{\phi}\right]$ of Eq.4.20 and take the time average to obtain

$$\begin{aligned} \left\langle \exp\left[\pm i\,l\,\Delta\hat{\phi}\right] \right\rangle &= \left\langle 1 \pm i\,l\,\Delta\hat{\phi} - \frac{1}{2} l^2\,\Delta\hat{\phi}^2 + \cdots \right\rangle \\ &= 1 \pm i\,l\left\langle \Delta\hat{\phi} \right\rangle - \frac{1}{2} l^2 \left\langle \Delta\hat{\phi}^2 \right\rangle + \cdots \end{aligned} \tag{4.21}$$

Since the mean of variance is zero in Eq.4.21, and average of the variance is $\left\langle \Delta\hat{\phi}^2 \right\rangle = \Delta\phi^2$, hence we obtain the expression [18, 43]

$$\left\langle \exp\left[\pm i\,l\,\Delta\hat{\phi}\right] \right\rangle = 1 - \frac{1}{2} l^2\,\Delta\phi^2 + \cdots \qquad \approx \mathrm{e}^{-\frac{1}{2} l^2\,\Delta\phi^2}. \tag{4.22}$$

The condition that $l\,\Delta\hat{\phi}$ is small can always be met for small l by shortening the lengths

of the virtual segments. Using Eq.4.22, we can write Eq.4.20 as

$$\left\langle \prod_{j=1}^{n} \mathrm{e}^{\pm i\, l\, \delta\phi_i} \right\rangle = \left\langle \exp\left[\pm i\, l \left\langle \hat{\phi} \right\rangle\right] \right\rangle \left\langle \exp\left[\pm i\, l\, \Delta\hat{\phi}\right] \right\rangle$$
$$= \mathrm{e}^{\pm i\, l\, \phi_0}\, \mathrm{e}^{-\frac{1}{2} l^2\, \Delta\phi^2}. \tag{4.23}$$

And finally, with the expression obtained in Eq.4.23, the output density matrix in Eq.4.19 can be rewritten as

$$\hat{\rho}_{\mathrm{out}} = |R_{p,l}(r)|^2 \begin{pmatrix} 1 & \mathrm{e}^{i\, l\, (2\,\theta + \phi_0)} \mathrm{e}^{-\frac{1}{2} l^2\, \Delta\phi^2} \\ \mathrm{e}^{-i\, l\, (2\,\theta + \phi_0)} \mathrm{e}^{-\frac{1}{2} l^2\, \Delta\phi^2} & 1 \end{pmatrix}. \tag{4.24}$$

The state represented by $\hat{\rho}_{\mathrm{out}}$ is no longer pure due to presence of the dephasing term $\mathrm{e}^{-\frac{1}{2} l^2\, \Delta\phi^2}$ in the off-diagonal terms and the rate of decoherence is much faster for larger values of l.

4.4 Summary

To summarize, we discussed how decoherence of an optical photon in optical fiber impedes the long distance transmission of qubit and qudit state. It takes away the quantum properties of photon by randomizing the phase relationship, the density matrix transitions from pure to mixed state.

Chapter 5
Entanglement Sudden Death in Single Mode fiber

5.1 Introduction

Entanglement is a fundamental resource for existence of key quantum communication technologies such as Quantum Key Distribution (QKD), Quantum dense coding, Quantum teleportation, and Quantum network. It is essential resource for any capacity achieving quantum communication. Perfect quantum communication is equivalent to distribution of perfect entanglement [59]. If we can transport a qubit without decoherence then entanglement shared by qubit will also be distributed perfectly, however the effect of environmental noise inevitably impair our ability to send quantum states over long distance. In the case of photonic qubit, the distribution of entangled pair is done by the use of optical fibers but they are limited by unavoidable transmission losses and entanglement sudden death (ESD) caused by decoherence. This distribution approach is limited to 100km for polarization entangled photon under optimistic assumptions [60, 61, 62, 63, 64]. Classically, a repeater is used to increase the transmission distance by amplifying the signal and sending it over again but that approach is forbidden in quantum theory [36].

An alternative technology called Quantum repeater is used for long distance distribution of entangled state as shown in Figure 5.1. It uses two pairs of entangled state carried over an optical fiber from a spontaneous parametric down-conversion (SPDC) source and then it does a entanglement swapping by doing a Bell measurement [37, 65, 38]. The SPDC and the Bell measurement are probabilistic in nature and optical fibers are prone to losses, combining the three sources of error the overall rate for error-free distribution of entanglement will decrease as the number of repeaters between the two distribution point is increased. Also, as the number of repeaters are increased the network complexity increases

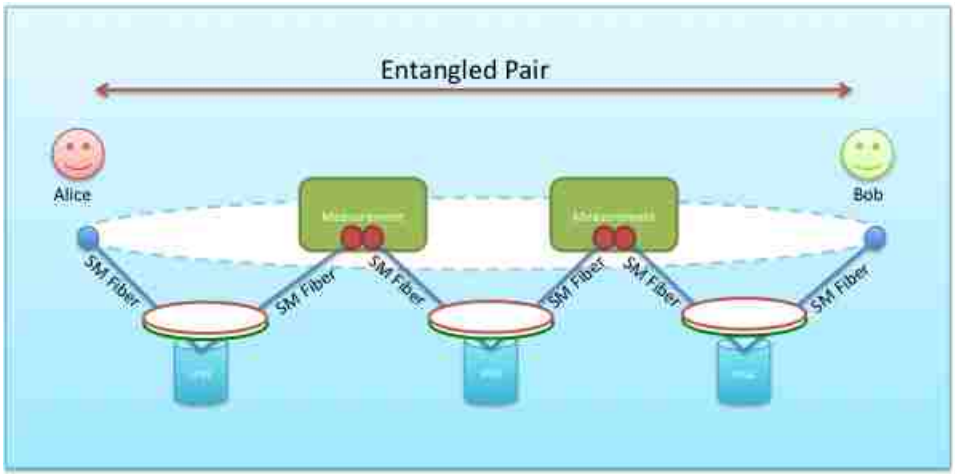

Figure 5.1: Quantum repeater that uses entangled photons and entanglement swapping technique to increase the effective communication distance, where photons are carried over the optical fiber to the Bell measurement site.

and hence associated losses also increase. This brings us back to the original question of error free and efficient distribution of entangled state.

It is very important to devise techniques that minimizes the loss of entanglement caused by decoherence of photon in optical fiber so that the length over which the entangled photon pair can be efficiently distributed is increased without increasing the number of repeaters between the two points. In this chapter, I analytically show that fluctuation in refractive index of optical fiber causes decoherence and subsequently loss of entanglement.

5.2 Entanglement

Historically entanglement has played a crucial role in the development of quantum physics. Initially it was thought to be a qualitative feature distinguishing quantum theory from classical theory but latter its characterization by Bell's inequality made this distinction quantitative and its non-local feature available for experimental verification. It is a kind of correlation that can not be generated classically.

We can also define quantum correlation operationally in context of quantum information. If we find a correlation in a quantum system that can not be simulated classically, then we usually attribute them as quantum effect and label them as quantum correlation.

We give a brief introduction to the concept of entangled states in the subsequent sections and later describe a measure called concurrence to quantify entanglement.

5.2.1 Multipartite Entanglement

A quantum system composed of N physically distinct subsystem is called multipartite quantum system. The Hilbert space $\mathcal{H}_S$ associated with the multipartite system is given by the tensor product on N individual Hilbert spaces of subsystems: $\mathcal{H}_S = \mathcal{H}_1 \otimes \cdots \otimes \mathcal{H}_N$, where $\mathcal{H}_i$ for $1 \leq i \leq N$ represents the Hilbert space associated with i-th subsystemt [66, 67, 68]. Due to vector nature of total Hilbert space $\mathcal{H}_S$, not all states necessarily may be written as the product of some other states. In other words, a pure quantum state $|\psi\rangle$, that can be written as

$$|\psi\rangle = \sum_{j_1 \cdots j_N} c_{j_1 \cdots j_N} |j_1\rangle \otimes \cdots \otimes |j_N\rangle, \tag{5.1}$$

where $\{|j_i\rangle\}$ is the basis for the i-th subsystem, and $c_{j_1 \cdots j_N}$ are normalized complex coefficients. In general a quantum state on $\mathcal{H}_S$ can not be written as equation (5.1), that is product of the individual state of subsystem. In other words, it is not possible to attribute a state vector to individual system to represent the state of the complete system and this is precisely the phenomenon of entanglement [66, 67, 68].

Definition 1 (***Separable pure state***) *A pure state $|\psi\rangle \in \mathcal{H}_S$ is separable if it is a product state. That is, if it can be written as*

$$|\psi\rangle = |\psi_1\rangle \otimes \cdots \otimes |\psi_N\rangle, \tag{5.2}$$

for some $|\psi_1\rangle \in \mathcal{H}_S, \cdots$ and $|\psi_N\rangle \in \mathcal{H}_N$.

Definition 2 (***Entangled pure state***) *A pure state $|\psi\rangle \in \mathcal{H}_S$ is entangled if it is not separable.*

In realistic scenario, mixed states are more abundant in nature because decoherence and other imperfect quantum operations leads to loss of information about the state of

the system. The state is represented by a trace-1 normalized density matrix ρ, that is an element of the space $\mathcal{D}(\mathcal{H}_S)$ of positive semidefinite operators acting on a Hilbert space $\mathcal{H}_S$ The definition of entanglement for mixed state is more subtle and it is given by [69]:

Definition 3 (***Separable state***) *A state $\rho \in \mathcal{D}(\mathcal{H}_S)$ is separable if it can be expressed as a convex combination of pure product states*

$$\rho = \sum_i p_i \, \rho_1^i \otimes \cdots \otimes \rho_N^i, \tag{5.3}$$

such that $\rho_i \in \mathcal{H}_i$, $p_i \geq 0$ and $\sum_i p_i = 1$.

The states of the form (5.3) can trivially be prepared by *Local Operations and Classical Communication* 'LOCC', where first member samples from the distribution p_i, informs all other members of the outcome i, and then each member X locally creates ρ_X^i and discards the information about the outcome i. These state are created from scratch by LOCC and hence their correlations can be described classically.

Definition 4 (***Entangled state***) *A state $\rho \in D(\mathcal{H}_S)$ is entangled if it can not be expressed as a convex combination of pure product states i.e. it is not separable.*

Entangled states can not be created from scratch using LOCC and separable states, hence all their correlations can not be described classically.

5.2.2 Bipartite Entanglement

A quantum system composed of two physically distinct subsystem is called bipartite quantum system. The Hilbert space $\mathcal{H}_S$ associated with the bipartite system is given by the tensor product $\mathcal{H}_1 \otimes \mathcal{H}_2$, where $\mathcal{H}_1$ and $\mathcal{H}_2$ represent the two subsystems respecitevely [66, 67, 68]. Due to vector nature of total Hilbert space $\mathcal{H}_S$, not all states necessarily may be written as the product of some other states. In other words, a pure quantum state

$|\psi\rangle_{AB}$, that can be written as

$$|\psi\rangle = \sum_{j_1 j_2} c_{j_1 j_2} |j_1\rangle \otimes |j_2\rangle, \tag{5.4}$$

where $\{|j_1\rangle\}$ and $\{|j_2\rangle\}$ are the basis of the system 1 and 2 respectively, and $c_{j_1 j_2}$ are normalized complex coefficients, are called *separable state*. A quantum state vector on $\mathcal{H}_S$ that can not be written as a product of state vector of the individual subsystem are called *entangled pure state*.

- **Pure State: Maximally Entangled State**

For any pure bipartite pure state $|\psi\rangle$ there always exists a product basis $\left|\phi_j^1 \phi_j^2\right\rangle$ in terms of which a state $|\psi\rangle$ can be written as

$$|\psi\rangle = \sum_{j=0}^{r-1} c_j \left|\phi_j^1 \phi_j^2\right\rangle, \tag{5.5}$$

where $r \leq d = min\{d_1, d_2\}$ and $c_j \geq 0$ for all j. This decomposition is called Schmidt decomposition and r and c_j are called Schmidt rank and Schmidt coefficients of $|\psi\rangle$ respectively. A pure state is entangled if $r > 1$. For a finite dimensional system, maximally entangled state pure state are defined in terms of Schmidt decomposition such that

$$\left|\phi^+\right\rangle = \frac{1}{\sqrt{d}} \sum_{j=0}^{d-1} \left|\phi_j^1 \phi_j^2\right\rangle. \tag{5.6}$$

For spin-half two qubit system ($d_1 = d_2 = 2$), the maximally entangled states are defined as four Bell states and expressed in computational basis as

$$\left|\Psi^\pm\right\rangle = \frac{1}{\sqrt{2}}(|01\rangle \pm |10\rangle) \tag{5.7}$$

$$\left|\Phi^\pm\right\rangle = \frac{1}{\sqrt{2}}(|00\rangle \pm |11\rangle). \tag{5.8}$$

- **Mixed State: Werner State**

Werner state are mixtures of maximally entangled bell state $|\Psi^-\rangle$ with white noise and has the form

$$\rho_1 = r\left|\Psi^{\pm}\right\rangle\left\langle\Psi^{\pm}\right| + \frac{1-r}{4}\mathbb{I} \tag{5.9}$$

$$\rho_2 = r\left|\Phi^{\pm}\right\rangle\left\langle\Phi^{\pm}\right| + \frac{1-r}{4}\mathbb{I}, \tag{5.10}$$

where $0 \leq r \leq 1$ [69, 70]. It is a subclass of Bell-diagonal states, where the density matrix in computational basis is nonvanashing only along the diagonal and antidiagonal and has "X" form. The purity $P = \mathrm{Tr}\,(\rho^2)$ of Werner state only depends on the purity parameter r and it is given by $P = (1 + 3r^2)/4$. For $r = 0$, the state is a maximally entangled state and for $r = 1$ the state is a completly mixed state [71, 72].

5.3 Entanglement Measure

Entanglement being an essential resource for any kind of quantum information task, it is very important to be able to compare and quantify entanglement of states. In general, quantification of entanglement is a formidable task and typically involves optimization, whose computational resource grows fast with system size. Effort required to quantify of entanglement for an arbitrary state becomes practically impossible for handful of particles. Given the complexity and importance of the task, there exists several proposed quantifier based on efficiency of quantum information protocols or operational approach, axiomatic approach, geometric aspect etc, each having some advantage over others in some sense. In this section we just describe one operational measure for quantification of entanglement for the two qubit system and it is called concurrence.

5.3.1 Entanglement of Formation and Concurrence

Entanglement of formation E_F is one of the important entanglement quantifier and it is defined as:

$$E_F(\rho) \equiv \inf_{\{p_i,\psi_i\}} \sum_i p_i E(|\psi_i\rangle\langle\psi_i|) \equiv \inf_{\{p_i,\psi_i\}} \sum_i p_i S(\mathrm{Tr}_B\{|\psi_i\rangle\langle\psi_i|\}), \tag{5.11}$$

where $\rho = \sum_i p_i |\psi_i\rangle\langle\psi_i|$ and $S(\rho) = -\mathrm{Tr}[\rho \log_2 \rho]$ is the von Neumann entropy. In other words, entanglement of formation is the infimum average entropy of entanglement over all possible pure state decomposition of the given state [67].

In general, the quantity E_F is computationally difficult to calculate except for the case of two-qubit system. For two-qubit system a closed form analytic expression for E_F is defined in terms of an intermediate quantity called *concurrence* C. It was first introduced introduced by Hills and Wootters for the case of rank 2 matrices, and later generalized for any two-qubit state [73]. It is defined as

$$C(\rho_{AB}) \equiv max\{0, \lambda_1 - \lambda_2 - \lambda_3 - \lambda_4\}, \tag{5.12}$$

where the λ_i are, in decreasing order, the square roots of the eigenvalues of the matrix $\rho_{AB}.\tilde{\rho}_{AB}$ where $\tilde{\rho}_{AB} \equiv \sigma_y \otimes \sigma_y \rho^*_{AB} \sigma_y \otimes \sigma_y$, σ_y is the Pauli matrix and ρ^* is elementwise complex conjugate of ρ. For general bipartite qubit state, an analytic expression exists for entanglement of formation in terms of concurrence [74]

$$E_F(\rho) = s\left(\frac{1 + \sqrt{1 - C^2(\rho)}}{2}\right), \tag{5.13}$$

where $s(x) = -x \log_2 x - (1-x)\log_2(1-x)$ is the Shannon entropy. The two qubit $E_F(\rho)$ and two qubit concurrence are monotonically related by above expression hence concurrence

is used to quantify entanglement rather than the E_F. It should be remembered that entanglement of formation is an entanglement measure, and the concurrence obtains its meaning via its relation to entanglement of formation and not vice versa.

5.4 Entanglement Sudden Death in Single-Mode Fiber

Entanglement is an essential resource and it distribution over long distances is inhibited by decoherence caused due to the refractive index fluctuation in the fiber. This decoherence ultimately leads to loss of entanglement for pure state and entanglement sudden death (ESD) for mixed state.

To understand the decoherence, we consider the setup shown in the Figure 5.2, where an entangled photon pair from a spontaneous parametric down conversion (SPDC) source is sent over single mode fiber. A general initial state for the two-qubit polarization entangled photon is given as

$$\left|\Psi_{in}^{+}\right\rangle = \alpha|HV\rangle + \beta|VH\rangle, \tag{5.14}$$

$$\left|\Phi_{in}^{+}\right\rangle = \alpha|HH\rangle + \beta|VV\rangle, \tag{5.15}$$

where we assume that $|\alpha^2| + |\beta^2| = 1$ and the computational basis is $\{HH, HV, VH, VV\}$.

As the photon passes through a section of fiber it acquires a phase ϕ proportional to the length of section. Here we choose a convention, where the phase gained by the horizontally polarized photon is $\exp(i\phi)$ and the phase gained by vertically polarized photon $\exp(-i\phi)$. Since the two photons travel through two different optical fiber with similar index profile,

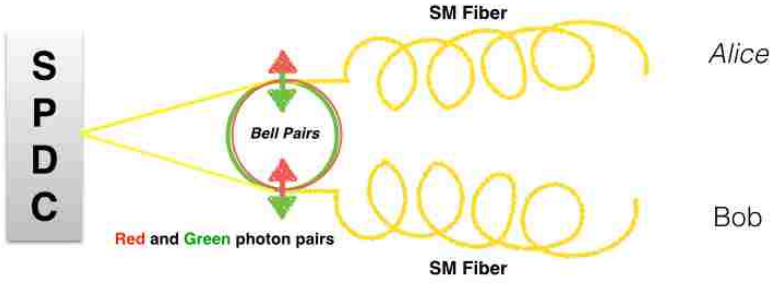

Figure 5.2: Decoherence of entangled photon in an experimental setup, where a Bell pair is created from spontaneous parametric down conversion (SPDC) and the photon pair is sent over the single-mode fiber.

the phase gained is given by :

$$\begin{aligned}
|HH\rangle &\Rightarrow \exp i(\phi_1 + \phi_2)|HH\rangle \\
|HV\rangle &\Rightarrow \exp i(\phi_1 - \phi_2)|HV\rangle \\
|VH\rangle &\Rightarrow \exp -i(\phi_1 - \phi_2)|VH\rangle \\
|VV\rangle &\Rightarrow \exp -i(\phi_1 + \phi_2)|VV\rangle.
\end{aligned} \tag{5.16}$$

After the photon, with initial state $|\Psi^+\rangle$, passes through the j_{th} section of the fiber, it acquires a phase according to the transformation given in equation (5.16). The output state is given by

$$\left|\Psi^+_{out}\right\rangle = \alpha \mathrm{e}^{i\left(\delta\phi_j^1 - \delta\phi_j^2\right)}|HV\rangle + \beta \mathrm{e}^{-i\left(\delta\phi_j^1 - \delta\phi_j^2\right)}|VH\rangle, \tag{5.17}$$

and the corresponding density matrix is given by

$$\hat{\rho}^{\Psi^+}_{j_{\text{out}}} = \left|\Psi^+_{out}\right\rangle\left\langle\Psi^+_{out}\right| \tag{5.18}$$

$$= \left(\alpha \mathrm{e}^{i\left(\delta\phi^1_j - \delta\phi^2_j\right)}|HV\rangle + \beta \mathrm{e}^{-i\left(\delta\phi^1_j - \delta\phi^2 j\right)}|VH\rangle\right)\left(\alpha^* \mathrm{e}^{-i\left(\delta\phi^1_j - \delta\phi^2_j\right)}\langle HV| + \beta^* \mathrm{e}^{i\left(\delta\phi^1_j - \delta\phi^2_j\right)}\langle VH|\right) \tag{5.19}$$

$$= \left|\alpha^2\right||HV\rangle\langle HV| + \alpha\beta^* \mathrm{e}^{i2\left(\delta\phi^1_j - \delta\phi^2_j\right)}|HV\rangle\langle VH| + \beta\alpha^* \mathrm{e}^{-i2\left(\delta\phi^1_j - \phi^2_j\right)}|VH\rangle\langle HV| \tag{5.20}$$

$$+ \left|\beta^2\right||VH\rangle\langle VH|. \tag{5.21}$$

$$\hat{\rho}^{\Psi^+}_{j_{\text{out}}} = \begin{pmatrix} 0 & 0 & 0 & 0 \\ 0 & \left|\alpha^2\right| & \alpha\beta^* \mathrm{e}^{i2\left(\delta\phi^1_j - \delta\phi^2_j\right)} & 0 \\ 0 & \beta\alpha^* \mathrm{e}^{-i2\left(\delta\phi^1_j - \delta\phi^2_j\right)} & \left|\beta^2\right| & 0 \\ 0 & 0 & 0 & 0 \end{pmatrix}. \tag{5.22}$$

Similarly applying the transformation equation (5.16) for the other two-qubit entangled state, $|\Phi^+\rangle$, that passes through j_{th} section of the fiber, the output state is given by

$$\left|\Phi^+_{out}\right\rangle = \alpha \mathrm{e}^{i\left(\delta\phi^1_j + \delta\phi^2_j\right)}|HH\rangle + \beta \mathrm{e}^{-i\left(\delta\phi^1_j + \delta\phi^2_j\right)}|VV\rangle, \tag{5.23}$$

and the corresponding density matrix is given by

$$\hat{\rho}^{\Phi^+}_{j_{\text{out}}} = \left|\Phi^+_{out}\right\rangle\left\langle\Phi^+_{out}\right| \tag{5.24}$$

$$= \left(\alpha \mathrm{e}^{i\left(\delta\phi^1_j + \delta\phi^2_j\right)}|HH\rangle + \beta \mathrm{e}^{-i\left(\delta\phi^1_j + \delta\phi^2_j\right)}|VV\rangle\right)\left(\alpha^* \mathrm{e}^{-i\left(\delta\phi^1_j + \delta\phi^2_j\right)}\langle HH| + \beta^* \mathrm{e}^{i\left(\delta\phi^1_j + \delta\phi^2_j\right)}\langle VV|\right) \tag{5.25}$$

$$= \left|\alpha^2\right||HH\rangle\langle HH| + \alpha\beta^* \mathrm{e}^{i2\left(\delta\phi^1_j + \delta\phi^2_j\right)}|HH\rangle\langle VV| + \beta\alpha^* \mathrm{e}^{-i2\left(\delta\phi^1_j + \delta\phi^2_j\right)}|VV\rangle\langle HH| \tag{5.26}$$

$$+ \left|\beta^2\right||VV\rangle\langle VV|. \tag{5.27}$$

$$\hat{\rho}^{\Phi^+}_{j_{\text{out}}} = \begin{pmatrix} |\alpha^2| & 0 & 0 & \alpha\beta^* e^{i2\left(\delta\phi_j^1+\delta\phi_j^2\right)} \\ 0 & 0 & 0 & 0 \\ 0 & 0 & 0 & 0 \\ \beta\alpha^* e^{-i2\left(\delta\phi_j^1+\delta\phi_j^2\right)} & 0 & 0 & |\beta^2| \end{pmatrix}. \tag{5.28}$$

5.4.1 Decoherence Model

To further understand the model for decoherence of entangled photon pair in optical fiber, we first recall the model of a single mode fiber from Chapter 2.

In a realistic birefringent optical fiber which is typically of lengths 10-1000 km, the polarization qubits are likely to experience random effects due to changes in temperature, stress, etc. during propagation. The characteristic length scales for such changes, in a single mode fiber, are generally smaller than the fiber beat-lengths [16]. We approximate the communication channel as continuously connected fiber segments, as shown in Figure 5.3, of constant birefringence and constant length. In this derivation, we consider a communication channel with no dispersion.

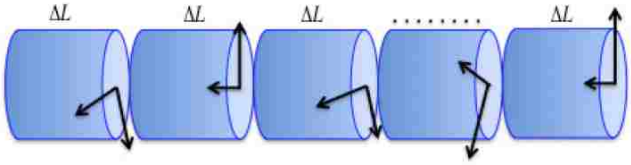

Figure 5.3: The fiber is modeled as concatenated segments of fiber of length ΔL with constant birefringence Δn.

We model the random dephasing by continuously concatenating pieces of fiber with randomly generated lengths $\triangle L$. The total propagation length thus can be split into segments of length ΔL with constant Δn. The absolute phase difference $\delta\phi$ acquired by the photon after propagating through the j^{th} segment is given by

$$\delta\phi_j = \Delta\beta_j \Delta L, \tag{5.29}$$

where $\Delta\beta_j$ is the constant birefringence for the segment of length ΔL of the fiber. The

birefriengence across these sections are modeled as Gaussian distribution with a zero mean and a known variance. Here, birefriengence is defined as the difference between the propagation constant of slow and fast modes. It can be expressed as

$$\Delta\beta = \frac{\omega n_s}{c} - \frac{\omega n_f}{c} = \frac{\omega \Delta n}{c}, \tag{5.30}$$

where ω is the angular frequency, c is the speed of light, and $\Delta n = n_s - n_f$ is the differential effective refractive index between slow (s) and fast (f) modes [13]. Here we assume that the fiber only exhibits linear birefrengence. These segments constitute a single phase profile associated with a particular instance of birefringent noise and corresponding changes in the refractive index difference $\triangle n$. Ensemble averaging over profiles gives density matrix for the output state depicting the random dephasing in the fiber.

Now, we consider the two states $|\Phi^+\rangle$ and $|\Psi^+\rangle$ as defined in equation (5.14) and equation (5.15). As these states propagate through the i-th section of fiber, they dephase according to the transformation given in equation (5.16) to a final state given by equation (5.17) and equation (5.23). After propagating through all the sections of fiber of length L, the output density matrices for the state $|\Phi^+\rangle$ and $|\Psi^+\rangle$ are given by

$$\hat{\rho}^{\Psi^+}_{j_{\text{out}}} = \begin{pmatrix} 0 & 0 & 0 & 0 \\ 0 & |\alpha^2| & \alpha\beta^* \prod_{j=1}^{n} \mathrm{e}^{i2\left(\delta\phi_j^1 - \delta\phi_j^2\right)} & 0 \\ 0 & \beta\alpha^* \prod_{j=1}^{n} \mathrm{e}^{-i2\left(\delta\phi_j^1 - \delta\phi_j^2\right)} & |\beta^2| & 0 \\ 0 & 0 & 0 & 0 \end{pmatrix}. \tag{5.31}$$

$$\hat{\rho}^{\Phi^+}_{j_{\text{out}}} = \begin{pmatrix} |\alpha^2| & 0 & 0 & \alpha\beta^* \prod_{j=1}^{n} \mathrm{e}^{i2\left(\delta\phi_j^1 + \delta\phi_j^2\right)} \\ 0 & 0 & 0 & 0 \\ 0 & 0 & 0 & 0 \\ \beta\alpha^* \prod_{j=1}^{n} \mathrm{e}^{-i2\left(\delta\phi_j^1 + \delta\phi_j^2\right)} & 0 & 0 & |\beta^2| \end{pmatrix}. \tag{5.32}$$

We then model the set of acquired phases $\{\delta\phi_1^1, \delta\phi_2^1, ..., \delta\phi_n^1\}$ and $\{\delta\phi_1^2, \delta\phi_2^2, ..., \delta\phi_n^2\}$ as random variable $\hat{\phi}^1$ and $\hat{\phi}^2$ with a mean $\left\langle \hat{\phi}^1 \right\rangle = \left\langle \hat{\phi}^2 \right\rangle = 0$ and a nonzero variance $\left\langle \Delta\hat{\phi}^{1^2} \right\rangle = \left\langle \Delta\hat{\phi}^{2^2} \right\rangle = \Delta\phi^2$; since the two optical fibers carrying the entangled pair are of the same type.

The product terms in off-diagonal elements of density matrix equation (5.32) and equation (5.31) can be written as

$$\begin{aligned}\prod_{j=1}^{n} \mathrm{e}^{\pm i2\delta\phi_i} &= \exp\left[2\sum_{j=1}^{n}(\pm i\delta\phi_i)\right] \\ &= \exp\left[2\sum_{j=1}^{n}\left(\pm i\left\langle\hat{\phi}\right\rangle \pm i\Delta\hat{\phi}\right)\right] \\ &= \exp\left[\pm i2n\left\langle\hat{\phi}\right\rangle\right]\exp\left[\pm i2\Delta\hat{\phi}\right] \\ &= \exp\left[\pm i2\Delta\hat{\phi}\right], \end{aligned} \tag{5.33}$$

where we substitute the mean and variance from the above model for random phase. We simplify it and obtain the last expression by using the fact that the mean of the random variables is zero. We then Taylor expand the factor $\exp\left[\pm i2\Delta\hat{\phi}\right]$ of equation (5.33) and take the average to obtain

$$\begin{aligned}\left\langle\exp\left[\pm i2\Delta\hat{\phi}\right]\right\rangle &= \left\langle 1 \pm i2\Delta\hat{\phi} - \frac{1}{2}(2)^2\Delta\hat{\phi}^2 + \cdots\right\rangle \\ &= 1 \pm i2\left\langle\Delta\hat{\phi}\right\rangle - \frac{1}{2}(2)^2\left\langle\Delta\hat{\phi}^2\right\rangle + \cdots \end{aligned} \tag{5.34}$$

Since the mean of variance is zero in equation (5.34) and average of the variance is $\left\langle\Delta\hat{\phi}^2\right\rangle = \Delta\phi^2$, hence we obtain the expression

$$\left\langle\exp\left[\pm i2\Delta\hat{\phi}\right]\right\rangle = 1 - \frac{1}{2}(2)^2\Delta\phi^2 + \cdots \qquad \approx \mathrm{e}^{-2\Delta\phi^2}. \tag{5.35}$$

We substitute back the approximation obtained in equation (5.34) and equation (5.35) in the off-diagonal term of the density matrix equation (5.31) and equation (5.32) to obtain

the final output density matrix for the two states.

$$\hat{\rho}^{\Psi^+}_{j_{\text{out}}} \approx \begin{pmatrix} 0 & 0 & 0 & 0 \\ 0 & |\alpha^2| & \alpha\beta^* \mathrm{e}^{-4\Delta\phi^2} & 0 \\ 0 & \beta\alpha^* \mathrm{e}^{-4\Delta\phi^2} & |\beta^2| & 0 \\ 0 & 0 & 0 & 0 \end{pmatrix}. \tag{5.36}$$

$$\hat{\rho}^{\Phi^+}_{j_{\text{out}}} \approx \begin{pmatrix} |\alpha^2| & 0 & 0 & \alpha\beta^* \mathrm{e}^{-4\Delta\phi^2} \\ 0 & 0 & 0 & 0 \\ 0 & 0 & 0 & 0 \\ \beta\alpha^* \mathrm{e}^{-4\Delta\phi^2} & 0 & 0 & |\beta^2| \end{pmatrix}. \tag{5.37}$$

From the output density matrix equation (5.36) and equation (5.37), we find that two-qubit entangled state of the of the form

$$\left|\Psi^+_{in}\right\rangle = \alpha|HV\rangle \pm \beta|VH\rangle. \tag{5.38}$$

$$\left|\Phi^+_{in}\right\rangle = \alpha|HH\rangle \pm \beta|VV\rangle \tag{5.39}$$

decohere at an exponentially rate as they propagate through the optical fiber. Here, $\Delta\phi^2$ is the standard deviation of random phase in the fiber.

5.4.2 Entanglement Death

To quantify the amount of entanglement of a birartite mixed state we recall the result due to "Tu and Eberly" [75], where they quantify the entanglement for mixed state also called "X" state in terms of concurrence.

They examined the evolution of entanglement under noise-induced relaxation of an important class of bipartite density matrices called "X" state. The density matrix in this class only contain non-zero element in an "X" formation, along the main diagonal and

anti-diagonal and given as:

$$\rho^{AB} = \begin{pmatrix} a & 0 & 0 & w \\ 0 & b & z & 0 \\ 0 & z^* & c & 0 \\ w^* & 0 & 0 & d \end{pmatrix}, \tag{5.40}$$

where $a + b + c + d = 1$. The X mixed state arises naturally in a variety of situations [76, 77, 78] and it includes pure Bell states and well-known Werner mixed state [69] as a special case. For the X state defined in equation (5.40), the concurrence is computed as

$$C\big(\rho^{AB}\big) = 2\max\Big\{0, |z| - \sqrt{ad}, |w| - \sqrt{bc}\Big\}. \tag{5.41}$$

Using the result in equation (5.41), the concurrence for the two output density matrix equation (5.36) and equation (5.37) can easily be calculated and it can be shown that the entanglement decays to zero for a pure Bell state and entanglement sudden death (ESD) happens for Werner mixed state.

5.5 Summary

To summarize, we discussed the topic of entanglement in bipartite and multipartite system and a measure for quantification of entanglement. Later we showed that decoherence caused by refractive index fluctuation in fiber leads to loss of entanglement for Bell state and ESD for Werner state.

Chapter 6
Numerical Simulation[1]

6.1 Introduction

The distribution of quantum states over long distances is essential for emerging quantum technologies such as quantum networks and long distance quantum cryptography. Quantum networks and quantum cryptographic systems [31, 32] use photonic qubits as information carriers because of their quantum nature and low-loss coefficient pertaining to transmission, both in optical fiber [33] and in free space [34]. Nevertheless, the losses become significant when we envision transmission over hundreds of kilometers or more and is accompanied by decoherence.

Quantum information is often encoded in the polarization or orbital angular momentum degree of freedom of the photon, or some suitable combination of both degrees of freedom. Unavoidable couplings between photonic qubit and its environment introduce uncontrolled evolution of the qubit causing the qubit to lose its ability to exhibit coherent behavior. As a result, the phase of the qubit becomes randomized and the information stored in it is lost. Such decoherence processes stand as a serious obstacle towards achieving scalable quantum information processing.

To extend the lifetime of the qubit, we use a simple and effective technique of Dynamical decoupling (DD) where external pulse sequences applied to the system average out the qubit-environment interaction by time-reversing the effects of the interaction Hamiltonian. The idea of refocusing the phase diffusion by the application of repeated external pulses has been extensively studied and several DD strategies have been proposed. Notable examples of DD schemes are the periodic DD (PDD) [24], Carr-Purcell DD (CP) [79], Carr-Purcell-Meiboom -Gill (CPMG) [80], concatenated DD (CDD) [28] and Uhrig DD

[1]This chapter previously appeared as Manish K. Gupta and et al., Physical Review A 91, 032329 (2015), Bhaskar Roy Bardhan, Petr M. Anisimov, Manish K. Gupta and et al., Physical Review A 85, 022340 (2012). It is reprinted by permission of the American Physical Society.

(UDD) [81]. In quantum computing, DD has been typically used as an open-loop control scheme to reduce the errors which occur during the evolution of the quantum state.

To numerically simulate the effect of refractive index fluctuation in optical fiber on photonic qubi or qdit state, we first model the optical fiber of length L as concatenated segments of fixed Δn as shown in the Figure 6.1. The absolute phase difference acquired by the photon after propagating through the j^{th} segment is given by

$$\delta\phi_j = \Delta\beta_j \Delta L \tag{6.1}$$

where $\delta\phi$ is the acquired phase after traveling though the j^{th} segment of length ΔL in the fiber. These fiber segments together constitute a single phase profile for a particular instance of birefringent noise and corresponding changes in the refractive index Δn. The output state is obtained by averaging over all phase profiles.

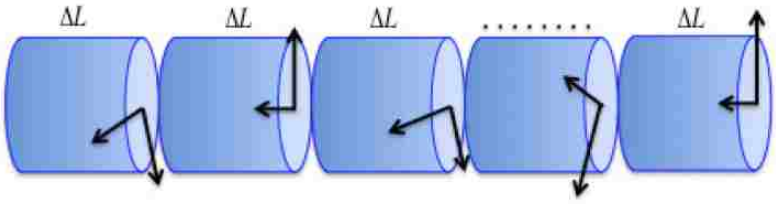

Figure 6.1: The fiber is modeled as concatenated segments of fiber of length ΔL with constant birefringence Δn.

6.2 Preserving Polarization Qubit in PM Fiber

We propose here the application of the CPMG sequence of dynamical decoupling for minimizing the random dephasing in polarization maintaining (PM) optical fibers. This sequence has been shown to be robust against a variety of dephasing and control pulse errors [82, 83, 3, 84]. We apply this sequence to flying polarization qubits in order to extend the useful range of a quantum communication channel. We simulate the CPMG pulses with spatially separated half-wave plates to suppress the dephasing of the input polarization qubits. This will be useful for the BB84 protocol [31] of quantum key distribution,

along with applications in the fields like optical quantum computing [85] and quantum networks [86], with the advantage of having low control overheads. Our proposed scheme helps to improve the range of communication channels without requiring any ancilla qubits and measurement.

6.2.1 Numerical Simulation

To characterize the effectiveness of our scheme, we use the fidelity $\mathcal{F}$ between the input state $|\psi_{\text{in}}\rangle$ and ρ_{out} as

$$\mathcal{F} = \langle\psi_{\text{in}}|\rho_{\text{out}}|\psi_{\text{in}}\rangle, \tag{6.2}$$

where $\rho_{\text{out}} = \frac{1}{n}\sum_{i=1}^{n}|\psi_i\rangle\langle\psi_i|$. Here n is the total number of randomly generated phase profiles, corresponding to the propagation operator $\hat{u}_i$ so that $|\psi_i\rangle = \hat{u}_i|\psi_{\text{in}}\rangle$ represents the simulated birefringent noise. Therefore, the fidelity being close to one implies that the input state is well-preserved against the dephasing.

For an arbitrary polarization state $\alpha|H\rangle + \beta|V\rangle$, our calculations show that after n randomly generated phase profiles, the average fidelity between the input and output states is

$$\mathcal{F}_{\text{Avg}} = \left\langle \cos^2(\theta) + \left(|\alpha|^2 - |\beta|^2\right)^2 \sin^2(\theta) \right\rangle. \tag{6.3}$$

Here θ is the total phase introduced by the birefringent fiber as well the waveplates. States which minimize the fidelity are given by $\frac{1}{\sqrt{2}}\big(|H\rangle + e^{i\phi}|V\rangle\big)$ and lie on the equator of the Poincaré sphere. However, equation (6.3) is valid for any general input state and our simulations, although targeted to improve the fidelity of the states that are useful for the BB84 protocol, hold for any general polarization state, and hence useful for practical implementations of sending a general quantum state through the channel. We observe that the fidelity drastically improves when we used the waveplates even for a large variation of the parameters of the random dephasing $\Delta\phi$. We illustrate this in Figure 6.2.

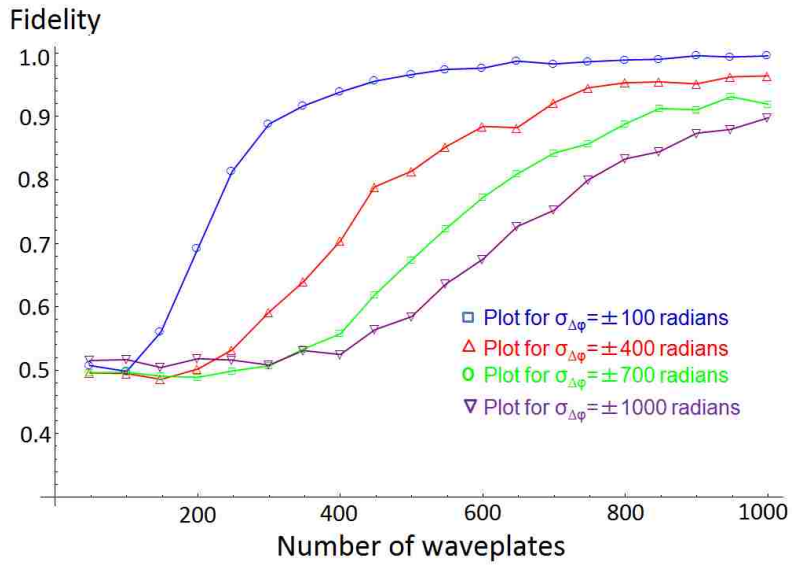

Figure 6.2: Fidelity obtained with CPMG waveplates in the optical fiber is shown with variation of the number of waveplates for different standard deviations of the randomly generated dephasing $\triangle\phi$ and fixed $L = 10\text{km}, \langle\triangle L\rangle = 10\text{m}$ and $\sigma_{\triangle L} = 3\text{m}$.

We developed our dephasing model in a dimensionless manner so we can model any realistic fiber length. In Figure 6.3, the contour plot of the fidelity is shown with respect to the standard deviations $\triangle L$ and $\triangle\phi$. This plot illustrates that high fidelity can be obtained for a reasonably large range of random fluctuations. Therefore, we show how to preserve photonic qubits against dephasing over realistic lengths of optical fiber.

The variation of fidelity for different fiber lengths is plotted in Figure 6.4, which shows that polarization qubits can be preserved up to an excellent fidelity using the CPMG sequence for a wide range of the total fiber length. Moreover, for a given length of the fiber, we can estimate the minimum number of waveplates or the distance between the waveplates required to achieve high fidelity. For instance, for a total fiber length of L=10 km, the estimated number of waveplates from Figure 6.2 is 610 to obtain a fidelity of 0.98. Using this, the rough estimate of the inter-waveplate distance L_τ is 8.2 m when we considered birefringence fluctuations Δn on a length scale of 10 m (which is fairly realistic for the long-distance communication purposes) along the fiber.

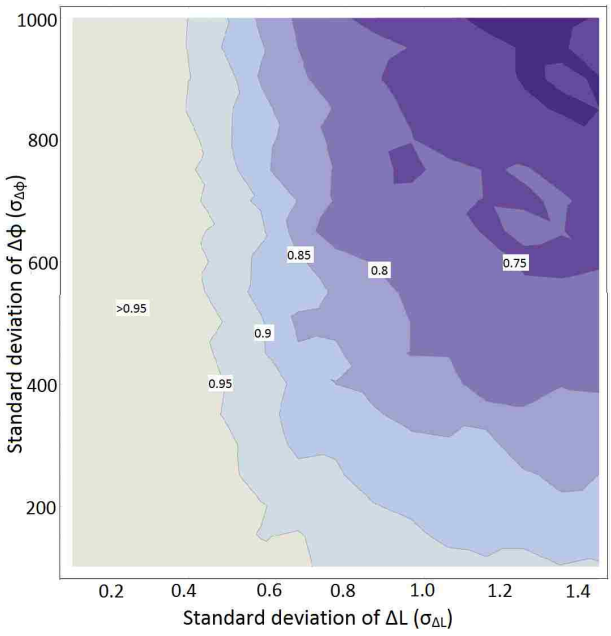

Figure 6.3: Contour plot of the fidelity with the variations of the standard deviations of $\triangle L$ and $\triangle\phi$. Lighter regions show higher values of the fidelity. The simulation is done with fixed $L = 10\text{km}, \langle\triangle L\rangle = 10\text{m}$.

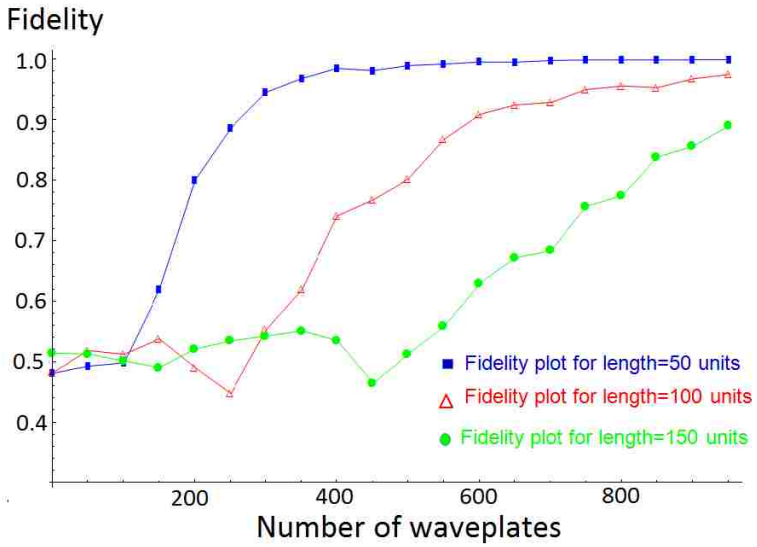

Figure 6.4: Fidelity variation for different fiber lengths with $\langle\triangle L\rangle = 10\text{m}, \sigma_{\triangle L} = 3\text{m}$ and $\sigma_{\triangle\phi} = \pm 100$ radians.

6.3 Preserving Polarization Qubit in SM Fiber

In the past, techniques based on DD control have been proposed by Wu and Lidar [25] and others [87, 88, 89] for preserving the polarization qubit in an optical fiber, however, no

specific scheme has been studied in single-mode fiber that are not polarization preserving. In our previous work, we proposed the Carr-Purcell-Meiboom-Gill (CPMG) DD pulse sequence for preserving polarization qubit in a polarization-maintaining fiber where the birefringence of the fiber was simulated as a Gaussian-distributed, zero-mean random process [90]. We numerically showed that effect of decoherence can be minimized with the use of ideal pulses implemented using suitability oriented half-wave plates (HWP) and a fidelity greater than 99% can be achieved [27].

Polarization-maintaining fibers are less widely used in telecommunication in comparison to single-mode fiber since they are costly. For this reason, we propose a scheme to preserve the polarization qubit in a single-mode fiber with a more realistic birefringence noise profile, using the Knill dynamical decoupling (KDD) pulse sequence [3]. We numerically show that when the self correcting KDD pulse sequence is implemented, using HWPs in a single-mode fiber, then a polarization qubit can be preserved with fidelity greater than 99%. In reality, manufacturing a fiber with perfect wave plates is a difficult task. Hence, we also show that in the presence of 0.5% rotation error in a pulse, a fidelity greater than 96% can be achieved. Since any state can be preserved with high fidelity it can be used as delay line or as quantum memory to store photon qubit for short period of time.

6.3.1 Numerical Simulation

We numerically show that state of polarization can be preserved against decoherence caused by the birefringence present in a single-mode fiber by introducing half-wave plates (HWPs) at predetermined positions along the fiber. Since the manufacturing of fibers with waveplates at appropriate positions is limited by manufacturing accuracy, we also show that such intrinsic error can also be minimized when KDD is used.

To preserve the coherence of the polarization qubit in a single-mode fiber, we use DD pulse sequences implemented with HWPs. We compare the effectiveness of CPMG and KDD pulse sequences in the presence of pulse imperfections to allow for intrinsic errors in

the HWP, and we show that as the fiber length increases, the accumulation of errors due to pulse imperfection can be better suppressed with the KDD sequence as compared to the CPMG sequence.

The birefringence of a single-mode fiber is modeled by generating a set of values according to the Rayleigh distribution, whose probability density function is given as

$$f(x,\sigma) = \frac{x}{\sigma^2} e^{-x^2/(2\sigma^2)},\ x \geq 0 \tag{6.4}$$

where $\sigma \geq 0$, is the scale parameter of the distribution, and x is the distance along the fiber. Each value is the phase error acquired by the photon as it travels a distance ΔL along the fiber. A noise profile of the fiber is extrapolated from these phase error values.

We then calculate the fidelity of a specific DD pulse sequence in a fiber of a particular length, number of sections, and initial polarization state. For each section of fiber, the initial state of photon is allowed to freely evolve for a distance according to

$$\mathbb{M}_z(\delta\phi_j) = \begin{pmatrix} \mathrm{e}^{i\frac{\delta\phi_j}{2}} & 0 \\ 0 & \mathrm{e}^{-i\frac{\delta\phi_j}{2}} \end{pmatrix}, \tag{6.5}$$

where, $\delta\phi_j$ includes the phase error from the Rayleigh distribution. The pulse error is then calculated from the normal distribution with zero mean, and the state is rotated according to the particular DD pulse sequence being analyzed. This is repeated for each section in the fiber. We then compare the output state with input state and use fidelity as a measure of effectiveness in preserving the state of photon. Fidelity is defined as

$$\mathcal{F} = |\langle\psi_i|\,\psi_f\rangle|^2 = \langle\psi_i|\widehat{\rho}_{\mathrm{out}}|\psi_i\rangle, \tag{6.6}$$

where ψ_f and ψ_i represent the final and initial state respectively and $\widehat{\rho}_{\mathrm{out}} = \frac{1}{n}\sum |\psi_{out}\rangle\langle\psi_{out}|$ is average output state over n fiber noise profiles.

To compare the effectiveness of KDD and CPMG pulse sequences in suppressing the decoherence, we first run the simulation for a single-mode fiber of length 500 meters in absence of pulse error. The result of the simulation is shown in Figure 6.5., where we find that in the absence of pulse errors, the two schemes perform equally well and require 800 wave plates to preserve the polarization qubit in a 500-meter single-mode fiber.

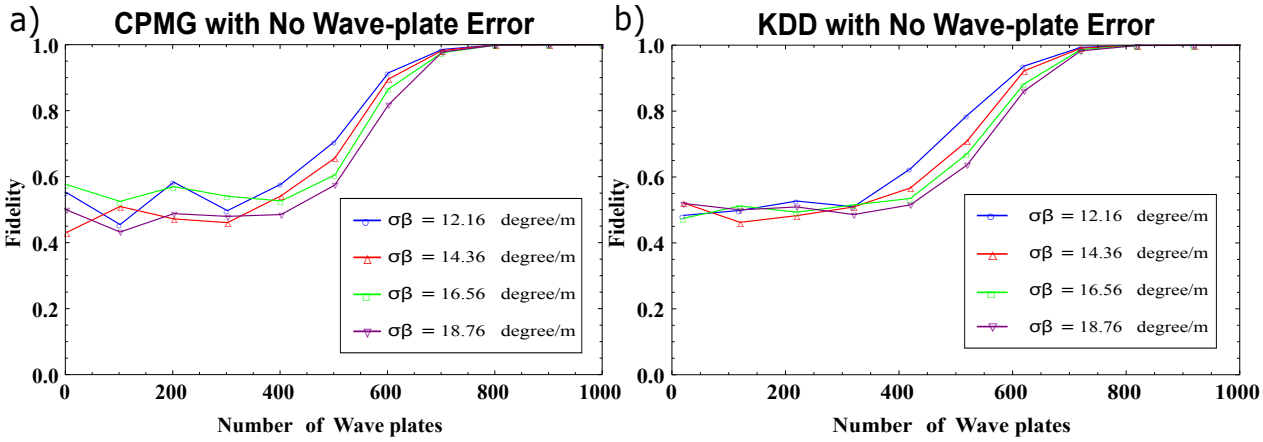

Figure 6.5: Fidelity of DD sequence in a 500 m single-mode fiber with perfect pulses. a) CPMG pulse sequence b) KDD pulse sequence.

We then introduce 0.5% error in the HWPs, distributed as Gaussian with zero mean and run the simulation for a 500-meter single-mode fiber. The result of the numerical simulation is show in Figure 6.6. The KDD sequence performs better when compared to CPMG sequence and achieves a fidelity of 96%. Furthermore, when errors in the wave plate is increased from 0.5% to 1%, the fidelity of the CPMG sequence drops to 80% due to error accumulation, whereas the fidelity of the KDD sequence remains above 90% due to error cancellation as shown in Figure 6.7.

As the fiber length is increased from 500 meters to one kilometer, the pulse errors accumulate and the fidelity of CPMG falls, whereas the fidelity of the KDD sequence remains the same due to cancellation of errors, as shown in Figure 6.8.

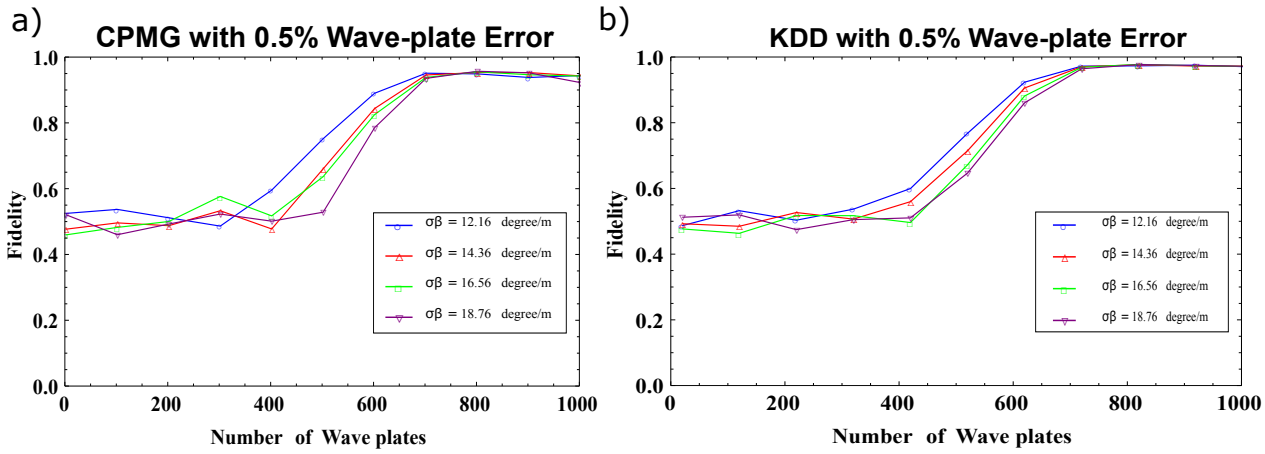

Figure 6.6: Fidelity of DD sequence in a 500 m single-mode fiber with 0.5% pulses error. a) CPMG pulse sequence b) KDD pulse sequence.

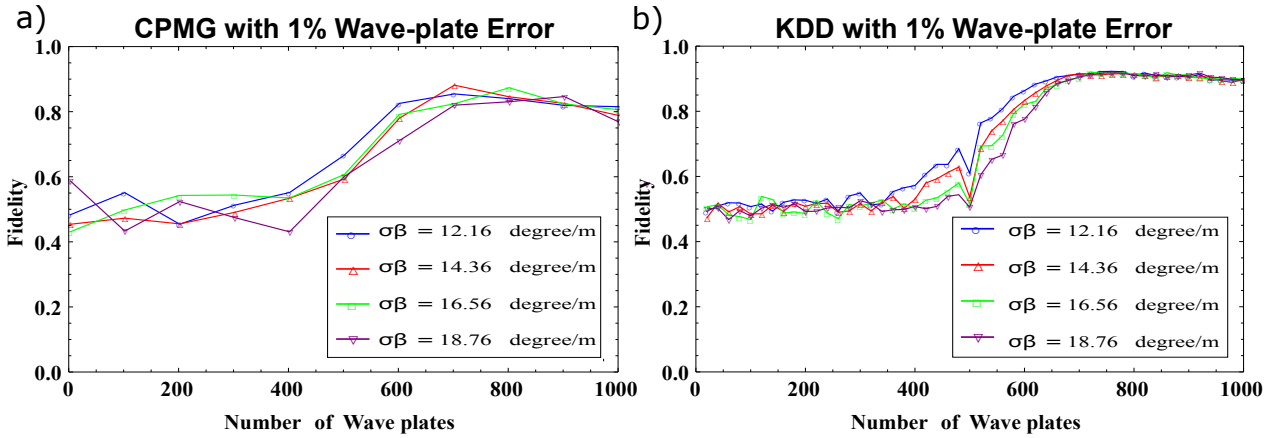

Figure 6.7: Fidelity of DD sequence in a 500 m single-mode fiber with 1% pulses error. a) CPMG pulse sequence b) KDD pulse sequence.

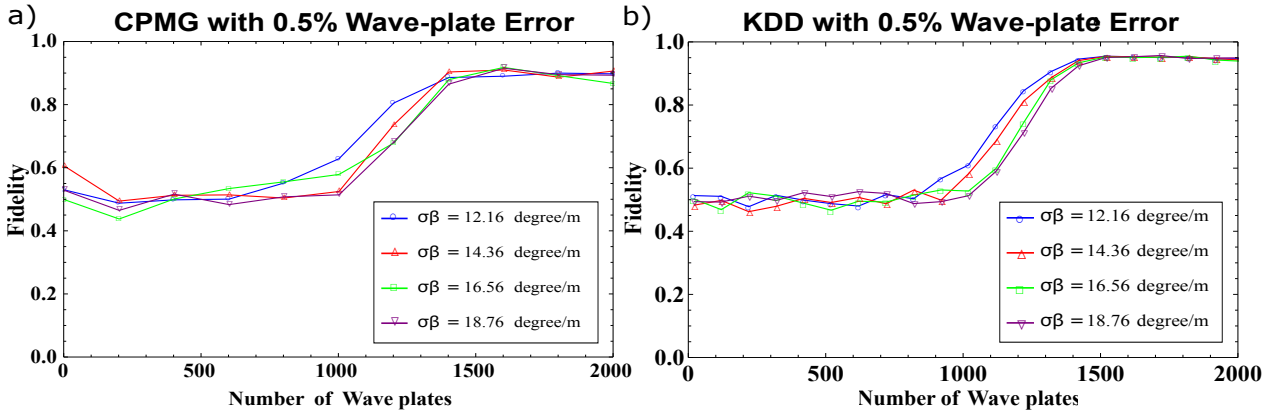

Figure 6.8: Fidelity of DD sequence in a 1 km single-mode fiber with 0.5% pulses error. a) CPMG pulse sequence b) KDD pulse sequence.

6.4 Preserving OAM Qudit state in MM Fiber

To understand the detrimental effects of noise encountered in the communication channel we numerically study three scenarios. First we analyze the decoherence of free evolving OAM photon in a fiber due to index of refraction fluctuations and then we analyze the effectiveness of open-loop control in preserving the coherence of the qubit, where the system is subjected to external, suitably tailored, space-dependent pulses which do not require measurement. Finally we analyze the impact of large values of quantum number l on decoherence suppression.

6.4.1 Numerical Simulation

Decoherence of a photonic state has its origin in optical index fluctuation of a fiber that can result from both intrinsic and extrinsic perturbations. We model axially varying index dephasing in an optical fiber of length L by a series of concatenated, homogeneous segments of length ΔL with constant Δn [18, 2, 27]. The index fluctuations across these segments is modeled by generating a set of values according to the Rayleigh distribution, whose probability density function is given as

$$f(x,\sigma) = \frac{x}{\sigma^2} e^{-x^2/(2\sigma^2)},\ x \geq 0 \tag{6.7}$$

where $\sigma \geq 0$, is the scale parameter of the distribution, and x is the distance along the fiber [17, 2]. A noise profile of the fiber is extrapolated from these phase error values. Here we assume that the fiber only exhibits linear index fluctuation as the radial dimension of the fiber is very small.

For our numerical analysis we consider the following input state

$$\begin{aligned} |\psi\rangle = \frac{1}{\sqrt{2\pi}}[&R_{p,l}(r)\exp(i\,l\,\theta)|p,l\rangle \\ &+R_{p,-l}(r)\exp(-i\,l\,\theta)|p,-l\rangle]. \end{aligned} \tag{6.8}$$

Since $R(p,l) = R(p,-l)$, we can normalize the state and rewrite the ket in matrix notation as:

$$|\psi\rangle = \frac{1}{\sqrt{2}} \begin{pmatrix} \mathrm{e}^{i\,l\phi} \\ \mathrm{e}^{-i\,l\phi} \end{pmatrix}. \tag{6.9}$$

We first calculate the fidelity of the fiber without any error suppression mechanism in place for a particular length, number of sections, and initial state. The initial state of the photon is allowed to freely evolve through each section of the fiber according to

$$\mathbb{M}_z(\delta\phi_j) = \begin{pmatrix} \mathrm{e}^{i\,l\,\frac{\delta\phi_j}{2}} & 0 \\ 0 & \mathrm{e}^{-i\,l\,\frac{\delta\phi_j}{2}} \end{pmatrix}, \tag{6.10}$$

where, $\delta\phi_j$ includes the phase error from the Rayleigh distribution. The freely evolved state is then compared with the input state. We use fidelity as a measure of effectiveness in preserving the state of photon and it is defined as

$$\mathcal{F} = |\langle\psi_i|\,\psi_f\rangle|^2, \tag{6.11}$$

where ψ_f and ψ_i represent the final and initial state respectively. The fidelity $\mathcal{F}$ is averaged over n fiber noise profiles.

When photon with state of the form equation (6.9) is launched into the fiber of length 500 m it completely dephases and fidelity remains at 50%. We then calculate fidelity for second scenario where the passive error suppression mechanism called the Carr-Purcell-Meiboom-Gill (CPMG) DD pulse sequence is used for a particular length, number of sections, and initial state [90, 24]. For each section of fiber, the initial state of photon is allowed to freely evolve for a certain distance according to equation (6.10) and then the state is rotated according to the CPMG DD pulse sequence, where the pulse sequence is implemented by inserting a dove prism. This prism is a well-known device in

optics that acts as image flipper in one transverse dimension, while leaving unchanged the image in the other transverse dimension [91]. This changes the OAM of a light beam from $l = 1$ to $l = -1$. This is repeated for each section in the fiber. We then compare the output state with input state and use fidelity as a measure of effectiveness in preserving the state of photon. We see that for $l = 2$ the photon state can be preserved with a fidelity greater than 99% as shown in Figure 6.9.

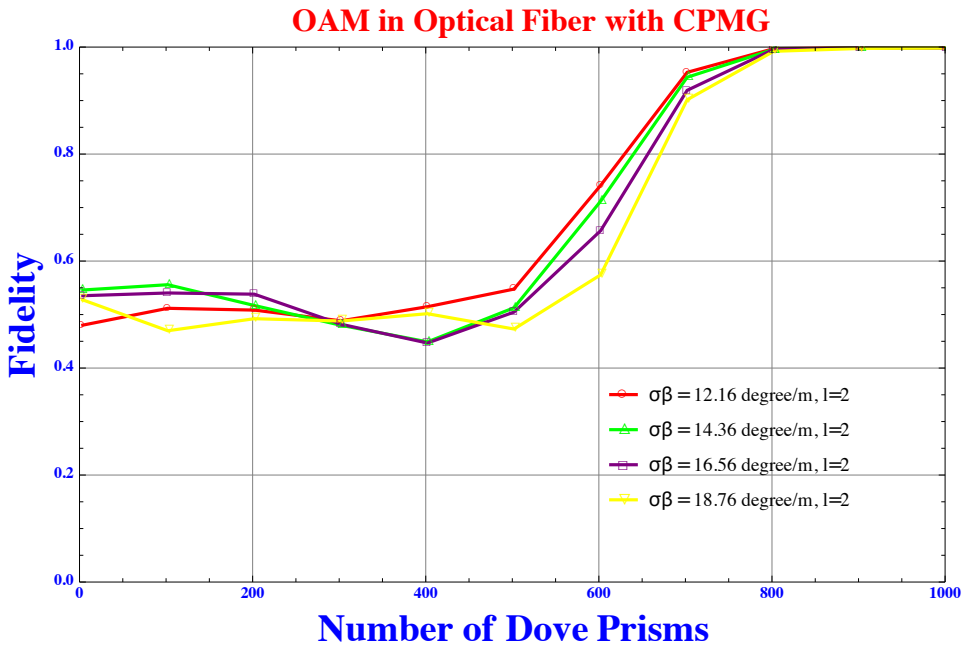

Figure 6.9: Fidelity of CPMG sequence in a 500 m optical fiber with perfect pulses. The result shown in the plot is for an OAM state with arbitrary ϕ and $l = 2$.

Finally we analyze the impact of large quantum number l on effectiveness of CPMG DD pulse sequence in preserving the OAM state of photon. We find that the fidelity decreases for same number of resource with increasing value of quantum number l such as $l = 10$ and $l = 50$ as shown in Figure 6.10 and Figure 6.11. As l is increased from 1 to 100, we see that the DD pulse sequence fails to preserve the OAM state of photon and it completely dephases as shown in the Figure 6.12. We note that there is no intuitive relation between the exponential noise scaling and number of prisms.

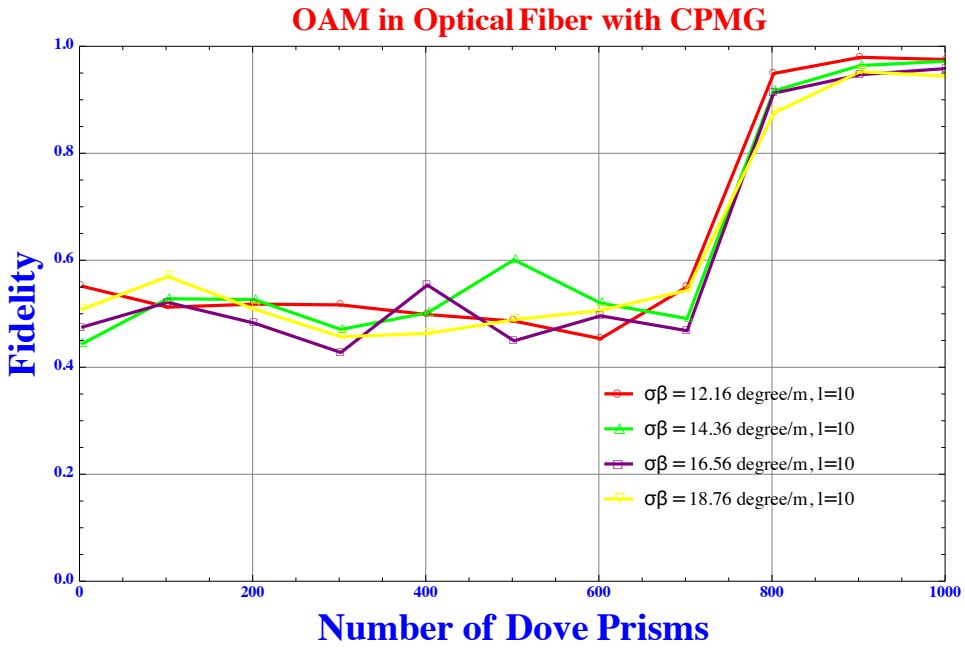

Figure 6.10: Fidelity of CPMG sequence in a 500 m optical fiber with perfect pulses. The result shown in the plot is for an OAM state with arbitrary ϕ and $l = 10$.

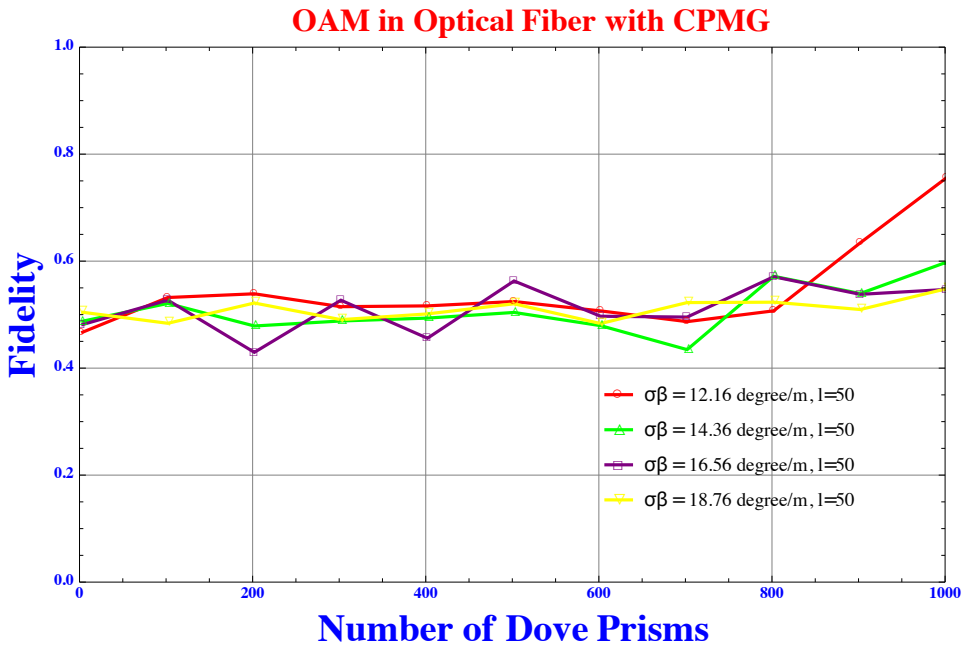

Figure 6.11: Fidelity of CPMG sequence in a 500 m optical fiber with perfect pulses. The result shown in the plot is for an OAM state with arbitrary ϕ and $l = 50$.

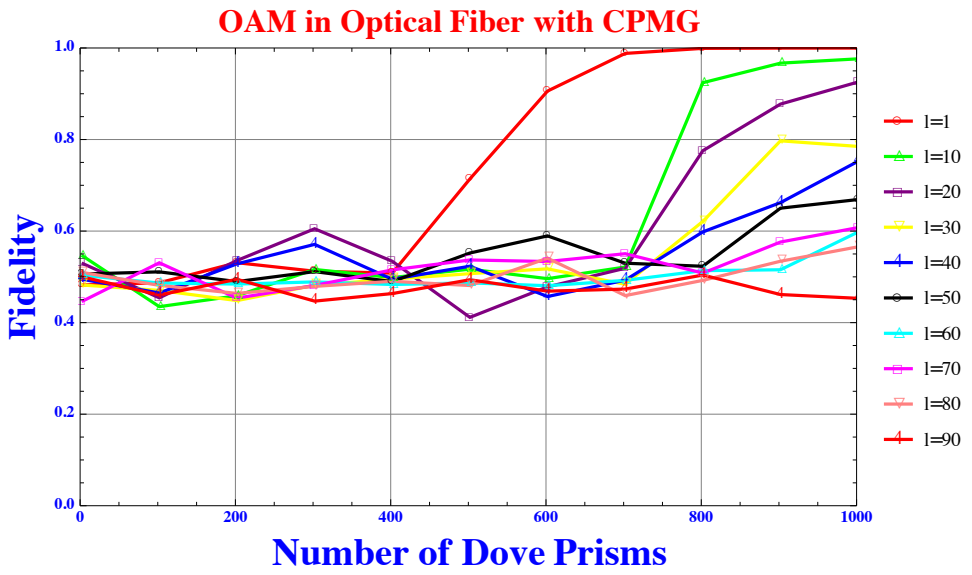

Figure 6.12: Fidelity of CPMG sequence in a 500 m optical fiber with perfect pulses. The result shown in the plot is for an OAM state with arbitrary ϕ and l between one and 100.

6.5 Saving Entanglement with DD

Entanglement is a fundamental resource for existence of key quantum communication technologies such as Quantum Key Distribution (QKD), Quantum dense coding, Quantum teleportation, and Quantum network. It is essential resource for any capacity achieving quantum communication. Perfect quantum communication is equivalent to distribution of perfect entanglement [59]. If we can transport a qubit without decoherence then entanglement shared by qubit will also be distributed perfectly, however the effect of environmental noise inevitably impair our ability to send quantum states over long distance.

Here we numerically simulate entanglement sudden death of polarization entangled photons in a single-mode fiber caused by the refractive index fluctuation. We numerically show the loss of entanglement for the Bell state and entanglement sudden death for Werner mixed state or "X" state [69, 75]. We additionally show that such a loss of entanglement can be mitigated to a large extent with a *open-loop* control technique called dynamical decoupling (DD) where the π-pulse is implemented using half-wave plate and we numerically show that entanglement can be preserved for longer distances in an optical fiber.

To quantify the entanglement in bipartite state, we use concurrence as a measure and it is defined as

$$C(\rho_{AB}) \equiv max\{0, \lambda_1 - \lambda_2 - \lambda_3 - \lambda_4\}, \tag{6.12}$$

where the λ_i are, in decreasing order, the square roots of the eigenvalues of the matrix $\rho_{AB}.\tilde{\rho}_{AB}$ where $\tilde{\rho}_{AB} \equiv \sigma_y \otimes \sigma_y \rho^*_{AB} \sigma_y \otimes \sigma_y$, σ_y is the Pauli matrix and ρ^* is elementwise complex conjugate of ρ. The value of $C = 1$ for maximally entangled state and $C = 0$ for completely mixed state.

6.5.1 Numerical Simulation

We first simulate the decay of entanglement for the case of polarization entangled photon in ϕ^+ Bell state in a single-mode fiber. The result of the numerical simulation is shown in Figure 6.13. As predicted by the decoherence model, discussed in the previous chapter, the concurrence decays to a very small value as the photon propagates through a 100m optical fiber.

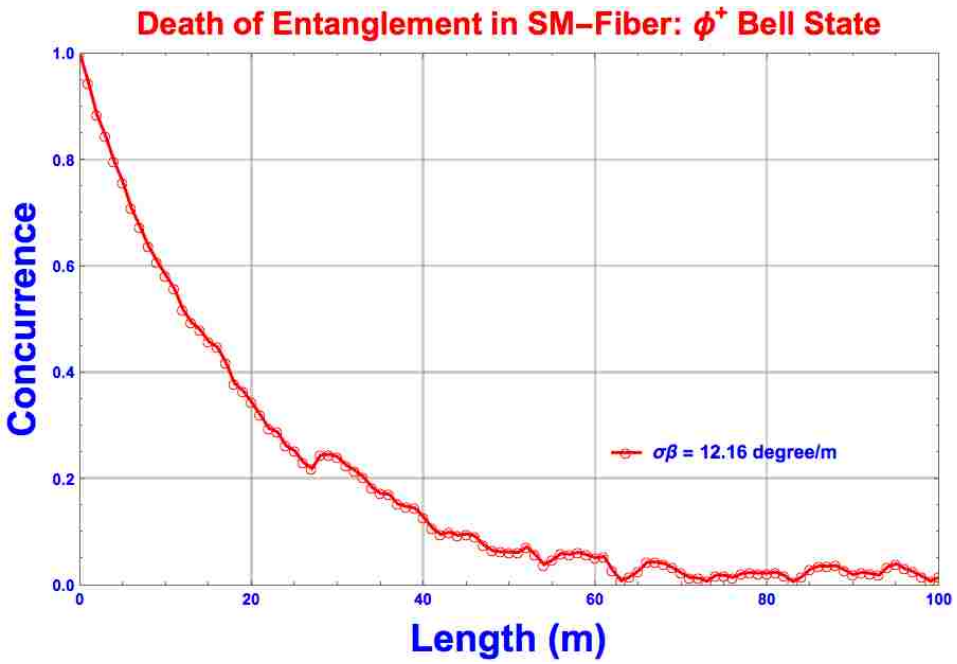

Figure 6.13: Decay of entanglement in a 100m Single Mode optical fiber. The input state is ϕ^+ state.

In the actual experiment, the entangled photons are never produced in pure state hence, we also simulate the propagation of X state, also called Extended Werner state [75, 69], in a single-mode fiber. The result of the numerical simulation for a particular value of the mixing parameter $r = 0.89$ is shown in Figure 6.14. As predicted by decoherence model we observe that the value of concurrence goes to zero, which is also called entanglement sudden death (ESD). To further analyze, we numerically simulate propagation of X state for a range of values of mixing parameter r, $0 \leq r \leq 1$. We again observe a region of ESD as shown in the Figure 6.15.

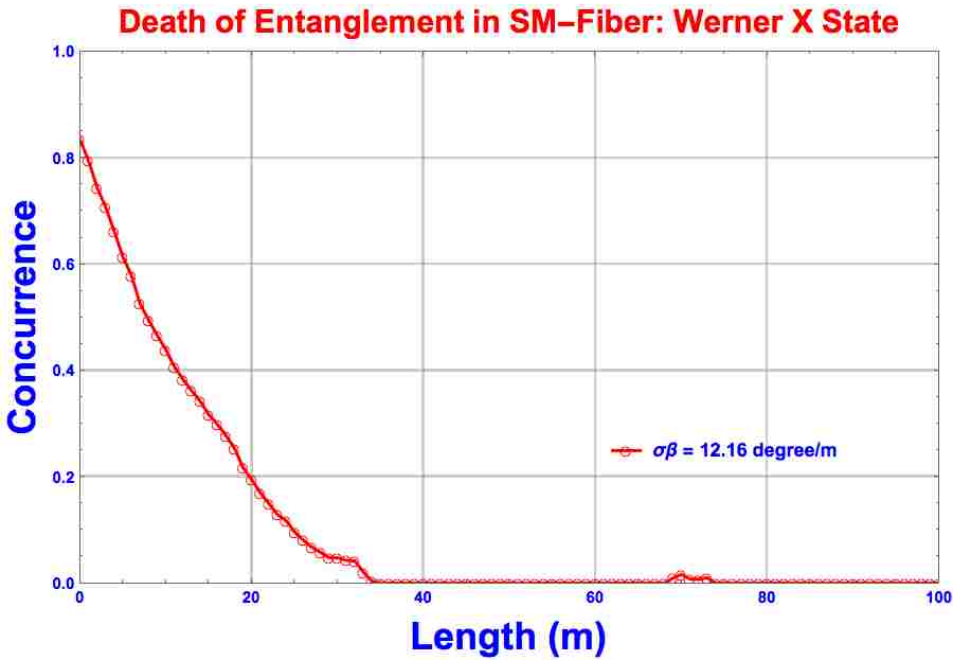

Figure 6.14: Decay of entanglement in a 100m Single Mode optical fiber. The input state is Werner X state.

To suppress the noise caused by the refractive index fluctuation in the optical fiber we use the passive error suppression mechanism called the Carr-Purcell-Meiboom-Gill (CPMG) DD pulse sequence. Where we apply a sequence of π pulse implemented using half-wave plates in an optical of a particular length. We numerically simulate the two scenarios where in the first case the initial state is ϕ^+ Bell state and in the second case the initial state is the X state is propagated through a 100m fiber with error suppression mechanism is in

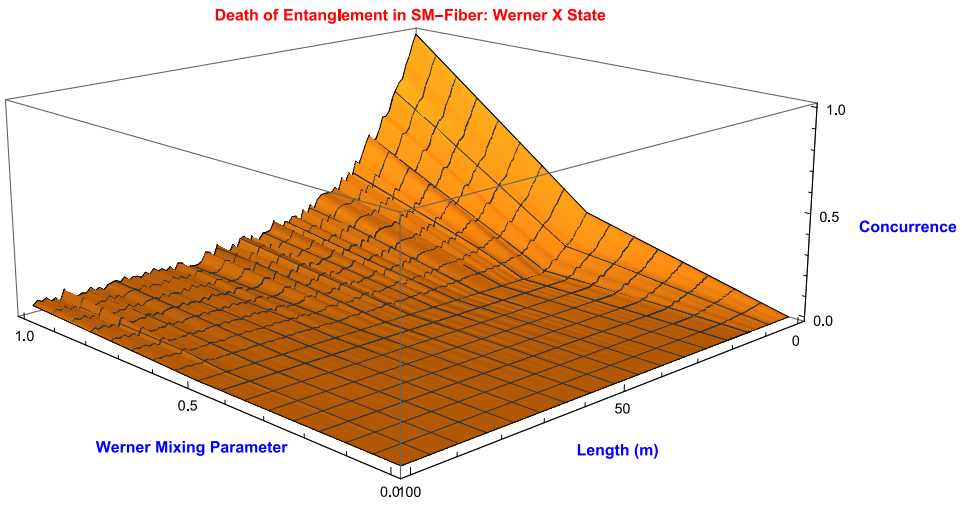

Figure 6.15: Decay of entanglement in a 100m Single Mode optical fiber. The input state is Werner X state. The mixing parameter varies from zero to one.

place. We observe that the entanglement can be preserved for the two states and the result of the numerical simulation is shown in Figure 6.16 and Figure 6.17.

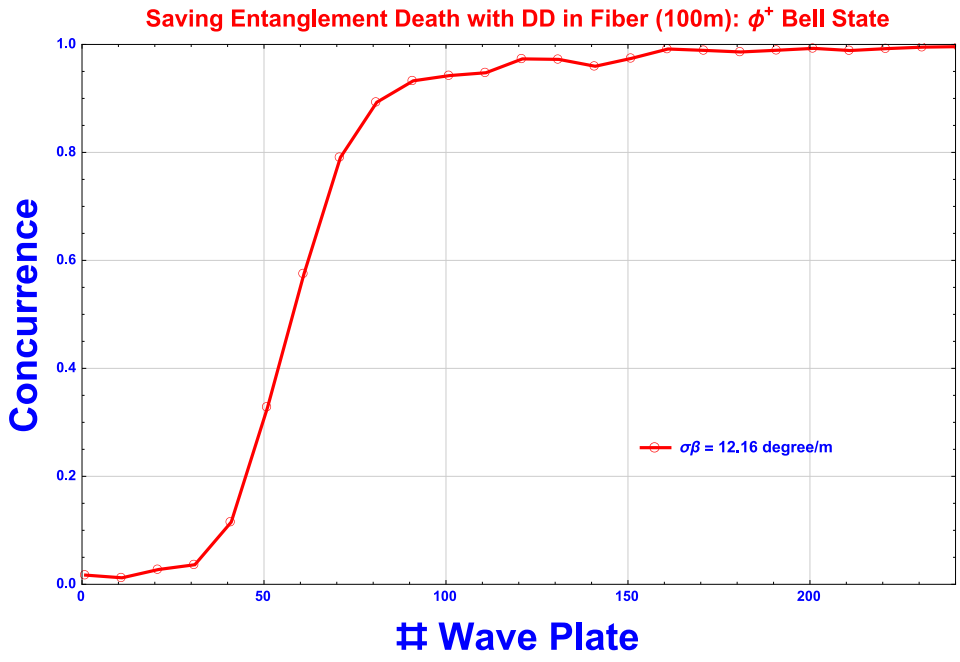

Figure 6.16: Entanglement decay is minimized by applying CPMG DD pulse implemented using Half-Wave plates. The input state is ϕ^+ state.

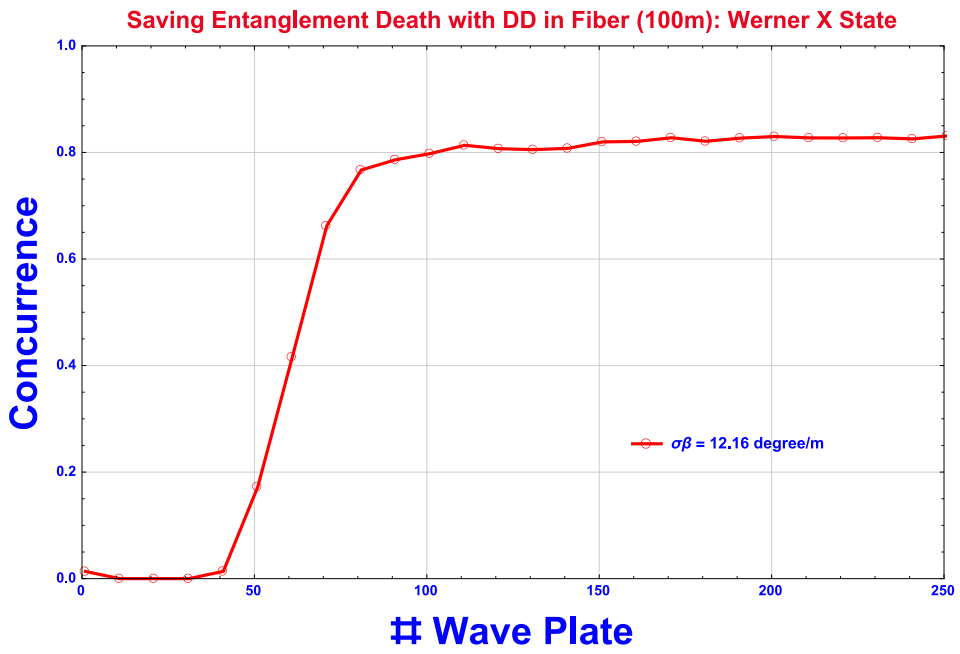

Figure 6.17: Entanglement decay is minimized by applying CPMG DD pulse implemented using Half-Wave plates. The input state is Werner X state.

6.6 Summary

To summarize, We numerically simulated the effect of refractive index fluctuation on polarization qubit in PM fiber and MM fiber and showed that DD can be used to preserve polarization qubit with a fidelity of 99% for ideal and non-ideal pulses. We numerically analyzed the impact of large values of quantum number l on decoherence and showed that DD can be used to minimize the effect of decoherence to a certain maximum value of l. We numerically simulated the effect of refractive index fluctuation in optical fiber on entangled Bell state and Werner mixed state and showed that DD can be used to extend the length over which entangled photons can be distributed over the optical fiber.

Chapter 7
Conclusions and Outlook

7.1 Summary of Results

In this thesis, we studied the problem of quantum communication from the perspective of pure dephasing caused by the refractive index fluctuation in the fiber. These fluctuations in refractive index are caused by asymmetry in the core of the fiber induced either during manufacturing or deployment. We showed how these fluctuations in the optical fiber can be numerically modeled.

We later derived the analytic model for decoherence of polarization qubit in single mode and multi-mode fiber and numerically showed that such a decoherence can be minimized up to 99% by using the technique of dynamical decoupling with the help of half waveplate in optical fiber, thus preserving the quantum state of qubit for longer distances. We numerically studied the effectiveness of CPMG and KDD sequence in preserving the state of the qubit in optical fiber with perfect pulses and later we showed that composite pulse such as KDD is superior in performance in case of pulse error.

Experiments show that the data rate for quantum communication using polarization qubit is low for practical purposes and other degrees of freedom of photon must be explored for increasing data rates. One such state photo is orbital angular momentum state which provides infinite dimensional Hilbert space for encoding data in angular momentum degree of freedom and thus providing a method to increase quantum communication data rates. We analytically showed that a certain maximum value of quantum number l may be used if data is encoded in angular momentum degree of freedom because the fluctuation in optical fiber will again cause decoherence and complete data loss. In addition, we numerically showed that if dynamical decoupling is used then the problem of decoherence can be minimized hence increase the rate of error free communication for longer distances.

Finally, we studied the problem of sending entangled photon over the single-mode optical fiber and derived the analytic model of decoherence for general entangled state and showed that decoherence will cause entanglement sudden death. We later numerically showed that the length over which entangled photon can be distributed can be increased by using the technique of dynamical decoupling thus increasing the length for distribution of entangled photon. The Table 7.1 lists all the scenario analyzed analytically and numerically simulated.

Table 7.1: State and Type of fiber.

State	Optical Fiber
Polarization Qubit	PM Fiber
Polarization Qubit	SM Fiber
Polarization Entangled Qubit	SM Fiber
OAM Qudit	MM Fiber

In the appendix, I have explored other directions of research not directly connecting to the theme of this thesis.

7.2 Future Directions

Performance analysis of different DD pulse sequences for OAM photon in optical fiber: In this thesis, we only analyzed the performance of CPMG pulse sequence in preserving the OAM photon but there are other pulse sequences such as UDD, CDD, PDD that needs to be compared because such sequences are known to cancel higher order errors. Further, an optimization study can be done on number of pulses required for a specific length of optical fiber.

Effect of pulse shaping error in optical fiber for OAM photon: Another avenue that needs to be explored for OAM photon is the effect of pulse shaping error in preserving the state of OAM photon. How does the shape of pulse affect the fidelity of DD pulse sequence ? Does use of composite pulse or error correcting pulse have any impact on preserving the state of OAM photon ?

Preserving multidimensional entanglement in optical fiber: A model for decoherence of multi-dimensional entangled state in optical fiber may be derived. Can such entangled state be preserved for long distances in optical fiber ? Does DD help in preserving the multidimensional entanglement or we need some combination of techniques to preserve ? Such questions would need to be explored.

References

[1] T. M. Cover and J. A. Thomas. *Elements of Information Theory.* Wiley & Sons, 1991.

[2] M. Wuilpart, P. Megret, M. Blondel, A.J. Rogers, and Y. Defosse. Measurement of the spatial distribution of birefringence in optical fibers. *Photonics Technology Letters, IEEE*, 13(8):836–838, Aug 2001.

[3] Alexandre M. Souza, Gonzalo A. Álvarez, and Dieter Suter. Robust dynamical decoupling for quantum computing and quantum memory. *Phys. Rev. Lett.*, 106:240501, Jun 2011.

[4] Charles H. Bennett and Stephen J. Wiesner. Communication via one- and two-particle operators on Einstein-Podolsky-Rosen states. *Phys. Rev. Lett.*, 69:2881–2884, Nov 1992.

[5] Michael A. Nielsen and L. Chuang. *Quantum Computation and Quantum Information.* Cambridge University Press, 2000.

[6] Robert G. Gallager. *Information theory and reliable communication.* John Wiley and Sons, 1968.

[7] Christopher Gerry and Peter Knight. *Introductory Quantum Optics.* Cambridge University Press, 2004.

[8] Pieter Kok and Brendon W. Lovett. *Introduction to Optical Quantum Information Processing.* Cambridge University Press, 2010.

[9] Rodney Loudon. *The Quantum Theory of Light.* Oxford University Press, 2000.

[10] J. J. Sakurai. *Modern Quantum Mechanics.* Addison Wesley, 1993.

[11] Bahaa E. A. Saleh and Malvin Carl Teich. *Fundamentals of Photonics*. John Wiley & Sons, Inc., 1991.

[12] Herwig Kogelnik, Robert M. Jopson, and Lynn E. Nelson. Chapter 15 - polarization-mode dispersion. In Ivan P. KaminowTingye Li, editor, *Optical Fiber Telecommunications IV-B (Fourth Edition)*, Optics and Photonics, pages 725 – 861. Academic Press, Burlington, fourth edition edition, 2002.

[13] Andrea Galtarossa and Curtis R. Menyuk. *Polarization Mode Dispersion*, volume 1 of *Optical and Fiber Communications Reports*. Springer, 2005.

[14] Max Born and Emil Wolf. *Principles of Optics*. Pergamon Press, 1989.

[15] Yi-chao Meng and Ming-hua Wu. Stress and modal birefringence of single-mode specialty optical fibers with three-stress regions. *Journal of Shanghai University (English Edition)*, 15(2):137–142, 2011.

[16] Andrea Galtarossa, Luca Palmieri, Marco Schiano, and Tiziana Tambosso. Measurements of beat length and perturbation length in long single-mode fibers. *Opt. Lett.*, 25(6):384–386, Mar 2000.

[17] X. Rong Li. *Probability, Random Signals, and Statistics*. CRC Press, 1999.

[18] Manish K. Gupta, Erik J. Navarro, Todd A. Moulder, Jason D. Mueller, Ashkan Balouchi, Katherine L. Brown, Hwang Lee, and Jonathan P. Dowling. Preserving photon qubits in an unknown quantum state with Knill dynamical decoupling: Towards an all optical quantum memory. *Phys. Rev. A*, 91:032329, Mar 2015.

[19] Peter W. Shor. Scheme for reducing decoherence in quantum computer memory. *Phys. Rev. A*, 52:R2493–R2496, Oct 1995.

[20] Andrew M. Steane. Efficient fault-tolerant quantum computing. *Nature*, 399(6732):124–126, 05 1999.

[21] J. Chiaverini, D. Leibfried, T. Schaetz, M. D. Barrett, R. B. Blakestad, J. Britton, W. M. Itano, J. D. Jost, E. Knill, C. Langer, R. Ozeri, and D. J. Wineland. Realization of quantum error correction. *Nature*, 432(7017):602–605, 12 2004.

[22] P. Zanardi and M. Rasetti. Noiseless quantum codes. *Phys. Rev. Lett.*, 79:3306–3309, Oct 1997.

[23] Lorenza Viola and Seth Lloyd. Dynamical suppression of decoherence in two-state quantum systems. *Phys. Rev. A*, 58:2733–2744, Oct 1998.

[24] Lorenza Viola, Emanuel Knill, and Seth Lloyd. Dynamical decoupling of open quantum systems. *Phys. Rev. Lett.*, 82:2417–2421, Mar 1999.

[25] Lian-Ao Wu and Daniel A. Lidar. Overcoming quantum noise in optical fibers. *Phys. Rev. A*, 70:062310, Dec 2004.

[26] Richard R. Ernst, Geoffrey Bodenhausen, and Alexander Wokaun. *Principles of Nuclear Magnetic Resonance in One and Two Dimensions*. Oxford University Press, 1990.

[27] Bhaskar Roy Bardhan, Petr M. Anisimov, Manish K. Gupta, Katherine L. Brown, N. Cody Jones, Hwang Lee, and Jonathan P. Dowling. Dynamical decoupling in optical fibers: Preserving polarization qubits from birefringent dephasing. *Phys. Rev. A*, 85:022340, Feb 2012.

[28] K. Khodjasteh and D. A. Lidar. Fault-tolerant quantum dynamical decoupling. *Phys. Rev. Lett.*, 95:180501, Oct 2005.

[29] Kaveh Khodjasteh and Daniel A. Lidar. Performance of deterministic dynamical decoupling schemes: Concatenated and periodic pulse sequences. *Phys. Rev. A*, 75:062310, Jun 2007.

[30] M. H. Levitt. *Progress in Nuclear Magnetic Resonance Spectroscopy*, chapter Composite pulses, page 1396 1411. New York, NY: Wiley, 1996.

[31] C.H. Bennett and G. Brassard. Quantum cryptography: Public key distribution and coin tossing. In *Proceedings of the IEEE International Conference on Computers, Systems, and Signal Processing*, 1984.

[32] Nicolas Gisin, Grégoire Ribordy, Wolfgang Tittel, and Hugo Zbinden. Quantum cryptography. *Rev. Mod. Phys.*, 74:145–195, Mar 2002.

[33] D. Stucki, N. Walenta, F. Vannel, R. T. Thew, N. Gisin, H. Zbinden, S. Gray, C. R. Towery, and S. Ten. High rate, long-distance quantum key distribution over 250km of ultra low loss fibres. *New J. Phys.*, 11:075003, 2009.

[34] R. Ursin, F. Tiefenbacher, T. Schmitt-Manderbach, H. Weier, T. Scheidl, M. Lindenthal, B. Blauensteiner, T. Jennewein, J. Perdigues, P. Trojek, B. Omer, M. Furst, M. Meyenburg, J. Rarity, Z. Sodnik, C. Barbieri, H. Weinfurter, and A. Zeilinger. Entanglement-based quantum communication over 144[thinsp]km. *Nat Phys*, 3(7):481–486, 07 2007.

[35] D. Dieks. Communication by {EPR} devices. *Physics Letters A*, 92(6):271–272, 1982.

[36] W. K. Wootters and W. H. Zurek. A single quantum cannot be cloned. *Nature*, 299(5886):802–803, 10 1982.

[37] H.-J. Briegel, W. Dür, J. I. Cirac, and P. Zoller. Quantum repeaters: The role of imperfect local operations in quantum communication. *Phys. Rev. Lett.*, 81:5932–5935, Dec 1998.

[38] Nicolas Sangouard, Christoph Simon, Hugues de Riedmatten, and Nicolas Gisin. Quantum repeaters based on atomic ensembles and linear optics. *Rev. Mod. Phys.*, 83:33–80, Mar 2011.

[39] P. van Loock, T. D. Ladd, K. Sanaka, F. Yamaguchi, Kae Nemoto, W. J. Munro, and Y. Yamamoto. Hybrid quantum repeater using bright coherent light. *Phys. Rev. Lett.*, 96:240501, Jun 2006.

[40] J. Minář, Hugues de Riedmatten, and Nicolas Sangouard. Quantum repeaters based on heralded qubit amplifiers. *Phys. Rev. A*, 85:032313, Mar 2012.

[41] Zhen-Sheng Yuan, Yu-Ao Chen, Bo Zhao, Shuai Chen, Jorg Schmiedmayer, and Jian-Wei Pan. Experimental demonstration of a bdcz quantum repeater node. *Nature*, 454(7208):1098–1101, 08 2008.

[42] Nicolas Sangouard, Romain Dubessy, and Christoph Simon. Quantum repeaters based on single trapped ions. *Phys. Rev. A*, 79:042340, Apr 2009.

[43] Bhaskar Roy Bardhan, Kebei Jiang, and Jonathan P. Dowling. Effects of phase fluctuations on phase sensitivity and visibility of path-entangled photon fock states. *Phys. Rev. A*, 88:023857, Aug 2013.

[44] L. Allen, Stephen M. Barnett, and Miles J. Padgett. *Optical Angular Momentum*. CRC Press, 2003.

[45] David L. Andrews. *Structured Light and Its Applications: An Introduction to Phase-Structured Beams and Nanoscale Optical Forces*. Academic Press, 2008.

[46] L. Allen, M. W. Beijersbergen, R. J. C. Spreeuw, and J. P. Woerdman. Orbital angular momentum of light and the transformation of Laguerre-Gaussian laser modes. *Phys. Rev. A*, 45:8185–8189, Jun 1992.

[47] Helle Bechmann-Pasquinucci and Asher Peres. Quantum cryptography with 3-state systems. *Phys. Rev. Lett.*, 85:3313–3316, Oct 2000.

[48] Vahid Karimipour, Alireza Bahraminasab, and Saber Bagherinezhad. Entanglement swapping of generalized cat states and secret sharing. *Phys. Rev. A*, 65:042320, Apr 2002.

[49] Stephen D. Bartlett, Hubert de Guise, and Barry C. Sanders. Quantum encodings in spin systems and harmonic oscillators. *Phys. Rev. A*, 65:052316, May 2002.

[50] Matthias Fitzi, Nicolas Gisin, and Ueli Maurer. Quantum Solution to the Byzantine Agreement Problem. *Phys. Rev. Lett.*, 87:217901, Nov 2001.

[51] Andris Ambainis. A new protocol and lower bounds for quantum coin flipping. *Journal of Computer and System Sciences*, 68(2):398 – 416, 2004. Special Issue on {STOC} 2001.

[52] Artur K. Ekert. Quantum cryptography based on bell's theorem. *Phys. Rev. Lett.*, 67:661–663, Aug 1991.

[53] A. R. Dixon, Z. L. Yuan, J. F. Dynes, A. W. Sharpe, and A. J. Shields. Continuous operation of high bit rate quantum key distribution. *Applied Physics Letters*, 96(16):–, 2010.

[54] S. Etcheverry, G. Canas, E. S. Gomez, W. A. T. Nogueira, C. Saavedra, G. B. Xavier, and G. Lima. Quantum key distribution session with 16-dimensional photonic states. *Sci. Rep.*, 3, 07 2013.

[55] Gabriel Molina-Terriza, Juan P. Torres, and Lluis Torner. Management of the angular momentum of light: Preparation of photons in multidimensional vector states of angular momentum. *Phys. Rev. Lett.*, 88:013601, Dec 2001.

[56] H. Bechmann-Pasquinucci and W. Tittel. Quantum cryptography using larger alphabets. *Phys. Rev. A*, 61:062308, May 2000.

[57] Simon Groblacher, Thomas Jennewein, Alipasha Vaziri, Gregor Weihs, and Anton Zeilinger. Experimental quantum cryptography with qutrits. *New Journal of Physics*, 8(5):75, 2006.

[58] Nenad Bozinovic, Yang Yue, Yongxiong Ren, Moshe Tur, Poul Kristensen, Hao Huang, Alan E. Willner, and Siddharth Ramachandran. Terabit-scale orbital angular momentum mode division multiplexing in fibers. *Science*, 340(6140):1545–1548, 2013.

[59] Martin B. Plenio and Shashank Virmani. An Introduction to entanglement measures. *Quant. Inf. Comput.*, 7:1–51, 2007.

[60] Xiaoying Li, Paul L. Voss, Jun Chen, Jay E. Sharping, and Prem Kumar. Storage and long-distance distribution of telecommunications-band polarization entanglement generated in an optical fiber. *Opt. Lett.*, 30(10):1201–1203, May 2005.

[61] Cristian Antonelli, Mark Shtaif, and Misha Brodsky. Distance limitations on the entanglement distribution over optical fiber due to chromatic and polarization mode dispersion. In *CLEO:2011 - Laser Applications to Photonic Applications*, page CThX3. Optical Society of America, 2011.

[62] Hannes Hübel, Michael R. Vanner, Thomas Lederer, Bibiane Blauensteiner, Thomas Lorünser, Andreas Poppe, and Anton Zeilinger. High-fidelity transmission of polarization encoded qubits from an entangled source over 100 km of fiber. *Opt. Express*, 15(12):7853–7862, Jun 2007.

[63] Han Chuen Lim, Akio Yoshizawa, Hidemi Tsuchida, and Kazuro Kikuchi. Distribution of polarization-entangled photon-pairs produced via spontaneous parametric down-conversion within a local-area fiber network: Theoretical model and experiment. *Opt. Express*, 16(19):14512–14523, Sep 2008.

[64] Chuang Liang, Kim Fook Lee, Jun Chen, and P. Kumar. Distribution of fiber-generated polarization entangled photon-pairs over 100 km of standard fiber

in oc-192 wdm environment. In *Optical Fiber Communication Conference, 2006 and the 2006 National Fiber Optic Engineers Conference. OFC 2006*, pages 1–3, March 2006.

[65] L. M. Duan, M. D. Lukin, J. I. Cirac, and P. Zoller. Long-distance quantum communication with atomic ensembles and linear optics. *Nature*, 414(6862):413–418, 11 2001.

[66] Florian Mintert, Andr R.R. Carvalho, Marek Ku, and Andreas Buchleitner. Measures and dynamics of entangled states. *Physics Reports*, 415(4):207 – 259, 2005.

[67] Leandro Aolita, Fernando de Melo, and Luiz Davidovich. Open-system dynamics of entanglement:a key issues review. *Reports on Progress in Physics*, 78(4):042001, 2015.

[68] Chiara Macchiavello. On the role of entanglement in quantum information. *Physica A: Statistical Mechanics and its Applications*, 338(12):68 – 75, 2004. Proceedings of the conference A Nonlinear World: the Real World, 2nd International Conference on Frontier Science.

[69] Reinhard F. Werner. Quantum states with Einstein-Podolsky-Rosen correlations admitting a hidden-variable model. *Phys. Rev. A*, 40:4277–4281, Oct 1989.

[70] Ryszard Horodecki, Paweł Horodecki, Michał Horodecki, and Karol Horodecki. Quantum entanglement. *Rev. Mod. Phys.*, 81:865–942, Jun 2009.

[71] Frank Verstraete and Michael M. Wolf. Entanglement versus bell violations and their behavior under local filtering operations. *Phys. Rev. Lett.*, 89:170401, Oct 2002.

[72] R. Lo Franco, A. D'Arrigo, G. Falci, G. Compagno, and E. Paladino. Preserving entanglement and nonlocality in solid-state qubits by dynamical decoupling. *Phys. Rev. B*, 90:054304, Aug 2014.

[73] Scott Hill and William K. Wootters. Entanglement of a pair of quantum bits. *Phys. Rev. Lett.*, 78:5022–5025, Jun 1997.

[74] William K. Wootters. Entanglement of formation of an arbitrary state of two qubits. *Phys. Rev. Lett.*, 80:2245–2248, Mar 1998.

[75] Ting Yu and J. H. Eberly. Evolution from entanglement to decoherence of bipartite mixed "x" states. *Quantum Info. Comput.*, 7(5):459–468, July 2007.

[76] Jin Wang, Herman Batelaan, Jeremy Podany, and Anthony F Starace. Entanglement evolution in the presence of decoherence. *Journal of Physics B: Atomic, Molecular and Optical Physics*, 39(21):4343, 2006.

[77] J. S. Pratt. Universality in the entanglement structure of ferromagnets. *Phys. Rev. Lett.*, 93:237205, Dec 2004.

[78] S. Bose, I. Fuentes-Guridi, P. L. Knight, and V. Vedral. Subsystem purity as an enforcer of entanglement. *Phys. Rev. Lett.*, 87:050401, Jul 2001.

[79] H. Y. Carr and E. M. Purcell. Effects of diffusion on free precession in nuclear magnetic resonance experiments. *Phys. Rev.*, 94:630–638, May 1954.

[80] S. Meiboom and D. Gill. Modified spinecho method for measuring nuclear relaxation times. *Review of Scientific Instruments*, 29(8):688–691, 1958.

[81] Götz S. Uhrig. Keeping a Quantum Bit Alive by Optimized π-Pulse Sequences. *Phys. Rev. Lett.*, 98:100504, Mar 2007.

[82] John J. L. Morton, Alexei M. Tyryshkin, Arzhang Ardavan, Kyriakos Porfyrakis, S. A. Lyon, and G. Andrew D. Briggs. Measuring errors in single-qubit rotations by pulsed electron paramagnetic resonance. *Phys. Rev. A*, 71:012332, Jan 2005.

[83] Łukasz Cywiński, Roman M. Lutchyn, Cody P. Nave, and S. Das Sarma. How to enhance dephasing time in superconducting qubits. *Phys. Rev. B*, 77:174509, May 2008.

[84] Ashok Ajoy, Gonzalo A. Álvarez, and Dieter Suter. Optimal pulse spacing for dynamical decoupling in the presence of a purely dephasing spin bath. *Phys. Rev. A*, 83:032303, Mar 2011.

[85] Pieter Kok, W. J. Munro, Kae Nemoto, T. C. Ralph, Jonathan P. Dowling, and G. J. Milburn. Linear optical quantum computing with photonic qubits. *Rev. Mod. Phys.*, 79:135–174, Jan 2007.

[86] T. Chaneliere, D. N. Matsukevich, S. D. Jenkins, S. Y. Lan, T. A. B. Kennedy, and A. Kuzmich. Storage and retrieval of single photons transmitted between remote quantum memories. *Nature*, 438(7069):833–836, 12 2005.

[87] S. Massar and S. Popescu. Reducing polarization mode dispersion with controlled polarization rotations. *New J. Phys.*, 9:158, 2007.

[88] S. Damodarakurup, M. Lucamarini, G. Di Giuseppe, D. Vitali, and P. Tombesi. Experimental inhibition of decoherence on flying qubits via "bang-bang" control. *Phys. Rev. Lett.*, 103:040502, Jul 2009.

[89] M. Lucamarini, G. Di. Giuseppe, D. Vitali, and P. Tombesi. Open-loop and closed-loop control of flying qubits. *J. Phys. B: At. Mol. Opt. Phys.*, 44:154005, 2011.

[90] S. Meiboom and D. Gill. Modified spinecho method for measuring nuclear relaxation times. *Review of Scientific Instruments*, 29(8):688–691, 1958.

[91] N. González, G. Molina-Terriza, and J. P. Torres. How a dove prism transforms the orbital angular momentum of a light beam. *Opt. Express*, 14(20):9093–9102, Oct 2006.

[92] Vittorio Giovannetti, Seth Lloyd, and Lorenzo Maccone. Advances in quantum metrology. *Nat Photon*, 5(4):222–229, 04 2011.

[93] Florian Wolfgramm, Chiara Vitelli, Federica A. Beduini, Nicolas Godbout, and Morgan W. Mitchell. Entanglement-enhanced probing of a delicate material system. *Nat Photon*, 7(1):28–32, 01 2013.

[94] Michael A. Taylor, Jiri Janousek, Vincent Daria, Joachim Knittel, Boris Hage, BachorHans-A., and Warwick P. Bowen. Biological measurement beyond the quantum limit. *Nat Photon*, 7(3):229–233, 03 2013.

[95] Barry C. Sanders. Quantum dynamics of the nonlinear rotator and the effects of continual spin measurement. *Phys. Rev. A*, 40:2417–2427, Sep 1989.

[96] Hwang Lee, Pieter Kok, and Jonathan P. Dowling. A quantum rosetta stone for interferometry. *Journal of Modern Optics*, 49(14-15):2325–2338, 2002.

[97] G. Gilbert and Y. S. Weinstein. Aspects of practical remote quantum sensing. *Journal of Modern Optics*, 55(19-20):3283–3291, 11 2008.

[98] Mark A. Rubin and Sumanth Kaushik. Loss-induced limits to phase measurement precision with maximally entangled states. *Phys. Rev. A*, 75:053805, May 2007.

[99] U. Dorner, R. Demkowicz-Dobrzanski, B. J. Smith, J. S. Lundeen, W. Wasilewski, K. Banaszek, and I. A. Walmsley. Optimal quantum phase estimation. *Phys. Rev. Lett.*, 102:040403, Jan 2009.

[100] R. Demkowicz-Dobrzanski, U. Dorner, B. J. Smith, J. S. Lundeen, W. Wasilewski, K. Banaszek, and I. A. Walmsley. Quantum phase estimation with lossy interferometers. *Phys. Rev. A*, 80:013825, Jul 2009.

[101] Kacprowicz M., Demkowicz-Dobrzanski R., Wasilewski W., Banaszek K., and Walmsley I. A. Experimental quantum-enhanced estimation of a lossy phase shift. *Nat Photon*, 4(6):357–360, 06 2010.

[102] Hossein T. Dinani and Dominic W. Berry. Loss-resistant unambiguous phase measurement. *Phys. Rev. A*, 90:023856, Aug 2014.

[103] Stefan Scheel. Decoherence of nonclassical states of light can be very efficiently used in optical sensor technology. *Journal of Modern Optics*, 50(8):1327–1334, 05 2003.

[104] A. Neville, M. Berry J. L. O'Brien H. Cable R. Whittaker, C. Erven and J. C. F. Matthews. Quantum-enhanced absorption spectroscopy. *arXiv:1508.00849*, 2015.

[105] J. D. Jackson. *Classical electrodynamics*. Wiley, 1999.

[106] R. G. Beausoleil, W. J. Munro, and T. P. Spiller. Applications of coherent population transfer to quantum information processing. *Journal of Modern Optics*, 51(11):1559–1601, 07 2004.

[107] D. A. Steck. Sodium d line data. 2001.

[108] J. R. Jeffers, N. Imoto, and R. Loudon. Quantum optics of traveling-wave attenuators and amplifiers. *Phys. Rev. A*, 47:3346–3359, Apr 1993.

[109] R. Loudon. *The quantum theory of light*. Oxford University Press, 2001.

[110] Tae-Woo Lee, Sean D. Huver, Hwang Lee, Lev Kaplan, Steven B. McCracken, Changjun Min, Dmitry B. Uskov, Christoph F. Wildfeuer, Georgios Veronis, and Jonathan P. Dowling. Optimization of quantum interferometric metrological sensors in the presence of photon loss. *Phys. Rev. A*, 80:063803, Dec 2009.

[111] Samuel L. Braunstein and Carlton M. Caves. Statistical distance and the geometry of quantum states. *Phys. Rev. Lett.*, 72:3439–3443, May 1994.

[112] *D. Bratton and J. Kennedy, Proceedings of the 2007 IEEE Swarm Intelligence Symposium*, 2007.

Appendix A
Quantum enhanced spectroscopy with entangled multi-photon states

A.1 Introduction

The goal of quantum metrology is to obtain the most precise measurements possible with minimal resources [92]. Many types of high-precision measurement use a form of interferometry. In interferometers, the unknown parameter is imprinted as the relative phase between a superposition of states. Measurement of the output state, after quantum interference, gives information about the unknown parameter.

One particular example is optical interferometry with Mach-Zehnder interferometers. In this case, using N independent photons gives $1/\sqrt{N}$ scaling for the uncertainty of phase measurements, which is known as the standard quantum limit. However, using N entangled photons gives $1/N$ scaling for the phase uncertainty, which is often called the Heisenberg limit. This enhancement in sensitivity is of much importance in probing delicate systems such as atoms [93] and biological samples [94].

A well-known type of entangled states is NOON states [95, 96]. NOON states saturate the Heisenberg limit. However, in the presence of absorption, NOON states perform poorly [97, 98] and other states must be considered [99, 100, 101, 102]. Even with such states, the advantage over the standard quantum limit is reduced by loss. However, we can take advantage of the sensitivity of nonclassical properties of quantum states to absorption. The sensitivity of quantum coherence can be used efficiently to estimate absorption [103], and also estimate physical quantities that the absorption depends on.

In Ref. [104] a sub-shot-noise measurement of absorption is obtained using heralded single photons. In that work, a non-interferometric setup was used, where all the information is obtained from absorption, and the quantum enhancement results from sub-Poissonian statistics of single photons. According to the Kramers-Kronig relation, absorption is

accompanied by a phase shift [105]. However, the information from the phase is only accessible if we take advantage of superposition and interference.

One would think, since NOON states have coherence which is highly sensitive to loss, they could be the best candidates to sense loss or a parameter which causes loss in the system. However, here we show that for the task of spectroscopy, when there is an advantage to using entangled states, it is possible to find more general entangled states that perform better than NOON states.

The system we are considering here is an ensemble of atoms. We are interested in measuring a transition frequency of the atoms. If this ensemble is probed by a beam of photons, the absorption of photons, and phase shift imposed on the probe, both depend on the transition frequency of atoms. We consider a Mach-Zehnder interferometer with the atomic ensemble placed in one of the arms of the interferometer. We optimize over the state in the arms of the interferometer and find the state from which we obtain the maximum information about the atomic transition frequency.

A.2 Interferometric scheme

Consider a Mach-Zehnder interferometer, as shown in Figure A.1, with an ensemble of atoms placed in the upper arm of the interferometer. Here, we consider an ensemble of identical two-level atoms in the absence of Doppler broadening and dipole dephasing. This simple model gives a good qualitative description of the problem. Assuming that all atoms interact equally with the input quantum state and that there is no interaction between atoms, using the dipole and rotating-wave approximation the susceptibility of the ensemble is given by [8, 106]

$$\chi(\Delta) = \chi'(\Delta) + i\chi''(\Delta) = \frac{2\mathcal{N}\mu^2}{\hbar\varepsilon_0}\frac{\Delta + i\gamma_s}{\Delta^2 + \gamma_s^2}, \tag{A.1}$$

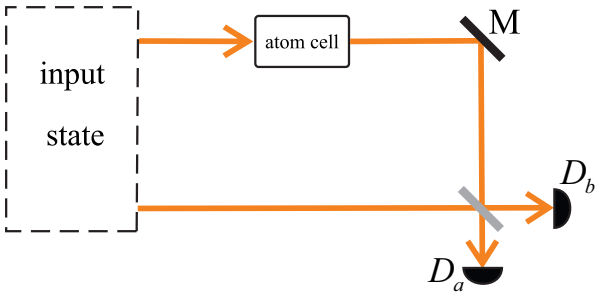

Figure A.1: A Mach-Zehnder interferometer with an ensemble of atoms placed in the upper arm. D_a and D_b are photon number detectors in the output modes.

where $\Delta = \omega - \omega_0$ is the detuning between ω_0, the transition frequency of atoms, and ω, the frequency of input photons, γ_s is the spontaneous decay rate of the excited state, $\mathcal{N}$ is the number density of atoms, μ is the electric dipole moment, $\hbar$ is the reduced Planck constant and ε_0 is the vacuum permittivity. Details of the derivation of this susceptibility based on interaction of an ensemble of atoms with quantized light are given in Refs. [8, 106].

The imaginary and real parts of the susceptibility are plotted in Figure A.2. In this figure we have used data for the D1 transition line of sodium from Ref. [107]; i.e. $\mu = 0.704 \times 10^{-29}$ C $\cdot$ m and $\gamma_s = 61.354 \times 10^6$ s^{-1}. For the number density of atoms we have used $\mathcal{N} = 2.5 \times 10^{16}$ m^{-3}.

Knowing the susceptibility of the atomic medium, the effect of the atomic ensemble in the upper arm of the Mach-Zehnder interferometer can be modeled by the beam splitter model proposed in Refs. [108, 109]. Normally, one beam splitter is used to model loss

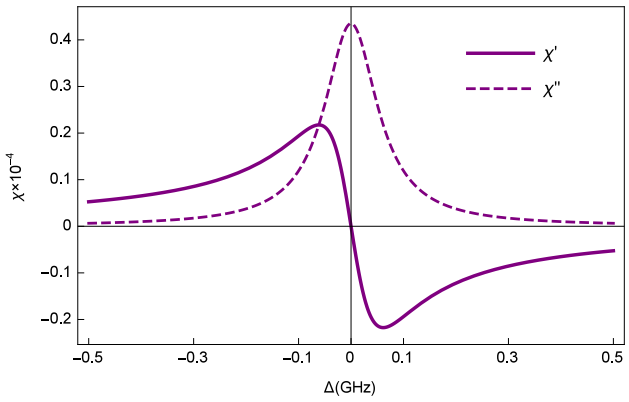

Figure A.2: Real (solid line) and imaginary (dashed line) parts of susceptibility, χ' and χ'' respectively, for an ensemble of two level atoms.

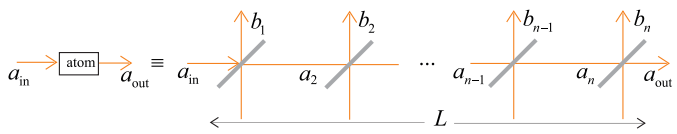

Figure A.3: Beam splitter model to model the interaction of photons with the ensemble of atoms.

in each of the arms of a Mach-Zehnder interferometer [100, 102, 110]. However, here we consider a line of n beam splitters, shown in Figure A.3 where each beam splitter represents one of the atoms in the ensemble. The kth beam splitter transforms the creation operator $a_k^\dagger$ according to

$$a_k^\dagger = \sqrt{t(\omega)}a_{k+1}^\dagger + \sqrt{r(\omega)}b_k^\dagger, \tag{A.2}$$

where $t(\omega)$ and $r(\omega)$ are the transmissivity and reflectivity of the beam splitter, ω is the frequency of input photons, and b_k is the loss mode of the k-th beam splitter.

The effect of the atomic ensemble is obtained by applying all the beam splitters, and taking the limit as the number of beam splitters approaches infinity. The creation operator of the input mode $a_{\text{in}}^\dagger$ is therefore transformed to [108, 109]

$$\begin{aligned} a_{\text{in}}^\dagger = {} & a_{\text{out}}^\dagger e^{-i\frac{\omega L}{c}\sqrt{1+\chi}} \\ & -i\sqrt{\frac{\omega}{c}\chi''}\int_0^L e^{-i\frac{\omega}{c}(L-z)\sqrt{1+\chi}}b^\dagger(z)dz, \end{aligned} \tag{A.3}$$

where L is the length of the ensemble, ω is the frequency of the input photons, c is the speed of light and χ'' is the imaginary part of the susceptibility of the atomic ensemble $\chi = \chi' + i\chi''$. The real part of susceptibility, χ', describes dispersion and the imaginary part, χ'', describes absorption by the ensemble.

From Eq. (A.3), the transmissivity of the ensemble, T, and the phase shift imposed on the state from the ensemble, φ, can be written in terms of the imaginary and real parts of the susceptibility

$$T = e^{-\chi''\omega L/c}, \qquad \varphi = -\frac{\chi'\omega L}{2c}. \tag{A.4}$$

Here, we have used the approximation $\sqrt{1+\chi} \approx 1 + \chi/2$. The quantities T and φ are plotted in Figure A.4. This figure is plotted for $\omega_0 = 2\pi(508.33)$ THz, which is the D1 transition line of sodium [107], and $L = 1$ cm. As can be seen from Figure A.4, for detunings close to zero, φ has the highest slope. However, in this region, T is very small.

In the following section we find the optimal states to measure the transition frequency of the atoms i.e., Δ in this scheme.

A.3 Optimized states

We consider the general form of the state in the arms of the interferometer to be

$$|\psi\rangle = \sum_{k=0}^{N} \psi_k |N-k, k\rangle, \tag{A.5}$$

i.e., a pure state with the total photon number of N. We use Fisher information as the measure to quantify the metrological value of the states. According to the Cramér-Rao bound [111] the variance in estimating a parameter, Δ in this case, using an unbiased estimate, is lower bounded by the inverse of the Fisher information $F(\Delta)$

$$\mathrm{var}(\Delta) \geq 1/F(\Delta). \tag{A.6}$$

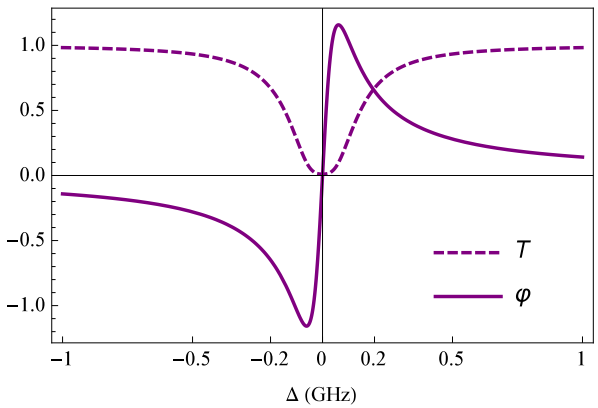

Figure A.4: Transmissivity T (dashed line) and phase shift φ (solid line) vs. detuning Δ.

Here, we are considering photon number detection in the output modes, thus we are using classical rather than quantum Fisher information. The Fisher information represents the amount of information about Δ contained in the measurement results. It is given as

$$F(\Delta) = \sum_{n_1,n_2} \frac{1}{P_{n_1,n_2}(\Delta)} \left(\frac{\partial P_{n_1,n_2}(\Delta)}{\partial \Delta} \right)^2, \tag{A.7}$$

where $P_{n_1,n_2}(\Delta)$ is the probability of detecting n_1 and n_2 photons in each of the output ports.

Considering the state given in Eq. (A.5), applying the atom cell transformation given in Eq. (A.3) on the first mode, and the last 50/50 beam splitter of the interferometer on both modes, we obtain

$$\begin{aligned} P_{n_1,n_2}(\omega) = & \sum_{k=0}^{n_1+n_2} \sum_{k'=0}^{n_1+n_2} \sum_{u=n_2-k}^{n_2} \sum_{v=n_2-k'}^{n_2} \psi_k \psi_{k'}^* \frac{n_1! n_2! (N-n_1-n_2)!}{\sqrt{k!k'!(N-k)!(N-k')!}} \left(\frac{1}{2}\right)^{n_1+n_2} (-1)^{k-n_2} \\ & \times \binom{N-k'}{N-n_1-n_2} \binom{N-k}{N-n_1-n_2} \binom{n_1+n_2-k}{u} \binom{n_1+n_2-k'}{v} \binom{k}{k+u-n_2} \binom{k'}{k'+v-n_2} \\ & \times \left(1-e^{-\omega L \chi''/c}\right)^{N-n_1-n_2} e^{i\omega \chi' L(k-k')/(2c)} e^{-\omega L \chi''(2n_1+2n_2-k-k')/(2c)}, \end{aligned} \tag{A.8}$$

where $\omega = \Delta + \omega_0$ is the frequency of the photons in the input state. Because we are quantifying the metrological value of the states via the Fisher information, we regard the optimal states to be those which maximize the Fisher information. We have found the optimal values of ψ_k numerically using the particle swarm optimization (PSO) algorithm.

In the PSO algorithm a swarm of particles search the space of ψ_k coefficients for those that maximize the Fisher information. Each particle has a velocity $\vec{v}$ and position $\vec{x}$ which are updated to $\vec{v}'$ and $\vec{x}'$ according to its best previous position $\vec{x}_\ell$, and the best position

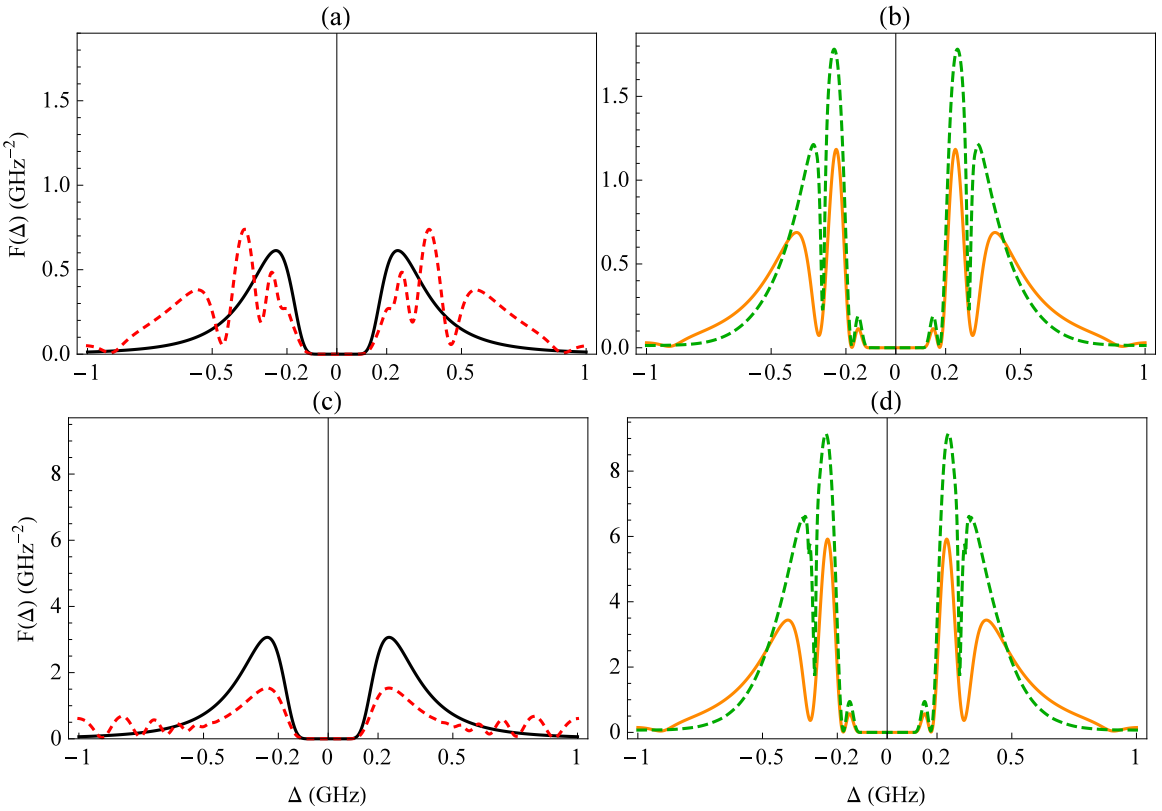

Figure A.5: Fisher information $F(\Delta)$ versus detuning Δ for $N = 2$ photons (upper row) and $N = 10$ (lower row). Solid-black line: N independent single photons $|1,0\rangle^{\otimes N}$. Dashed-red line: N-photon NOON state $(|N,0\rangle + |0,N\rangle)/\sqrt{2}$. Dashed green line: N-photon optimal state. Solid-orange line: N copies of single-photon NOON states $(|1,0\rangle + |0,1\rangle)/\sqrt{2}$.

of the entire swarm $\vec{x}_g$ as [112]

$$\vec{x}' = \vec{x} + \vec{v}',$$
$$\vec{v}' = \chi[\vec{v} + c_g r_g(\vec{x_g} - \vec{x}) + c_\ell r_\ell(\vec{x_\ell} - \vec{x})]. \tag{A.9}$$

Here, r_g and r_ℓ are uniform random numbers in the interval $[0,1]$, and χ, c_g and c_ℓ are constants. In our simulations, we used $\chi = 0.729$, $c_\ell = c_g = 2.05$ with 10 particles and 100 iterations.

We have found that the optimal state for a specific type of atoms, only depends on the product of the number density of atoms and cell length, $\mathcal{N}L$. This can be explained in the

following way. In Eqs. (A.4) and (A.8), we have $\omega\chi' L$ and $\omega\chi'' L$ which can be written as

$$\omega\chi L = \omega L(\chi' + \chi'') = \frac{2\mathcal{N}L\mu^2\omega_0}{\hbar\varepsilon_0\gamma_s}\frac{(\Delta/\gamma_s + i)(1 + \Delta/\omega_0)}{1 + (\Delta/\gamma_s)^2}. \tag{A.10}$$

For a given type of atom the multiplying factor at the front can only be varied via $\mathcal{N}$ or L. The other parameters, μ, ω_0 and γ_s can be varied by changing the type of atom. These parameters affect the variation of $\omega\chi$ in three ways:

1. They change the multiplicative factor at the front. As that factor can also be changed by varying $\mathcal{N}$ or L, that does not give any qualitatively different results than simply changing $\mathcal{N}$ or L.

2. The parameter γ_s appears in the ratio Δ/γ_s, and therefore provides a scaling to the variation of $\omega\chi L$ with Δ. It therefore does not qualitatively change the results.

3. The parameter ω_0 appears in the factor $(1 + \Delta/\omega_0)$. This factor affects the variation very little, because we consider a parameter regime where $\Delta/\omega_0 \ll 1$.

In the following we keep L constant at 1 cm and discuss the two cases: $\mathcal{N} > 10^{17}$ m^{-3} (large $\mathcal{N}$) and $\mathcal{N} < 10^{17}$ m^{-3} (small $\mathcal{N}$).

A.3.1 Large $\mathcal{N}$

For $\mathcal{N} > 10^{17}$ m^{-3}, we have found that numerically optimized states of the form given in Eq. (A.5) perform better than NOON states and independent single photons. In Figure A.5 we have compared the Fisher information of the N-photon optimal state, N independent single photon states $|1,0\rangle^{\otimes N}$, N copies of a single-photon NOON state $(|1,0\rangle + |0,1\rangle)/\sqrt{2}$, and an N-photon NOON state $(|N,0\rangle + |0,N\rangle)/\sqrt{2}$. This figure is plotted for $N = 2$ (upper row) and $N = 10$ (lower row). In this figure, we have used $\omega_0 = 2\pi(508.332)$ THz, which is the transition frequency of the D1 line of sodium [107], and an atom density of $\mathcal{N} = 2.5 \times 10^{17}$ m^{-3}.

Figure A.5 shows that, even for $N = 2$, the enhancement obtained by optimal states is significant. For larger photon numbers, as is shown in the graphs for $N = 10$, there is no further significant improvement in the enhancement of the optimal states. Moreover, the optimal states with high photon numbers are not experimentally achievable with the current technology. On the other hand, it may be possible to generate the optimal states for $N = 2$ with a scheme similar to the one proposed in Ref. [102].

Note that, close to resonance, for copies of single-photon NOON states the maximum peak is higher than for independent single photons and N-photon NOON states. This is as would be expected, since single-photon NOON states are the least sensitive NOON states to loss. From Figure A.5(c), we see that ten-photon NOON states perform worse than independent single photons close to resonance. However, far from resonance, their Fisher information is even higher than the numerically obtained optimal states. The reason why this is possible is that the optimal states are only optimal in the sense of giving the largest maximum Fisher information, but it is possible for other states to have larger Fisher information for detunings where the optimal states do not give their maximum Fisher information. On the other hand, as can be seen in Figure A.5(a), two-photon NOON states are less sensitive to loss (compared to ten-photon NOON states), and close to resonance they perform better than independent single photons.

The other thing to note from Figure A.5 is that to be able to work in the region with maximum Fisher information we need to have prior knowledge of the detuning. This is because the peaks of maximum Fisher information are quite narrow. In other words this scheme could be used to measure hyperfine splitting of atomic levels, or measure external effects, such as magnetic field, on the transition frequency of atoms.

In Figure A.6 we have plotted the values of the coefficients of the optimal states, ψ_k in the superposition (A.5), for a range of photon numbers from $N = 2$ to $N = 10$. This figure shows that the optimal states have higher amplitudes for the terms with higher photon numbers in the arm that contains the atomic ensemble. That is, when there are

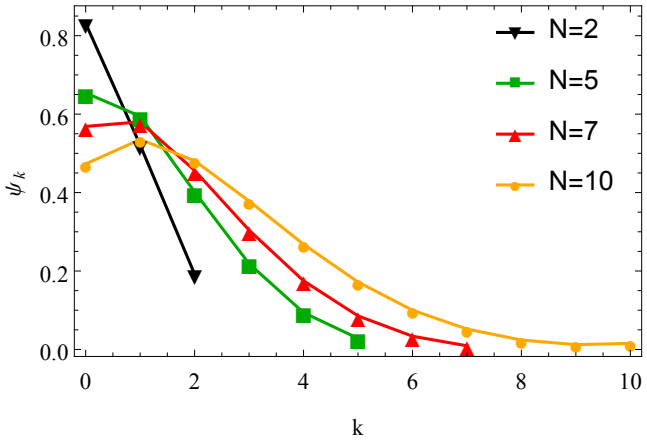

Figure A.6: Coefficients ψ_k of the optimal states, for four values of the total photon number N.

more photons in the arm with the ensemble, they are more likely to be lost, giving more information about Δ.

A.3.2 Small $\mathcal{N}$

For smaller values of $\mathcal{N}$ than considered in the previous subsection, the range of the phase shift is smaller (see Figure A.7). In this case, the optimal state is N independent single photons, $|1,0\rangle^{\otimes N}$. Having all the photons in the upper arm, only the loss is being probed, and no information is being obtained from the phase shift. The phase shift must be significant so that we can take advantage of interferometric schemes in spectroscopy. Surprisingly for $\mathcal{N} = 2.5 \times 10^{16}$ m^{-3} the maximum of the Fisher information for N independent single photons is even higher than the maximum of the Fisher information for the N-photon numerically optimized states with a larger number density of atoms which were considered in the previous subsection (see Figure A.8).

This could be understood from the variation of the transmissivity T and phase shift φ with $\mathcal{N}$, shown in Figure A.7. For smaller values of $\mathcal{N}$ the range of the phase shift is also smaller, which eliminates the advantage in using entangled states. In this case, the Fisher information is coming from the variation in the absorption. As $\mathcal{N}$ is decreased further, the dip in the absorption is reduced which results in a smaller Fisher information. For the

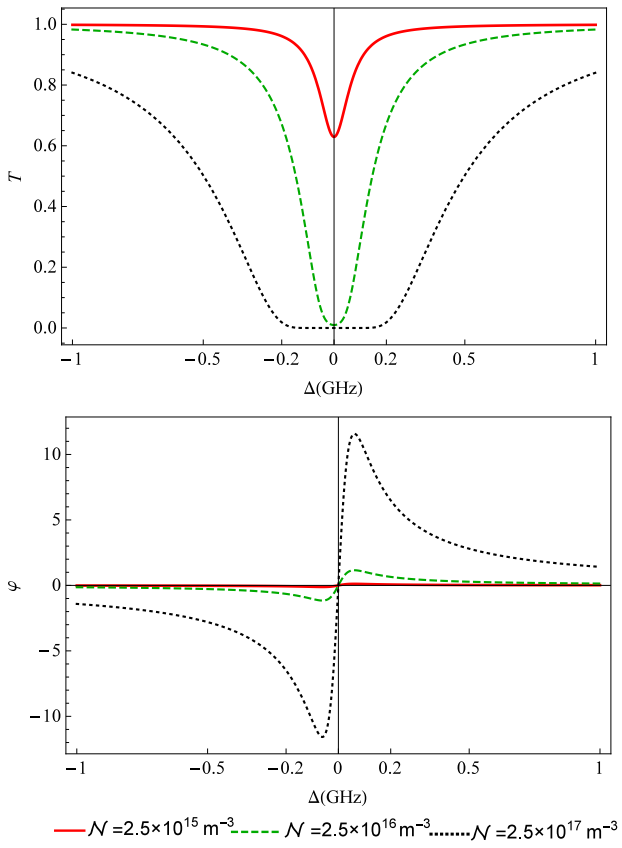

Figure A.7: Transmissivity T and phase shift φ versus Δ, for a range of values of number density of atoms $\mathcal{N}$.

higher densities, there is a larger phase shift, but it is in a region where the absorption is very high.

A.4 Conclusion

In this work we found optimal multi-photon states for measurement of the transition frequency of atoms. The scheme proposed here is an interferometric scheme with photon number detection in the output. In order to find the best states for measurement of the transition frequency, we numerically optimised for the states that provide the largest Fisher information.

For the number density of atoms we considered initially, the imposed phase on the probe is large, and it is advantageous to using information from both the absorption and

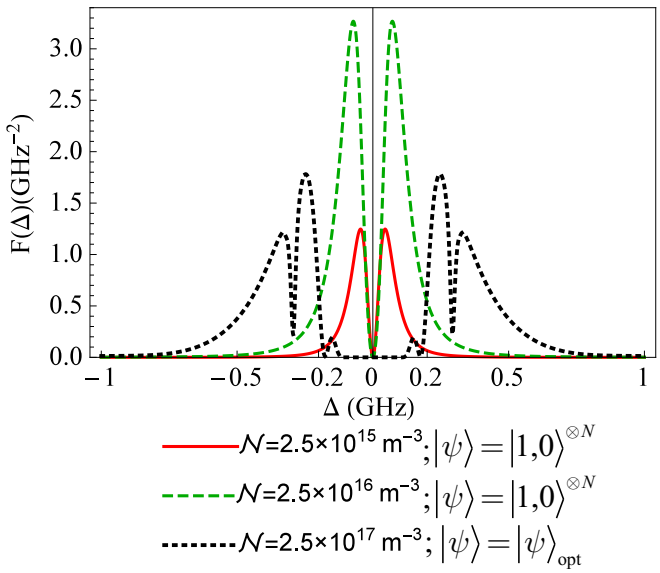

Figure A.8: Fisher information versus Δ for total number of photons $N = 2$, for a range of number densities of atoms $\mathcal{N}$. Solid, red line: N independent single photons with $\mathcal{N} = 2.5\times10^{15}$ m^{-3}. Dashed, green line: N independent single photons with $\mathcal{N} = 2.5\times10^{16}$ m^{-3}. Dashed, black line: numerically optimized state with $\mathcal{N} = 2.5 \times 10^{17}$ m^{-3}.

the phase shift for measuring the transition frequency. In this case, the optimal state is an entangled multi-photon state. This optimal state has a large weighting on the state with all photons in the arm with the atomic ensemble. On the other hand, for a smaller number density of atoms, the phase shift imposed on the probe is small and therefore the information from the phase shift is not significant enough to give any advantage. In this case, it is advantageous to pass all the photons through the atom cell and obtain all the information from absorption.

Surprisingly there is a value of the number density, $\mathcal{N} = 2.5 \times 10^{16}$ m^{-3}, for which N independent single photons have the highest Fisher information; even higher than the Fisher information for the N-photon numerically optimised states with a larger number density of atoms.

Appendix B
Reuse and Permissions

B.1 APS Copyright Policies

What is copyright? http://www.copyright.gov/

Copyright is a form of legal protection for original works of authorship. Copyright covers both published and unpublished works.

What does copyright protect?

Copyright, a form of intellectual property law, protects original works of authorship including literary, dramatic, musical, and artistic works, such as poetry, novels, movies, songs, computer software, and architecture. Copyright does not protect facts, ideas, systems, or methods of operation, although it may protect the way these things are expressed. See Circular 1, Copyright Basics, section "What Works Are Protected", see http://www.copyright.gov/circs/circ01.pdf

As the author of an APS-published article, may I use figures, tables, graphs, etc. in future publications?

Yes, as the author you have the right to use figures, tables, graphs, etc. in subsequent publications using files prepared and formatted by you or the APS-prepared versions. The appropriate bibliographic citation must be included.

As the author of an APS-published article, may I include my article or a portion of my article in my thesis or dissertation?

Yes, the author has the right to use the article or a portion of the article in a thesis or dissertation without requesting permission from APS, provided the bibliographic citation and the APS copyright credit line are given on the appropriate pages.

AMERICAN PHYSICAL SOCIETY LICENSE
TERMS AND CONDITIONS

May 19, 2016

This Agreement between Manish Kumar Gupta ("You") and American Physical Society ("American Physical Society") consists of your license details and the terms and conditions provided by American Physical Society and Copyright Clearance Center.

License Number	3867131405494
License date	May 13, 2016
Licensed Content Publisher	American Physical Society
Licensed Content Publication	Physical Review A
Licensed Content Title	Preserving photon qubits in an unknown quantum state with Knill dynamical decoupling: Towards an all optical quantum memory
Licensed Content Author	Manish K. Gupta et al.
Licensed Content Date	Mar 30, 2015
Licensed Content Volume Number	91
Type of Use	Thesis/Dissertation
Requestor type	Student
Format	Electronic
Portion	image/photo
Number of images/photos requested	6
Portion description	Figure: 1,2,3,4,5,6
Rights for	Main product
Duration of use	Life of Current Edition
Creation of copies for the disabled	no
With minor editing privileges	no
For distribution to	United States
In the following language(s)	Original language of publication
With incidental promotional use	no
The lifetime unit quantity of new product	0 to 499
The requesting person/organization is:	Manish Kumar Gupta
Order reference number	None
Title of your thesis / dissertation	MINIMIZING DECOHERENCE IN OPTICAL FIBER FOR LONG DISTANCE QUANTUM COMMUNICATION
Expected completion date	Aug 2016

AMERICAN PHYSICAL SOCIETY LICENSE
TERMS AND CONDITIONS

May 19, 2016

This Agreement between Manish Kumar Gupta ("You") and American Physical Society ("American Physical Society") consists of your license details and the terms and conditions provided by American Physical Society and Copyright Clearance Center.

License Number	3867131201898
License date	May 13, 2016
Licensed Content Publisher	American Physical Society
Licensed Content Publication	Physical Review A
Licensed Content Title	Dynamical decoupling in optical fibers: Preserving polarization qubits from birefringent dephasing
Licensed Content Author	Bhaskar Roy Bardhan et al.
Licensed Content Date	Feb 28, 2012
Licensed Content Volume Number	85
Type of Use	Thesis/Dissertation
Requestor type	Student
Format	Electronic
Portion	image/photo
Number of images/photos requested	5
Portion description	Figure: 1,2,3,4,5
Rights for	Main product
Duration of use	Life of Current Edition
Creation of copies for the disabled	no
With minor editing privileges	no
For distribution to	United States
In the following language(s)	Original language of publication
With incidental promotional use	no
The lifetime unit quantity of new product	0 to 499
The requesting person/organization is:	Manish Kumar Gupta
Order reference number	None
Title of your thesis / dissertation	MINIMIZING DECOHERENCE IN OPTICAL FIBER FOR LONG DISTANCE QUANTUM COMMUNICATION
Expected completion date	Aug 2016

Vita

Manish Kumar Gupta obtained his basic education at St. Michaels High School, Patna, Bihar, India. He then moved on to Banagalore, Karnataka India, where he obtained his bachelor in computer engineering degree. After obtaining a computer engineering he started his professional career in embedded design division at Hexaware Technologies, Mumbai, Maharastra, India and latter he worked in telecommunication for companies like Axes Technologies latter called Tech Mahindra (R & D) Services and Lucent Technologies Inc. and Motorola Inc.

Having worked in telecommunication Industry for more than 5 years; To advance his career he enrolled in Doctoral program in physics at Louisiana State University, Baton Rouge, United States and started his research work at Quantum Science and Technologies under the guidance of Dr. Jonathan P. Dowling. He first obtained a Masters in Science with major in physics and minor in electrical engineering and currently he is working to finish his PhD in physics.